UNIVERSITY OF MISKOLC

MIKOVINY SÁMUEL DOCTORAL SCHOOL OF EARTH SCIENCES

Head of the Doctoral School:
Prof. Dr. Péter Szűcs

HIGH-RESOLUTION FACIES INTERPRETATION OF QUATERNARY SEDIMENTARY SERIES FOR HYDROGEOLOGICAL MODELLING OF THE NYÍRSÉG-HAJDÚSÁG GROUNDWATER BODY, NE HUNGARY.

Ph.D. THESIS

AUTHOR:
Yetzabbel Gerarda Flores Carpio
Hydrogeological Engineer

SCIENTIFIC SUPERVISORS:

Prof. Dr. Péter Szűcs

Dr. Zoltán Püspöki

Institute of Water Resources and Environmental Management
Department of Hydrogeology and Engineering Geology

Miskolc, February 2024

DEDICATION

With heartfelt gratitude, I dedicate this work to my family and close friends. Your unwavering support, love, and encouragement have been invaluable in my travel to where I am today, and I am endlessly thankful for the warmth and strength you bring to me.

Specially, to my dearest husband, I am filled with profound gratitude for the love, partnership, and untiring devotion you bring into my life every day. Your presence has been a constant source of inspiration and joy. Thank you for being the anchor of my journey.

With love and gratitude,

Yetzabbel

ADVISOR'S FOREWORD

for the (PhD thesis)

"HIGH-RESOLUTION FACIES INTERPRETATION OF QUATERNARY SEDIMENTARY SERIES FOR HYDROGEOLOGICAL MODELLING OF THE NYÍRSÉG-HAJDÚSÁG GROUNDWATER BODY, NE HUNGARY"

by Yetzabbel G. Flores C.

The topic of the Candidate's thesis, high-resolution stratigraphy for hydrogeological modelling, is the focus of international research. The development introduced to the groundwater modelling workflow by the Candidate in the thesis pertains to geological modelling for porous aquifers, as applied in the case study of the regional Nyírség-Hajdúság Groundwater Body in NE Hungary. The suggested integrated application of high-resolution stratigraphy and hydrogeological data enables an accurate geological description of porous media aquifer systems characterized by high heterogeneity and medium depth, particularly at scales where the 2D geophysical field measurements are expensive or not time-efficient. This approach is relevant in contemporary hydrogeological practice and other geosciences.

The author explores new opportunities of the use of 1D geophysical data in densely drilled aquifers systems for hydrostratigraphic characterization. The 2D correlation of the data is based on facies correlation concepts and redefined in comparison with the hydraulic system patterns in the groundwater body. The assumption is grounded on the tight correlation between geological geometry and hydrogeological responses of the hydrogeological systems. The proposed methodology is suggested to enhance the 3D high-resolution interpretation of the geological framework of heterogeneous aquifer systems at regional scales.

An essential aspect of this thesis is the utilization of the results of the established hydrostratigraphic framework and hydraulic system for the 3D numerical modelling of the Nyírség-Hajdúság Groundwater Body. The optimization of the geometry and material properties assignment in accordance with facies proportions for each hydrostratigraphic unit has been proven to be an effective approach in the calibrating properties. The final model can inform by decision-making regarding management and sustainability plans, with the respective actualization of the hydrogeological data.

Her continuous efforts towards scientific research, her creativity, and the results presented in this thesis demostrate the Candidate's scientific knowledge and the suitability

for independent research. In our opinion, the Candidate's results, particularly those related to geological interpretation and groundwater modelling, merit publication in ranked international journals of hydrogeology or groundwater sustainability. We certify that this dissertation contains only valid data, and the presented results represent the Candidate's own work. In our opinion, it meets the scope and quality requirements set by the Mikoviny Sámuel Doctoral School of Earth Sciences. Based on the above, we fully support and recommend the public defense of the thesis and the award of the Ph.D. title.

01/03/2024

Prof. Dr. Péter Szűcs
University full professor

Dr. Zoltán Püspöki
Geological Survey of Hungary researcher

CONTENT

1 INTRODUCTION

Modern hydrogeology revolves around the concept of gravity-driven groundwater systems and their three fundamental factors: basin geometry, basin geology, and temporal changes in the water table (Tóth, 2009). These three factors converge to describe how groundwater flow transports various substances such as fluids, gases, solutes, colloids, particles, and heat from recharge areas to discharge sites (Tóth, 2015). Therefore, from a hydrogeological perspective, the spatial distribution of geological heterogeneity has gained significant importance, as it is recognized as one of the three primary controlling factors in aquifer production (Dutton, et al., 2003; Buday et al., 2015), model calibration (Cooley, 2004), recharge estimation (McCord et al., 1997), and is also the primary factor influencing solute transport (Bianchi and Pedretti, 2017).

Additionally, defining an exact geological framework for a specific site may be challenging; however, creating a reasonable approximation using stratigraphic and sedimentological concepts is achievable. This approach allows for the development of a comprehensive geological analysis that aligns with the objectives of groundwater investigations (Freeze and Cherry, 1979).

In the context of geothermal or petroleum projects, the targeted depth enables the joint evaluation of seismic and wireline log data (Torrado et al., 2020; Ben Mahrez et al., 2023). However, the situation differs when dealing with freshwater aquifers extending to depths of some hundred meters, as is the example in this research with maximum depths of 280 m. Such depths are too shallow for cost-effective seismic investigations and too deep for vertical geoelectric measurements (Kirsch, 2009). Consequently, wireline log correlations within this depth interval are challenging to support with additional 2D geophysical methods, which are essential for achieving sufficient horizontal resolution between them.

This situation contributes to the underestimation of 3D regional hydrogeological models and places greater reliance on 2D representations. These representations not only pertain to the geometrical configuration of the rock framework but also the hydrogeological data. This reliance on 2D representations occurs despite the significant heterogeneity and anisotropy properties of rocks and sediments, which are the primary determinants of preferential flow paths and sources of uncertainty (Maliva, 2016).

Therefore, the current research presents a methodological approach that enables us to recognize the 3D nature of the characteristics of the Southern Nyírség–Hajdúság

Groundwater Body. The proposed workflow integrates the 3D geological model developed using well-log correlation and geostatistical modelling with the hydrodynamic and hydrogeochemical patterns derived from a densely spatially referenced hydrogeological dataset. This correlation between the geometry of the rock framework and the hydraulic system patterns of the aquifer is evaluated, resulting in a robust hypothesis of the aquifer system concept. This approach facilitates the progression toward 3D numerical modelling.

1.1 Southern Nyírség–Hajdúság Groundwater Body – state of art.

The Southern Nyírség–Hajdúság Groundwater Body constitutes a complex aquifer system that has been exploited since 1830 due to its favorable specific yield capacity (Debreceni Vizmű Zrt., 2017a). Despite the abundance of wells, production data, hydrogeochemical information related to the study site, and previously published hydrogeological studies (Marton et al., 1980; Marton and Szanyi, 1997, 2000; Tóth and Almási, 2001), there is a notable absence of a comprehensive 3D regional hydrogeological model with the necessary resolution to precisely define the spatial continuity of aquifer layers. This precision is crucial for effective and sustainable water protection and management (Debreceni Vizmű Zrt., 2017b; Kinokow and Bredehoeft, 2020), particularly given the current increase in water demands of the region.

The initial study by Marton (1980), presented the regional flow net of the entire Nyírség Region in a two-dimensional section of 150 m depth, spanning from Sáránd in the southwest to Fehérgyarmat in the northeast (**Figure 1**). This research concluded that a significant volume of water is stored in the Pleistocene aquifer, characterized by low vertical infiltration rates attributed to a seepage factor five orders of magnitude lower than the horizontal hydraulic conductivity of the aquifer.

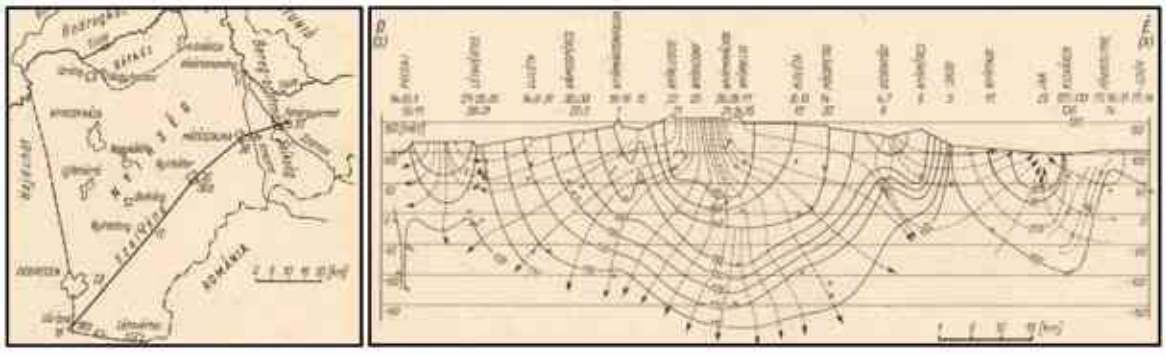

Figure 1. Regional flow net of Nyírség Region (Marton, 1982).

Despite the low recharge from precipitation, substantial supply potential exists across the extensive surface area of several thousand square kilometers. Additionally, the study found that the isotopic composition of water in the central area of the Nyírség Region closely

resembles contemporary rainwater, while at the edges, water samples exhibit similarities to Pleistocene waters.

In 1997, Marton and Szany made a significant contribution to the hydrogeological description of the Nyírség Region and its Quaternary sedimentary succession. They conducted a geostatistical investigation of the transmissivity of the Pleistocene aquifer, which was represented as a zero-order intrinsic random field modeled through an inverse procedure using a specific capacity dataset. Using Kriging interpolation, they generated a series of three transmissivity surfaces for different periods (**Figure 2**). The differences in these patterns were attributed to disturbances in the flow geometry, likely caused by significant leakage flux.

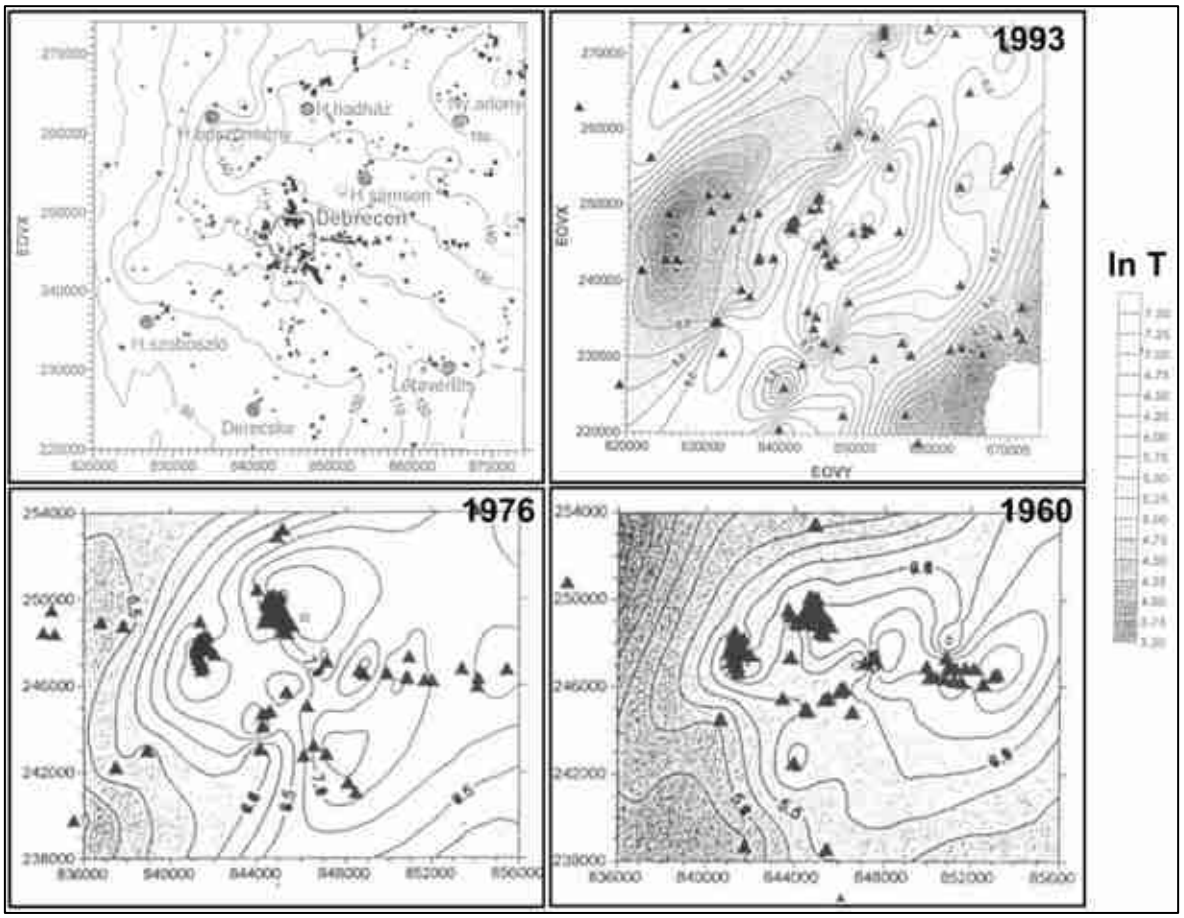

Figure 2. The geostatistical investigation of the transmisivity of the Pleistocene Aquifer around Debrecen in the Nyírség Region (Marton and Szanyi, 1997).

Starting from the early 20th century, the emphasis on drinking water supply in Debrecen shifted from surface and shallow water sources to deep aquifers. As a result, the currently operational wellfields of the city (WF-I, II, IV) (**Figure 3**) primarily tap into the Lower Pleistocene aquifer. Consequently, a study by Szany and Marton (2000) illustrates

how this intensive water production has gradually altered the natural flow conditions. A significant shift began in the 1970s, marked by a decline in the hydraulic head of the aquifer.

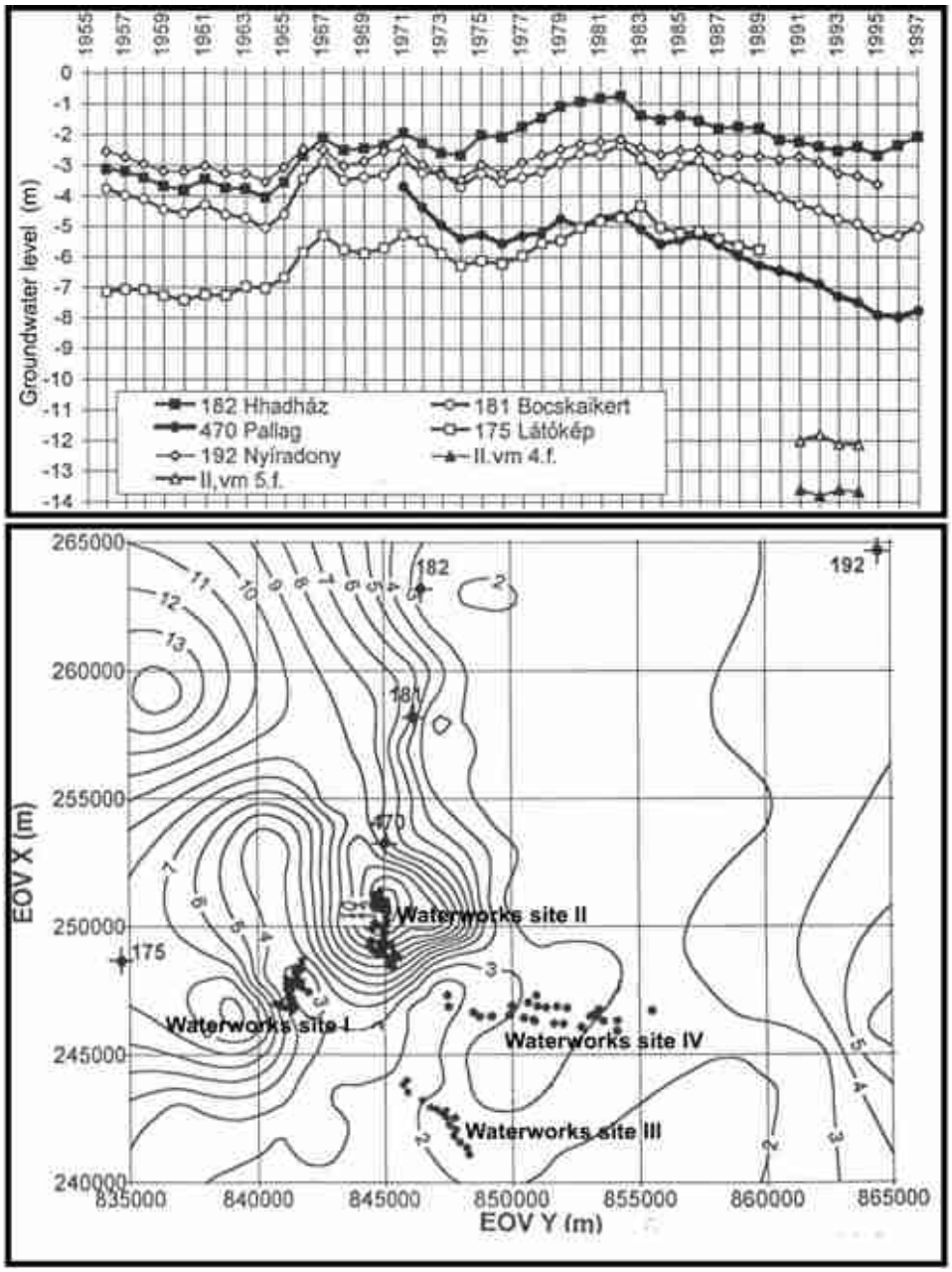

Figure 3. Changes in the water production of Debrecen between 1955 and 1997, and the water level in 1998 (Marton and Szanyi, 2000).

In addition, they highlighted two critical consequences of the imbalance in the water budget within the aquifer system. One relates to ecological damage (Szűcs and Madarász, 2006), while the other consequence is the alteration of hydraulic properties that elevate the risk of contamination of deeper aquifers (Simon et al., 2023). Marton and Szany investigation also revealed that aquitards can become significantly permeable under sustained, decades-long intensive pumping and increasing hydraulic gradients. This change

in the flow geometry raises serious questions about the protective properties of the intermediate 'waterproof' layers.

Subsequently, Szany (2004) introduced the first 3D local hydrogeological model of the area. The nearly 70 years of operation of the Debrecen Waterworks Sites offer an opportunity to comprehend both horizontal and vertical hydraulic conditions. By analyzing water level time series from wells screened at various depths, hydraulic head data was categorized into three different depth intervals: 1) wells screened from the shallow aquifer to 65-70 m depth with hydraulic head around 115 m a.s.l., 2) wells screened between 85 and 105 m with hydraulic head around 100 m a.s.l. and 3) wells screened between 120-170 m depth interval with hydraulic head around 92 m a.s.l. (Szanyi, 2004). The persistence of characteristic potential differences between these defined depth intervals underscores the significance of interbedded clayey aquicludes in shaping the flow regime of different hydrofacies within the aquifer system. Another local-scale model has been presented by Simon et al. 2023, focusing on how the imbalance in the regional water budget affects wetlands and, as a side effect, water-dependent ecosystems. This study concludes by examining wetland-groundwater interactions and their applicability to water retention planning.

Furthermore, Tóth and Almási (2001) introduced a fluid potential pattern for the Great Hungarian Plain. In their study, they combined the Quaternary succession, Zagyva Formation, and Újfalu Formation (before Törtel Formation) into what they referred to as the Great Plain Nagyalföld Aquifer. This aquifer is characterized by a gravity-driven flow regime and has an average permeability of 1000 md. It receives its recharge from the highlands of the Nyírség Region and has its primary discharge zone at the Tisza River. Additionally, two other studies have focused on the Great Hungarian Plain (Mádl-Szőnyi and Tóth, 2009; Ben Mahrez et al., 2023). The research by Madl Szőnyi (2009) aims to present the Duna-Tisza interfluve flow network at three different scales, while the recently published work by Ben Mahrez et al. (2023) introduces a subdivision of the previously mentioned Great Plain Nagyalföld Aquifer. This subdivision is vertically differentiated into three units as follows: Unit 1 comprises undifferentiated Quaternary sediments, and Unit 2 and Unit 3 pertain to the Zagyva Formation and partly to the Újfalu Formation.

Other studies in the region have also been conducted, primarily for geothermal purposes (Buday and Püspöki, 2011; Buday et al., 2015). In these investigations, the Algyő and Újfalu Formations took center stage, with the Quaternary Sequences being grouped into a single layer at the uppermost part of the study sites. Additionally, a 2D geophysical study

was conducted in the area with a focus on geothermal goals (Buday-Bódi et al., 2019). It was observed that the seismic section proved unsuitable for describing the Quaternary Sequences.

The first attempt to create high-resolution log correlation at the location of Debrecen city was performed by Püspöki (2016a,b), leading to the hypothesis of the existence of an incised valley in the region. Afterward, an intensive database development campaign was launched at the S.A.R.A. to investigate whether the presumed incised valley could be identified within a palaeogeographically relevant context (Püspöki, 2018; Flores, 2019). This extended database facilitated the establishment of a high-resolution 3D model using a sophisticated modelling software package equipped with authentic geostatistical tools. This endeavor developed through collaboration between SARA and the Mikoviny Sámuel Doctoral School since 2019, aimed to evaluate the stratigraphic characteristics and facies distributions of the study area.

1.2 Research motivation and aims

The doctoral research is motivated by the potential offered by the applied methodology for achieving a comprehensive 3D characterization of the porous Quaternary aquifer system within the Nyírség-Hajdúság Groundwater Body, situated in the intracontinental Pannonian Basin.

The study site possesses unique characteristics, including the depth of unconsolidated Quaternary sediments, a wealth of well-log data, and access to hydrogeological datasets. The imperative for a spatial geological definition of the Quaternary aquifer system stems from the escalating demand for water production in the region and the importance of safeguarding its quality, effective management, and sustainable planning to ensure the future availability of this vital resource.

With this motivation, the research objectives are as follows:

(1) To establish the 3D geological framework for the Quaternary aquifer system utilizing 1D geophysical data.

(2) To apply sequence stratigraphy for stratigraphic bounding surfaces identification.

(3) To utilize sequential indicator simulation and object-based simulation for 3D facies distribution modelling.

(4) To employ a integrated approach for the validation of the geological geometry, incorporating hydrogeological-hydrogeochemical information.

(5) To evaluate the hydraulic performance of the geological model on a regional scale.

(6) To extract insights from the case study that can contribute to understanding the effectiveness of the proposed integrated methodology in addressing similar conditions or challenges.

1.3 Description of the study area

1.3.1 Geographic location

The study area encompasses 1282 km^2 in the northeast region of the Great Hungarian Plain (**Figure 4a**), with 65.9% of the area belonging to the Southern Nyírség-Hajdúság Shallow Groundwater Body and 34.1% to the Northern Hortobágy-Nagykunság-Bihar Shallow Groundwater Body (**Figure 4b**). For simplicity, this research will refer to the study site as the Southern Nyírség-Hajdúság Groundwater Body (Southern-NHGWB). The maps and observation points are referenced in the 'EOV' coordinate system, spanning from EOVY= 824500 m to 887500 m (63 km range) and from EOVX= 216000 m to 273500 m (57.5 km range).

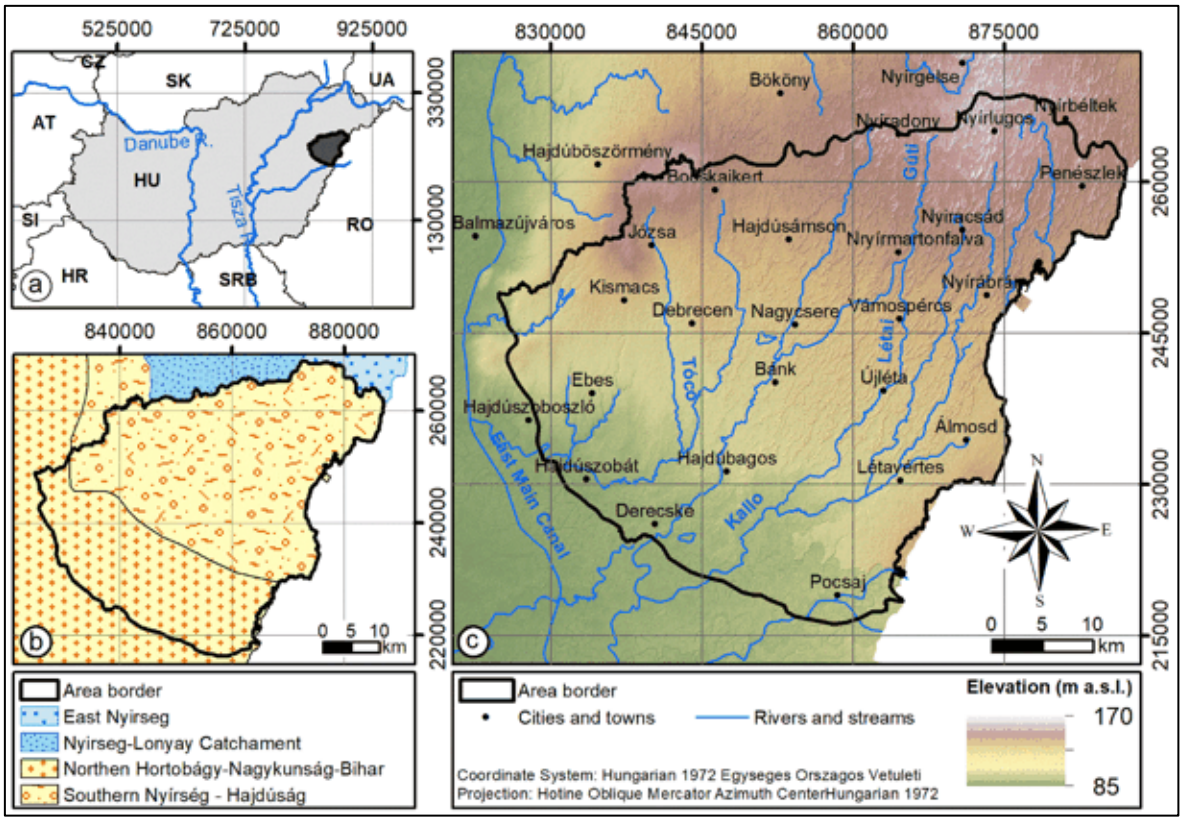

Figure 4. (a) Location of the Southern-NHGWB at NE of Hungary. (b) Shallow groundwater bodies of the National General Directorate of Water Management (ESRI Magyarország Kft. 2015). (c) Topography, morphology, and towns of the study site (Flores et al., 2023).

The Southern-NHGWB is characterized by an undulating plain with a complex parallel drainage network. The topography varies from 80 m a.s.l. in the lowlands

(Hajdúszovát and Pocsaj) to 170 m a.s.l. in the highlands (Nyírlugos). This region is bordered by the Berettyó and Hortobágy-Berettyó River Basins to the south and west, the Hungary-Romania border to the east, and the East Main Canal of Hungary to the west (ESRI Magyarország Kft., 2015) (**Figure 4c**). The area experiences a temperate continental climate characterized by mild winters and hot summers (VKKI, 2010). The average annual temperature hovers around 10-11°C, with seasonal fluctuations ranging from 23-24.5°C. Prevailing winds blow from the northwest to the southeast, while annual rainfall averages between 500 mm/y and 575 mm/y, and potential evapotranspiration falls within the range of 467 mm/y to 497 mm/y (NATÉR, 2023).

1.3.2 Geological and structural conditions

Bouguer anomaly and seismic data (Haas et al., 2014) have revealed a complex structure within the Nyírség region. It is characterized by a local sub-basin in the northern part, extending southward and intersecting the Derecske Trough. An inner elevated range oriented in the NE-SW direction is discernible. These structural elements have been active since the beginning of the Quaternary period, as indicated by Quaternary isopach data (**Figure 5**) (Wórum et al., 2020). They play a significant role in shaping the spatial distribution of facies and unconformity surfaces within the Quaternary sediments and even influence the region's current earthquake susceptibility (Gribovszki and Szeidovitz, 2006).

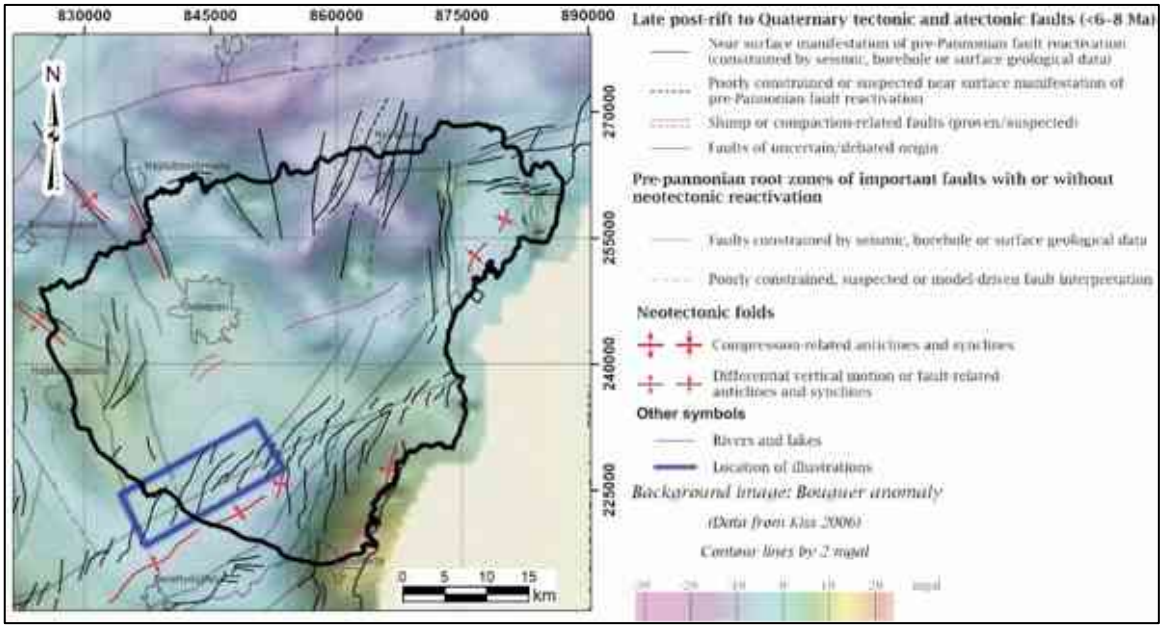

Figure 5. Tectonic lines and thickness of Quaternary sediments on the Great Hungarian Plain (Wórum et al., 2020).

Geologically, the depth of investigation reaches 280 meters, encompassing the entire Quaternary and a portion of the Pliocene sediments within the stratigraphic succession of the

northeastern part of the Great Hungarian Plain (GHP) (**Figure 6**). The described segment of the Pliocene sequence begins with the Újfalu Sandstone Unit, composed of alternating delta front and delta plain deposits consisting of sandstone, siltstone, and clay marl. Overlying it is the Zagyva Unit, characterized by fluvial and lacustrine sediments composed of medium to fine sand, silt, clay, and clay marl. This unit also contains coalified plant remnants and frequent lignite strips. Within the Zagyva Unit, one can observe the Nagyalföld Variegated Clay layer, representing a typical sequence of variegated clay interbedded with lignite and pebbly sand beds (Sztanó and Magyar, 2023).

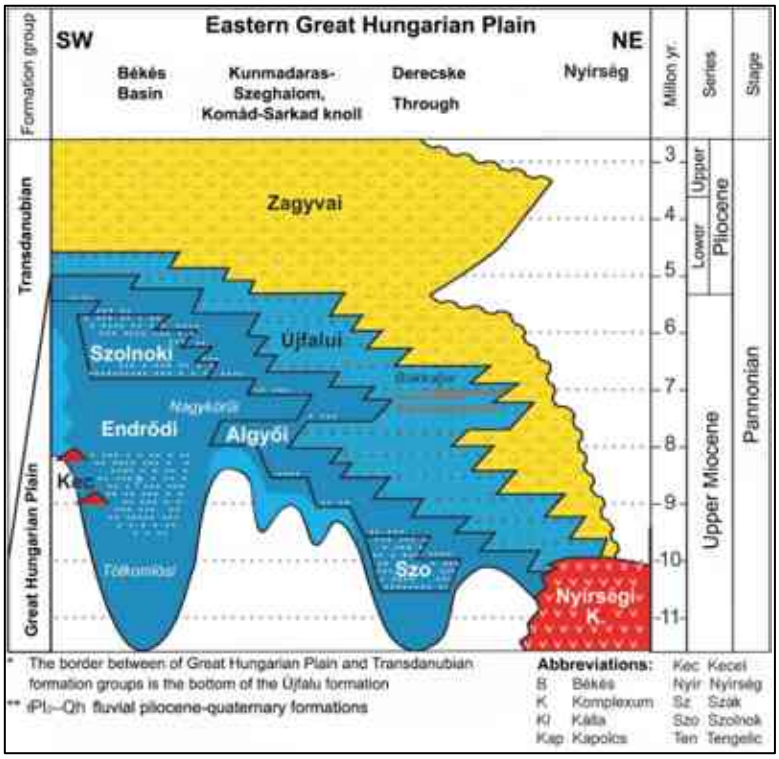

Figure 6. Pannonian lithostratigraphy of the Eastern Great Hungarian Plain (Sztanó and Magyar, 2023).

At the uppermost portion of the geological profile lie the fluvial fan deposits of the Quaternary period (**Figure 7**) (Borsy, 1982, 1990), which have been reshaped by the aeolian processes of the Late Pleistocene and Holocene epochs (Lóki, Hertelendi and Borsy, 1994). These deposits, forming fluvial fans, are surrounded by alluvial plains to the east, northeast, and northwest, marked by clear demarcations resulting from lateral erosion. Towards the west, they connect with a relatively elevated loess plateau, while the southern extent is characterized by recent alluvial plains. Several studies suggest that the considerable thickness of the Quaternary fluvial sequence in the area (approximately 250–300 meters) primarily accumulated due to drainage patterns shaped by the roughly northeast–southwest flow of the Tisza–Szamos system, somewhat mirroring the pre-Quaternary advancement

(Gábris and Nádor, 2007). Concerning the geological age attribution of the identified stratigraphic units in the area, the absence of cores and direct laboratory data presents a challenge, leading to the unavailability of direct evidence. Consequently, the ages are inferred from regional log correlations (Püspöki et al., 2013).

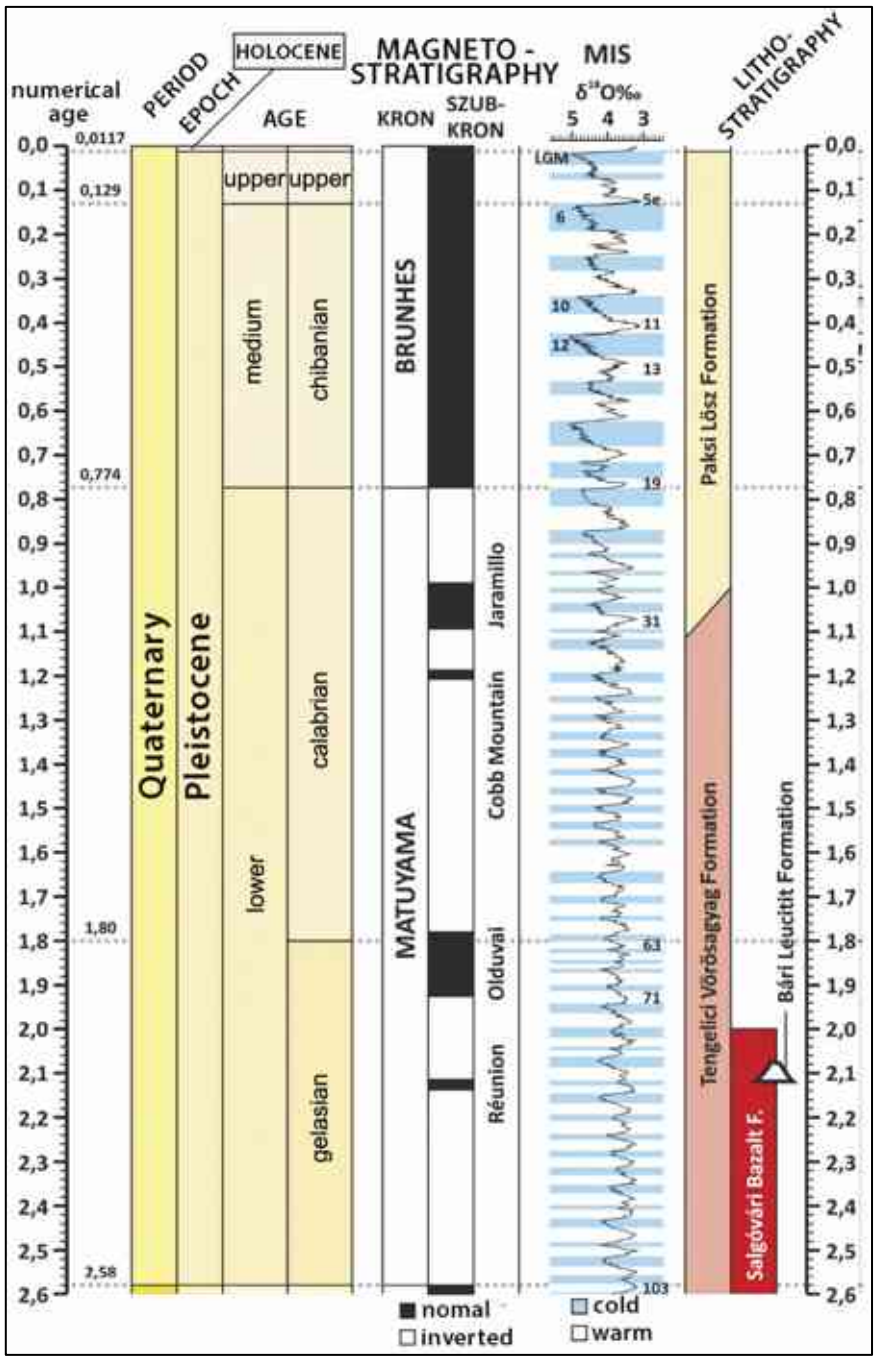

Figure 7. Quaternary sedimentary sequence of Hungary (Csillag et al., 2023)

1.3.3 Hydrogeological background

The hydrogeological characteristics of the extensive aquifer units in the Great Hungarian Plain were investigated within the framework of the Pannonian Basin Hydrogeological Research Program (PBHRP). This exploration led to the identification of

six hydrostratigraphic units based on lithological facies types and chronostratigraphy, which include the Pre-Neogene Aquiclude, Pre-Pannonian Aquifer, Endrőd Aquitard, Szolnok Aquifer, Algyő Aquitard, and the Nagyalföld Aquifer (Tóth and Almási, 2001). It is noteworthy that the depth of investigation within the study site primarily focuses on a section of the Nagyalföld Aquifer, acknowledged as one of Hungary's most significant non-karstic aquifers (Buday and Püspöki, 2011). The Nagyalföld Aquifer exhibits remarkable permeability, exceeding 1000 mD (Tóth and Almási, 2001).

In terms of hydrogeological perspective, the research study area is characterized as a gravity-driven unconfined zone (Tóth and Almási, 2001). Regional groundwater flow in the area typically follows a northeast to southwest direction, with the vicinity around Debrecen City serving as a transitional zone between the recharge area of Nyírség and the discharge area of Hortobágy (Erdélyi, 1976) (**Figure 4c**). The rate of recharge is predominantly determined by the effective infiltration of precipitation, ranging from 0 to 45 mm/year according to the average effective infiltration map provided by the National Adaptation Geoinformation System Project (NATéR, 2023). The water table is expected to attain an elevation of 155 m a.s.l. at Nyírlugos and Nyírbéltek, corresponding to the higher central surface of the Nyírség Region. In contrast, values as low as 80 m a.s.l. can be observed in topographic lowlands near Hajdúszovát and Hajdúszoboszló (NATÉR, 2023).

2 MATERIAL AND METHODS

2.1 Database

The investigation utilized a comprehensive database compiled by various institutions from 1969 to 1975, comprising a total of 512 production wells. Among these, 138 wells were obtained from the National Geological and Geophysical Database of Wells, known as the New Urbancsek Database. These wells provided crucial data on medium resistivity (R) (AM=40), self-potential (SP), natural gamma (NG), and geological log data necessary for mapping the subsurface geology of the aquifer system. Only 22 of these wells supplied information on deep resistivity (AM=120) and mud resistivity (ρ_i).

The dataset encompasses a total of 367 wells, all of which provide essential data for computing hydraulic parameters, such as pumping rates (Q), drawdown (s), and the locations of screen sections. Furthermore, data from 118 wells sourced from the National Hydrogeochemical Database (NHD) were utilized to assess chemical characteristics and water types at the horizon depth of the major aquifer system. For a comprehensive understanding of the database structure and information sources, please refer to **Table 1**.

Table 1. Structure of the available database for the research work (Flores et al., 2023).

	Data Type	Samples	Source	Institution
Geological and geophysical	Geologic log	130	New Urbancsek Data Base	SARA [1]
	Geophysical logs	138		
Hydrodynamic	Hydraulic head	366	Cadaster of Hungarian Drilled Wells. New Urbancsek Data Base	SARA [1] ME [2]
	Well diameter	466		
	Screen sections and production rate	369		
Geochemical	Water samples	118	National Geochemical Database	SARA [1]

Note(s): [1] Supervisory Authority for Regulatory Affairs. [2] University of Miskolc, Environmental Management Institute Library.

2.2 General workflow of the hydrogeological modelling process

The modelling process involves a structured algorithm that integrates both deterministic principles and subjective expertise. The workflow comprises two fundamental steps: (1) conceptualization and (2) numerical simulation, as illustrated in **Figure 8** (Anderson et al., 2015; Enemark et al., 2019). This underscores the necessity of incorporating a variety of techniques into the process to explore the local and regional expressions of variability in the studied system properties, aligning with the objectives of the research (Flores et al., 2023).

The comprehensive conceptualization of the groundwater system in the Southern-NHGWB utilizes all available data (**Table 1**) to delineate the geometry and to define the hydraulic properties of the hydrogeological framework, as well as to describe the flow pattern and geochemical evolution within the hydraulic system (**Figure 8**, Conceptual Model). Subsequently, the numerical simulation is employed to iteratively solve the groundwater governing flow equation (Kresic, 2006; Fetter, 2014) enabling the assessment of hydraulic head distribution for the discretized geometry under the specified initial and boundary conditions (**Figure 8**, Numerical Model). Finally, the calibration process is carried out to minimize the disparity between the calculated and observed hydraulic head distributions (**Figure 8**, Calibration).

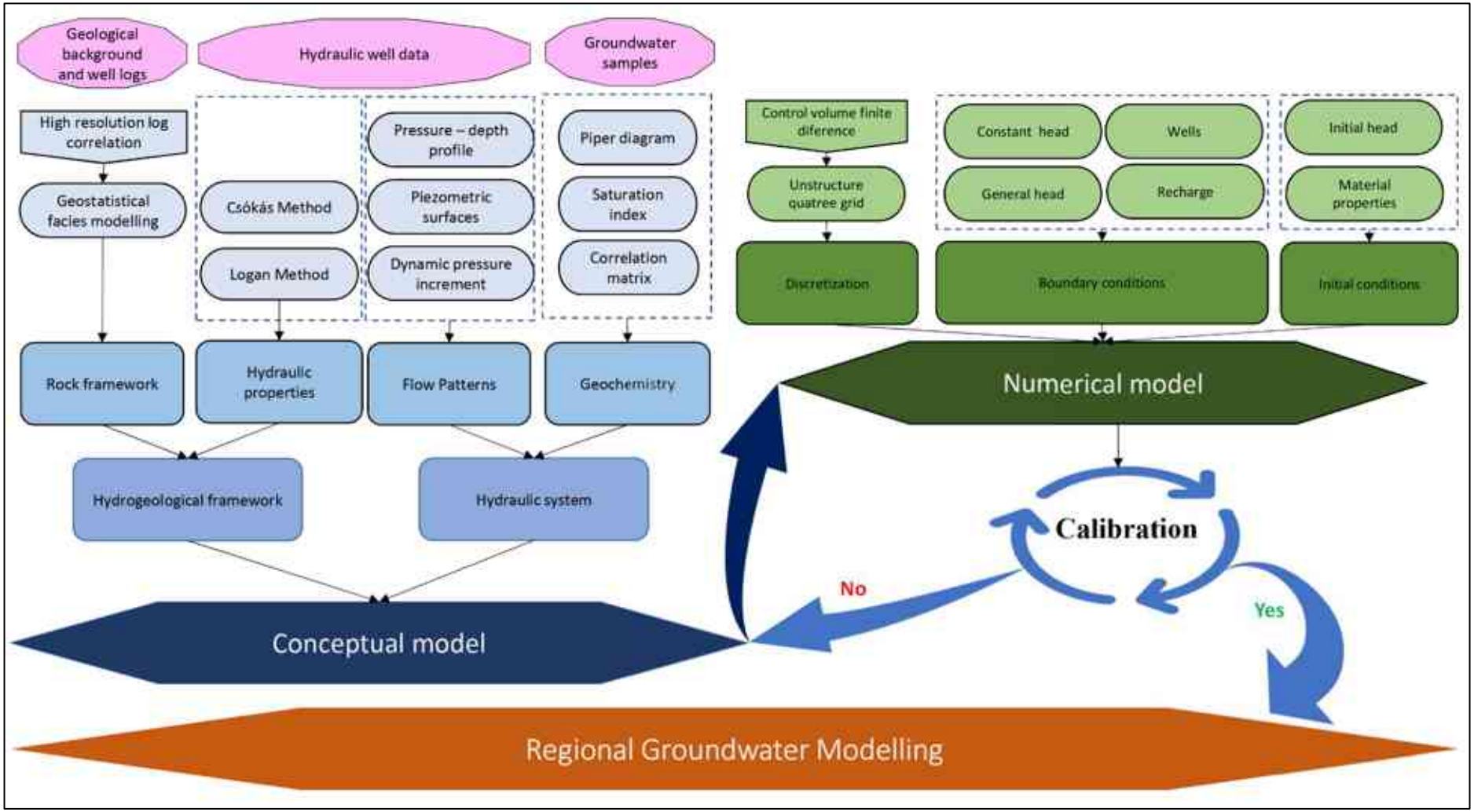

Figure 8. Implemented workflow for the regional groundwater modelling of the Nyírség-Hajdúság Groundwater Body.

2.3 Geological framework development

The initial phase of conceptualizing the aquifer involves establishing the geological framework. At this stage, high-resolution log correlation for stratigraphic discretization requires assumptions about the uniformity of the facies associations to explore the system's heterogeneity. Then, geostatistical methods such as object-based simulation or sequential indicator simulation will be utilized for mapping the 3D distribution of facies. TNavigator (refer to Appendix A) serves as the chosen tool due to its advanced visualization and analysis capabilities, which are essential for interpreting, constructing, and simulating the geological model as outlined in the proposed workflow. TNavigator facilitates the integration of diverse data types, such as well logs and geological interpretations, enabling the generation of detailed 3D models depicting subsurface structures and properties.

2.3.1 High-resolution log correlation

High-resolution log correlation employs sequence stratigraphy concepts (Cateneanu, 2022) in conjunction with systematic log correlation techniques to establish correlations between different wells. In cross-sections, logs are evenly spaced and display normalized spontaneous potential (SP) and/or natural gamma-ray (NG) on the left track, along with normalized medium electric resistivity (AM=40) on the right track. The space between the logs is filled with lithological log data obtained from cuttings during drilling (refer to Appendix B).

This process enables the identification of stratigraphic bounding surfaces and the definition of facies within the stratigraphic units based on lithostratigraphy and allostratigraphy concepts. Criteria such as log values, including spontaneous potential (SP), natural gamma-ray (NG), and resistivity (R), provide valuable insights into lithological variations and depositional environments. Additionally, log shape and stacking patterns offer information about sedimentary sequences and depositional processes. Vertical dimensions play a crucial role in determining the thickness and continuity of stratigraphic units. Furthermore, lithological descriptions, based on visual examination of cuttings or core samples, refine the interpretation of the facies. For further examples, refer to **Figure 9**.

Subsequently, stratigraphic surfaces were generated by interpolating the acquired well-tops using the geometric convergence algorithm (Maekawa et. al, 2007). This process is followed by the creation of a new discrete log for each well, introducing 11 categorical variables representing the identified facies within the stratigraphic units. The applied sequential stratigraphical approach may vary between lithostratigraphy and allostratigraphy

based on the density of the available well-log information for each unit. The facies log will be utilized in the geostatistical modelling of the 3D spatial distribution of facies, alongside the stratigraphic surfaces.

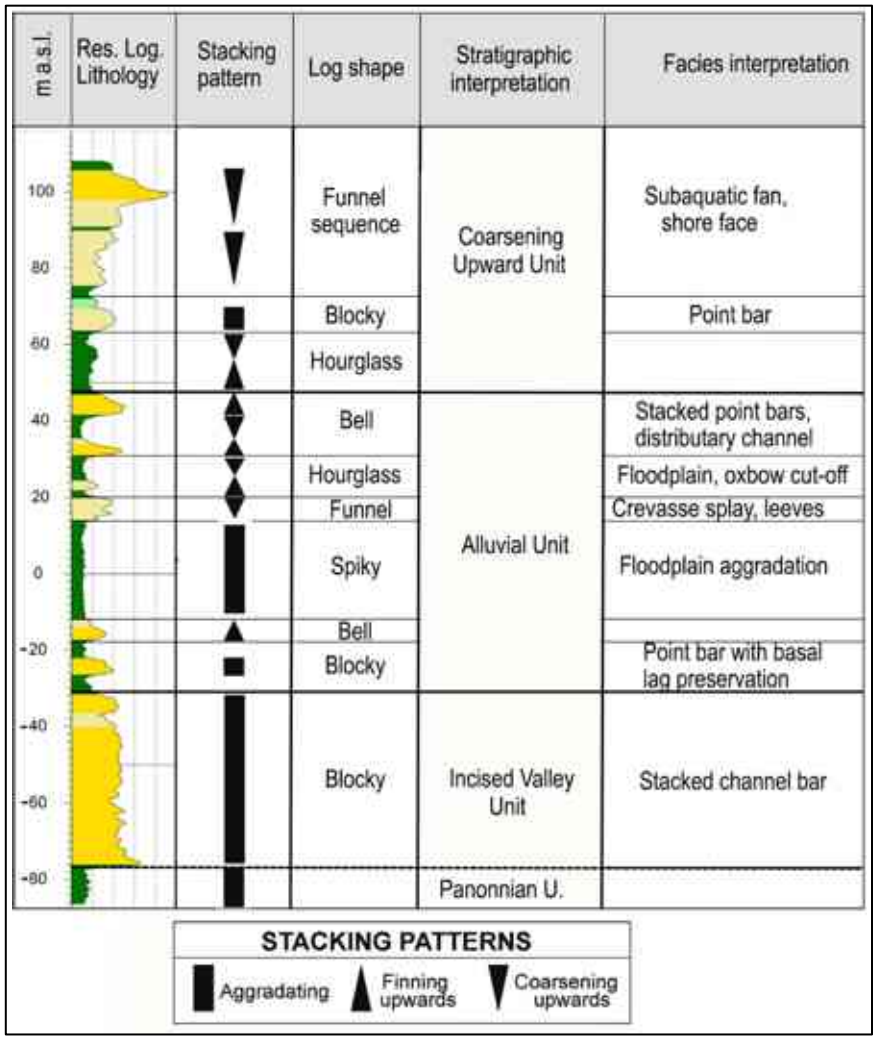

Figure 9. Resistivity log facies analysis observed in well data. The shape, scale, and stacking patterns log analysis was based on the work of Emery and Myers (1996) and Cateneanu (2022).

2.3.2 Geostatistical modelling

In the preceding section, the geological conceptual model was established, thus laying the groundwork for the initiation of the workflow for the geostatistical model of facies distribution (Pyrcz and Deutsch, 2014). The workflow is illustrated in **Figure 10**. The geostatistical modelling workflow begins with the structuring of the grid to discretize the model domain. These surfaces define the domain of interest for modelling, facilitating the aggregation and application of statistics, as they delineate the outer boundaries of the volume of interest (specific stratigraphic units). They play a crucial role in the gridding framework and the assessment of uniformity (**Figure 10**), serving as transitional zones between volume domains.

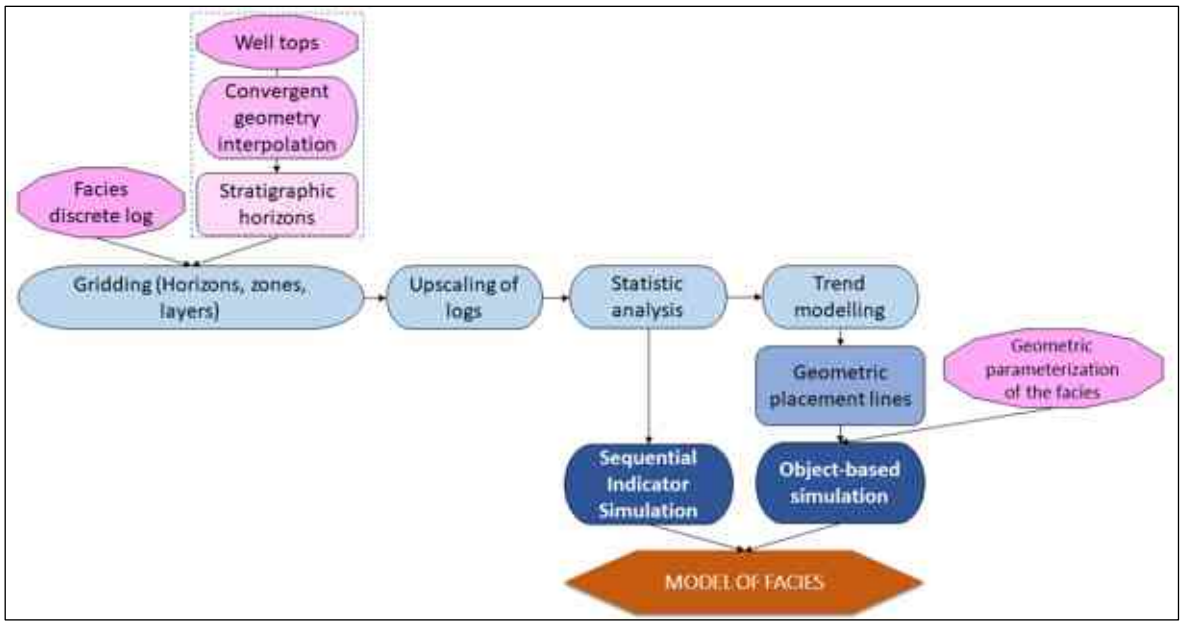

Figure 10. Workflow used to apply the facies modelling using geostatistical simulation methods. Adapted from Pyrcz and Deutsch (2014).

The layering of the volume domain involves identifying distinct regions, usually representing different facies, with consistent properties distributed under intrinsic hypothesis assumption. This hypothesis posits that the means remain constant and the semi-variogram values will depend only on the distance between the well locations. The thickness of the layers is chosen consequently with the thickness of the features considered important to be represented, with the aim of preserving essential information during the upscaling process from logs to the grid.

The construction of the trend model (**Figure 10**) is centered around modelling the locally varying direction of continuity and the locally variable mean or categorical proportion of the statistical inputs across all locations within the volume of interest (refer to Appendix C). This approach acknowledges the complexity and variability of the aquifer, thereby ensuring a practical modelling approach. It is reasonable to aggregate complex sets with widely different depositional and diagenetic controls together and assume that predictive models will emerge. Trend models can be developed using techniques including hand mapping, moving windows, inverse distance, and kriging.

Large-scale modelling involves modelling at a scale beyond geostatistical simulation, and its results can serve as a constraint for it. After defining the framework, regions, trends, and variable integration, geostatistical algorithms (**Figure 10**) can be employed to estimate and simulate the spatial distribution within the framework. This study employs two available algorithms: sequential indicator simulation, a cell-based method

rooted in variogram theory (refer to Appendix D), and object-based simulation, which idealizes the geometries of geological bodies (refer to Appendix E).

Sequential Indicator Simulation (SIS)

The sequential indicator method, developed by Journel and Alabert (1987), is a variogram-based designed to evaluate the likelihood of transitioning from the current category to any other category, without considering order relationships. It is rooted in the concept of Gaussian Simulation and extended to the Indicator-based model of uncertainty (Pyrcz and Deutsch, 2014). In this method (**Figure 11**), a set of mutually exclusive facies categories (s_f, f = 1, ..., F) are considered. At a specific location (u_j), the indicator transformation for a given facies (s_f) represents the probability of that facies prevailing at that location (1 if present, 0 otherwise).

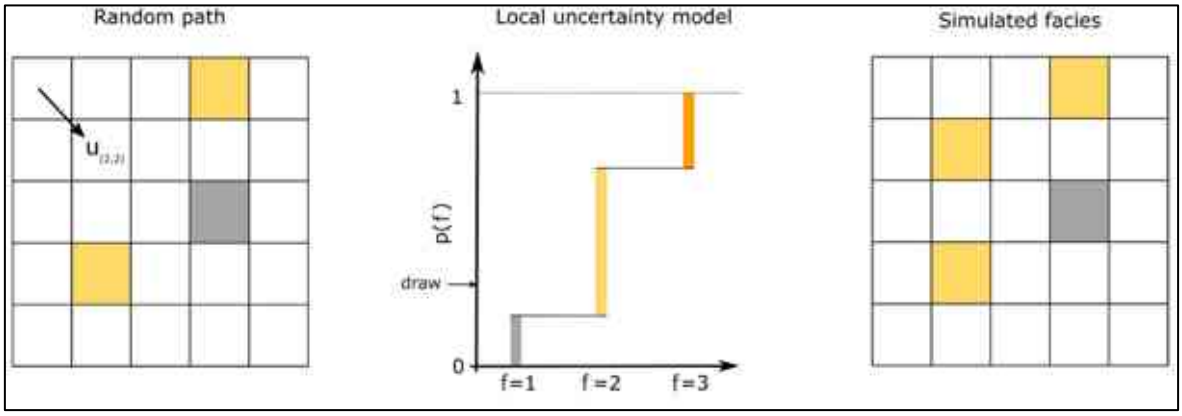

Figure 11. Representation of the three main stages of the SIS workflow (Mizuno and Deutsch, 2022). The analyzed categorical variables are indexed by f=1, 2, 3.

The algorithm systematically traverses nodes within the grid along a random path, searches for existing data, applies indicator kriging, and generates simulated values. This process is iterated across multiple realizations using distinct random number seeds. The SIS method (Alabert, 1987; Deutsch and Journel, 1998) finds utility in geological scenarios characterized by undefined geometries and high variability, particularly when factors such as anisotropy and variograms significantly influence the outcome.

Object-based stochastic simulation

The object-based modelling method (Deutsch and Wang, 1996) is specifically tailored to represent the idealized geometry of facies and finds widespread application in fluvial reservoir modeling. Within this method, parameterized architectural geometries are systematically inserted into the model domain until both global proportions and data conditioning criteria are satisfactorily fulfilled (Deutsch and Tran, 2002; Pyrcz and Deutsch,

2014). This approach relies on two fundamental considerations: firstly, the geometric parameterization, which serves to characterize geological heterogeneity across the model domain, and secondly, the strategic placement of background facies during the initialization phase of the model. The visually appealing results obtained from this method are often attributed to its adeptness in replicating idealized architectural element geometries (refer to **Figure 12**).

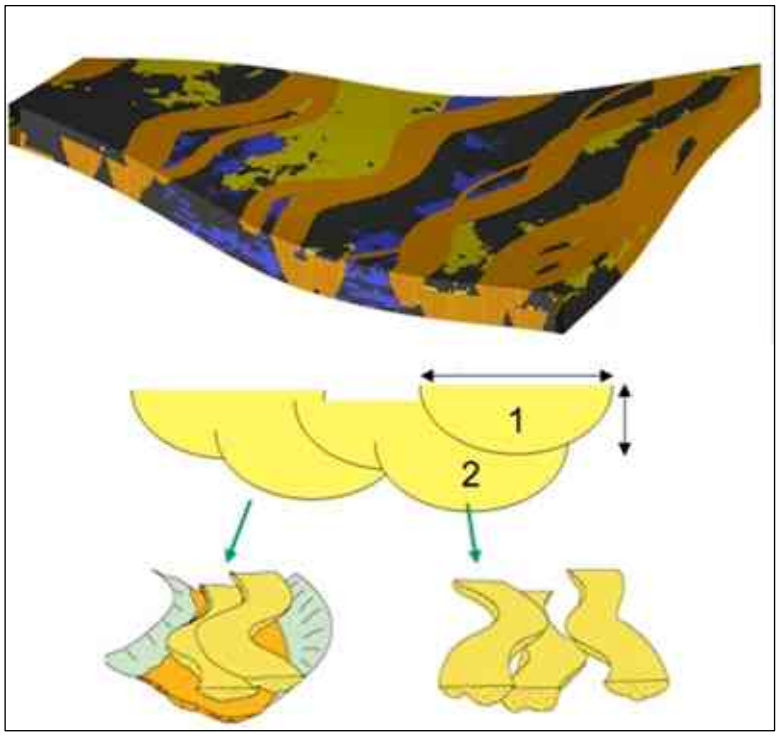

Figure 12. Initial geometric placement of a channel complex. (Rock Flow Dynamics, 2020).

These geometries are constructed through high-resolution log correlation and trend models. In geostatistical modelling, a 'facie' refers to a category that can be applied at various scales to delineate the model domain into regions with distinct property statistics (Pyrcz and Deutsch, 2014). These scales might include elements, stories with elements, or beds with stories. The facies within the model (or objects in object-based modelling) must represent components with significant volume contributions or a substantial impact on the aquifer's flow response.

2.4 Hydraulic parameters of aquifer units

In 1964, Logan proposed a method for estimating preliminary values of transmissivity using routine pumping tests when the pumping rate (Q), drawdown (s), and aquifer thickness (m) are available. This research has employed this method to approximate the hydraulic conductivity (k_h) of the sand bodies in unconfined and confined aquifers using **Equation 1** and **Equation 2**, respectively:

$$k_h = 2.43 \frac{Q}{s\,(2m-s)} \quad (1)$$

$$k_h = 1.22 \frac{Q}{s.m} \quad (2)$$

The reason for employing the Logan method (Logan, 1964) over other existing approaches, such as laboratory methods (Kozeny, 1927; Jelmer et al. 2017), or geophysical indirect measurements (Csókás, 1995; Bloch, 1991), is the availability of a dense dataset of pumping rate data in the area. This method allows for a clear initial assessment of the hydraulic properties of the different aquifer layers at the study site.

The Csókás (1995) method is an inversion-based model that allows the continuous measurement of the hydraulic conductivity along the aquifer system using geophysical logs. The estimation is done by applying the **Equation 3**:

$$k = C_k \frac{\varphi^3}{(1-\varphi)^4} \frac{\left(\log\frac{R_0}{R_w}\right)^2}{\left(\frac{R_0}{R_w}\varphi\right)^{1.2}}, \quad (3)$$

where φ is the porosity, R_0 is the resistivity of the rock, and R_w is the resistivity of the formation water. C_k is the proportional constant, calculated as follows:

$$C_k = 855.7 C_t {C_d}^2, \quad (4)$$

where C_t is a constant that varies according to the formation temperature (T) as $1 + 3.37 * 10^{-2}T + 2.21 * 10^{-4}T^2$, and C_d is the site constant proposed to be $5.22 * 10^{-4}$ for medium well-sorted sediments with a formation factor (F) less than 10. The formation factor is derived from **Equation 5:**

$$F = \frac{R_0}{R_w} \quad (5)$$

The application of the method requires geophysical well-log datasets, where are available self-potential (SP), natural gamma (NG), medium (AM=40), and long (AM=120) resistivity, and resistivity of the drilling mud (ρ_i).

The specific capacity (SC) of wells can be calculated by determining head losses as a function of pumping rates and time, as described by Risser, 2010 using **Equation 6**:

$$SC = \frac{Q}{s} \quad (6)$$

Here, SC represents the specific capacity in m³/d/m, Q is the pumping rate in m³/d, and s is the drawdown in the pumped well in meters. This calculation assumes a connection between subsurface flow and the well system, ensuring that the water leaving the groundwater system equals the water entering the well. As a result, any factor impacting the drawdown will also affect the specific capacity value for a given pumping rate.

2.5 Hydrodynamic parameters

Three hydrodynamic parameters characterize groundwater flow in a basinal environment (Tóth, 2009; Mádl-Szőnyi and Simon, 2016): Hydraulic head (h); regional patterns of pore pressure (p); and vertical pressure gradient (γ). Darcy's principle asserts that groundwater always flows from areas of high potential energy to areas of low potential energy (Darcy, 1856), in the direction of declining hydraulic head (h). Then, Hubbert (1940) validated Darcy's hypothesis by demonstrating the physical nature of the hydraulic head and its relation with the fluid's mechanical energy. The fluid potential (θ) is defined as the work (W) performed by a unit mass of fluid (m), then the energy content of fluid potential of a unit mass that moves from P_1 to P_2 is:

$$\theta = \frac{W}{m} = gz + \frac{v^2}{2} + \int_{p_0}^{p} \frac{dp}{\rho} \quad \textbf{(7)}$$

Under the assumption that groundwater flow velocities are negligibly low ($v \approx 0$), and the fluid is slightly compressible ($\rho \approx constant$), the expression of the fluid potential can be simplified to:

$$\theta = gz + \frac{p - p_0}{\rho} \quad \textbf{(8)}$$

The pressure (p) in a point (P), at the base of the manometers is:

$$p = \rho g \varphi + p_0, \quad \textbf{(9)}$$

where φ is the height of the water column above P, and p_0 is the atmospheric pressure on the fluid's surface in the manometer. Considering:

$$\varphi = h - z \quad \textbf{(10)}$$

where h is the hydraulic head and z is the elevation head at the given observation point P in meters. Substituting **Equation 9** and **10** into **Equation 8**, the fluid potential became:

$$\theta = gz + \frac{[\rho g(h-z)+p_0]-p_0}{\rho}, \quad \textbf{(11)}$$

or

$$\theta = gh \quad \textbf{(12)}$$

Assuming the atmospheric pressure as a datum ($p_0 = 0$), the relation can also be written as follows:

$$\theta = gh = gz + \frac{p}{\rho}, \quad \textbf{(13)}$$

or

$$h = z + \frac{p}{\rho g}, \quad \textbf{(14)}$$

where, ρ is the water density in kg/m^3, g is the gravity in m/s^2 and φ is the pressure head in meters calculated with **Equation 9** (Fetter, 2014).

To analyze the pore pressure and its gradients (Tóth, 2009), the regional pore pressure increments can be represented in a pressure-depth ($p(d)$) cartesian coordinate system, wherein the vertical axis represents depth below the land surface, and its origin is at $d = 0$. The horizontal axis represents pore pressures (p). The elevation of the water table below the land surface is denoted with d_0 (**Figure 13a**). The utilization of a pressure-depth profile ($p(d)$) instead of a pressure-elevation profile ($p(z)$) allows for the application of a unified hydrostratigraphic reference line for all measurement points, irrespective of their differences in elevation (z) location (**Figure 13b**).

The vertical pressure gradient (γ) is an expression of the direction and intensity of the vertical flow (Tóth, 2009). It is illustrated by the variation of the pressure in two surface points at different depths. For static fluids, the pore pressure increases with depth at a rate equal to the specific weight of the fluid (nominal pore pressure). However, for fluids in motion, the vertical component of flow causes it to increase according to:

$$\gamma = \frac{\mathrm{d}p}{\mathrm{d}d} \quad \textbf{(15)}$$

The dynamic pressure increment (Δp) is defined as the difference between the nominal and dynamic pressure. It is an indicator of the vertical flow direction from the water table. A positive increment ($+\Delta p$) suggests an upward flow direction, whereas a negative increment ($-\Delta p$) suggests a downward flow direction (Fogg and Keitler, 1981; Tóth, 2009). For the calculation of the dynamic pressure increment, the following equation is used:

$$\Delta p = \gamma_{st} \Delta h = p_{dyn} - p_{st}, \quad \textbf{(16)}$$

where γ_{st} is the gradient of the static fluid, Δh is the difference between the heads representing the static and flowing conditions. The static pressure term (p_{st}) can be calculated regardless the actual condition is static or dynamic. It is a calculated value of hypothetical static pressure also known as nominal hydrostratigraphic pressure, calculated by:

$$p_{st} = \rho g \varphi_{st} = \gamma_{st}(d - d_0), \quad \textbf{(17)}$$

while the dynamic pressure term (p_{dyn}) is determined by the measured pressure in the point P or water level in an open well. It is a physical quantity evaluated by **Equation 9**.

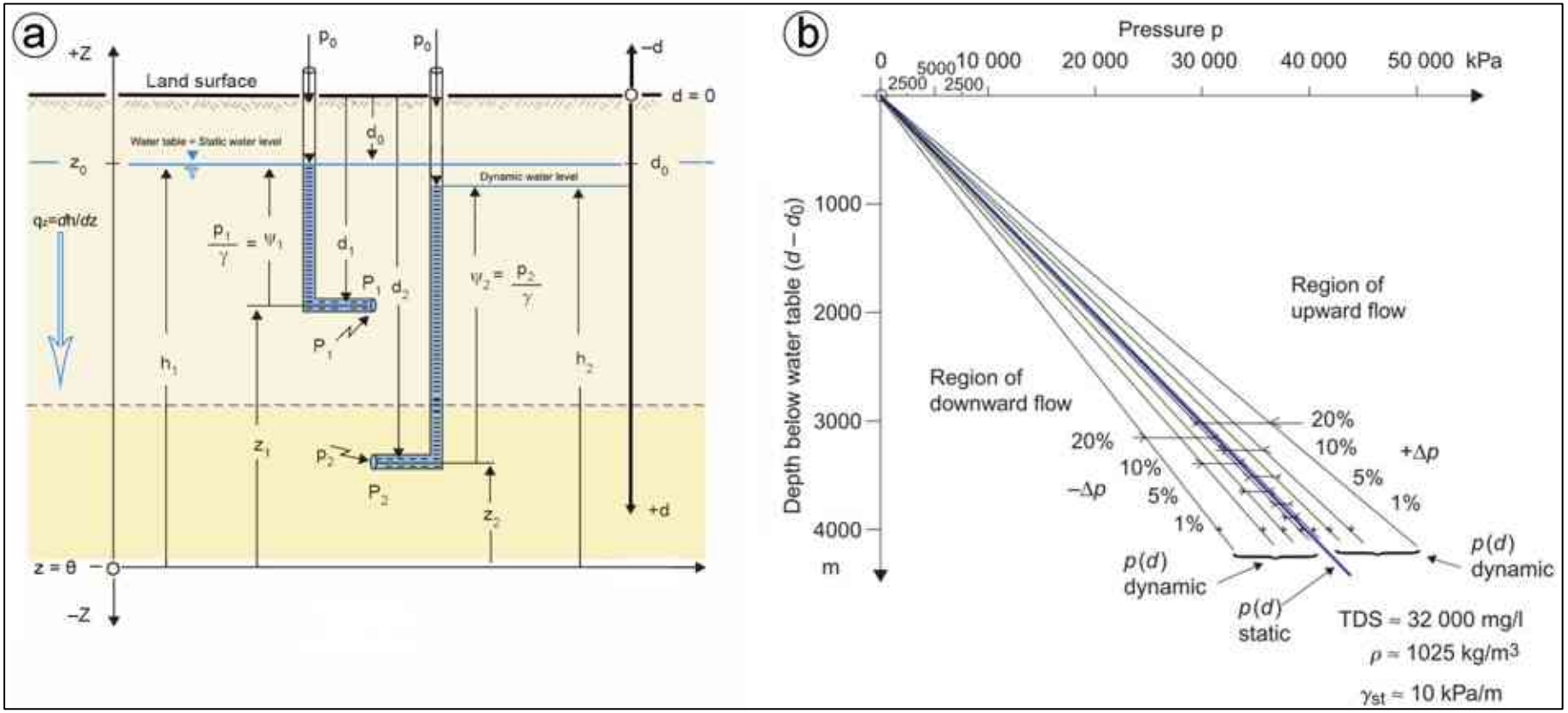

Figure 13. (**a**) Notations of hydrodinamic parameters. (**b**) Theoretical pressure-depth profile, and dynamic pressure increments referenced to the water table. The figure is addapted from Tóth (2009).

Therefore, distribution maps for each aquifer layer of each one of the hydrodynamic parameters ($h,\ \gamma,\ \Delta p$) are generated by Kriging Interpolation (Oliver and Webster, 2014) performed in Surfer 25.1.229.

2.6 Geochemical model

The analytical accuracy of the measurements of cations and anions in the water samples is obtained from the ionic balance error (IBE) within a limit of ±5% (Sasamoto et al., 2004). It was computed in milliequivalents per liter (mEq/l) as follows in **Equation 18** (Bayer et al., 2011):

$$\mathrm{IBE} = [(\mathrm{TC} - \mathrm{TA})/(\mathrm{TC} + \mathrm{TA})] \times 100, \quad \textbf{(18)}$$

where, TC is the sum of the total cations and TA is the sum of the total anions.

Hydrochemical facies are defined with a Piper plot (Piper, 1944). The Total Dissolved Solids (TDS) values were calculated to present the general chemical characteristics of the groundwater. The ratio of major ions was investigated to approximate the water-rock interaction processes, including mineral weathering and ion exchange. The Ca^{2+}+Mg^{2+}/HCO^{3-} +SO_4^{2-} ratio was calculated in mEq/L. Values smaller than 1 refer to silicate weathering or ion exchange **(Equation 19)**; meanwhile, values greater than 1 indicate carbonate weathering or reverse ion exchange **(Equation 20)** (Rajmohan and Elango, 2004).

$$\mathrm{Ca^{2+}} + 2\mathrm{NaX} \rightarrow 2\mathrm{Na^{+}} + \mathrm{CaX_2} \quad \textbf{(19)}$$

$$2\mathrm{Na^{+}} + 2\mathrm{CaX_2} \rightarrow \mathrm{Ca^{2+}} + 2\mathrm{NaX} \quad \textbf{(20)}$$

The mineral saturation in the groundwater of the aquifer system is determined by calculating the Saturation Index (SI) (Appelo and Postma, 2005) for calcite, dolomite, aragonite, gypsum, and halite using PHREEQC (Parkhurst and Appelo, 2013) according to **Equation 21**:

$$SI = log\frac{IAP}{K_{sp}} \quad \textbf{(21)}$$

where IAP refers to the ion activity product, and K_{sp} is the solubility product at a given temperature. If the value of the saturation index equals zero, the water is in a chemical equilibrium state with the mineral. A positive value of SI indicates that the groundwater is oversaturated, while a negative value refers to it being undersaturated concerning the mineral species.

The spatial distribution maps of the analyzed geochemical variables are plotted by interpolation of the data using the Kriging Method performed in Surfer 25.1.229. The two-

dimensional relationships between the physicochemical parameters were analyzed by Spearman's correlation matrix ('Spearman Rank Correlation Coefficient', 2008).

$$\rho = 1 - \frac{6 \sum d_i^2}{n(n^2-1)}, \quad \textbf{(22)}$$

where ρ is the Spearman rank correlation coefficient, d_i is the difference between the two ranks of each observation, and n is the number of observations.

2.7 Numerical model application

Numerical modelling attempts to represent the groundwater flow in a mathematical representation (Reilly, 2001). The process of solving the groundwater flow equation for the dependent variable (head) can be summarized in the following steps (refer to **Figure 8**): (1) code selection and discretization (independent variables x,y,z and time), (2) insertion of boundary conditions (hydrologic parameter), and (3) setup of initial conditions (material properties) (Anderson et al., 2015). Nowadays, there is a wide range of code options available in the field of hydrogeological modelling, such as Modflow 2005, Modflow USG, Modflow 6, Sutra, and others. These codes are often supported by graphical user interfaces like GMS, Visual Modflow, and Model Muse.

For this research, the Modflow-USG code is applied (Panday *et al.*, 2013). It is implemented within the Groundwater Modelling System (Aquaveo LLC, n.d.) graphical interface, to address the phenomenon under study. After completing the numerical modelling stage, the calibration process becomes essential to assess the base model's performance. During this step, we evaluate how well the model suits our problem. Adjustments may be made to address parameter sensitivity, data gaps, or inconsistencies in the conceptual model to improve the model's fit without compromising its reliability.

2.7.1 Code selection and discretization

To address the complexities inherent in modeling geometrically intricate aquifers, a strategic choice is made to utilize software capable of accommodating Unstructured Grids (USG) with the primary goal of achieving a more accurate representation of the aquifer's geometry. MODFLOW-USG is one such version that employs Control-Volume Finite-Difference (CVFD) Approximation (Panday *et al.*, 2013). In a CVFD model, spatial discretization can encompass various cell shapes, including rectangles, squares, hexagons, triangles, and irregular shapes (**Figure 14**). The capability of CVFD models extends beyond horizontal spatial discretization; it also encompasses the ability to adapt spatial discretization across vertical layers. This feature is particularly valuable in capturing the heterogeneity and

anisotropy that frequently characterize subsurface formations, ensuring a comprehensive representation of hydrogeological processes across the aquifer's depth

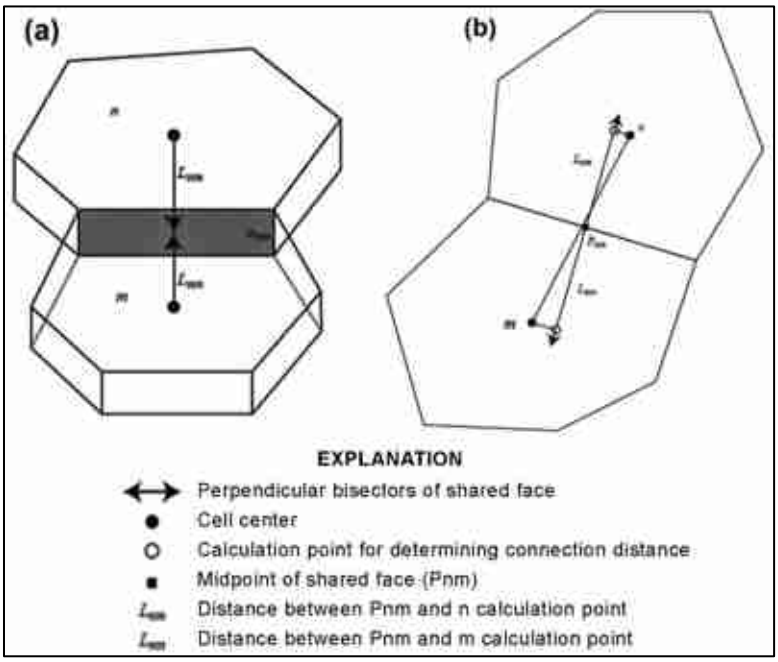

Figure 14. Plan view of finite-difference cells (n and m) in an unstructured grid as used in the CVFD. (**a**) Connection lengths are measured from the center of the cell. The flow area is shown in gray. (**b**) Geometry correction of the cell connection to bisect the shared face at the correct angle (Panday *et al.*, 2013).

The Control-Volume Finite-Difference (CVFD) method is a powerful numerical approach commonly used in hydrogeology and fluid dynamics for simulating and modelling flow and transport phenomena in porous media. It's a variant of the finite volume method designed to handle complex geometries and heterogeneous subsurface conditions. One of its distinguishing features lies in its capacity to accommodate larger nodal spacings in regions lying beyond the primary focus of the study. This attribute is particularly advantageous as it optimizes computational efficiency by prioritizing resources where they are most needed, thus enabling a more effective allocation of computational resources and enhancing the overall efficiency of the modeling process.

Model layers discretization dimensions

The design of horizontal nodal spacing must align with the modeling objectives, striking a balance between reasonable runtimes and the ease of data management and visualization of results. The primary consideration in this decision-making process stems from the size of the problem domain. Additionally, various factors must be taken into account, including solution accuracy, the location of calibration targets, configuration of

perimeter boundaries, parameter heterogeneity, presence of faults, conduits, barriers, and sources and sinks (Anderson et al., 2015).

The required number of layers in the model domain aims to represent vertical variability in hydrostratigraphy and/or simulate vertical changes in hydraulic heads. Typically, one layer corresponds to a hydrostratigraphic unit, although assigning more than one layer to a single unit may be necessary to capture changes in hydraulic properties or the hydraulic system within the unit (Anderson et al., 2015).

Contrary to horizontal discretization, abrupt changes in vertical dimensions typically pose fewer challenges because a high percentage of model domains are dominated by horizontal flow (Haitjema, 2006). General guidelines for vertical discretization are lacking, and significantly larger vertical nodal spacing relative to horizontal nodal spacing does not necessarily lead to errors. This is because most models incorporate some degree of vertical anisotropy, which diminishes the vertical component of flow and directs it horizontally (K_h/K_v). For example, if $K_h/K_v = 100$, the vertical node spacing can be 10 times larger than the horizontal without losing numerical accuracy (Anderson et al., 2015).

2.7.2 Initial conditions

Initial conditions encompass the setup of the starting head of the flow domain and the initial estimation of material properties, as depicted in **Figure 8**. The hydraulic characteristics of the layers are delineated by three material properties: hydraulic conductivity, storativity, and effective porosity. These attributes are assigned to each cell, element, or node within the layer's network, with adjustments often made during the calibration process.

Hydraulic conductivity (k) serves as a fundamental governing parameter in groundwater flow dynamics. In the initial model approximation, k is typically assumed to be constant within a given layer. However, geological materials rarely exhibit isotropic and homogeneous characteristics. While the assumption of isotropic horizontal conductivity ($k_x = k_y$) is often appropriate in many scenarios, the presence of fractures, sedimentary structures, or other geological features within the aquifer may introduce significant vertical anisotropy that must be carefully considered (k_x/k_y), leading to preferential directions of the flow paths (Maliva, 2016).

Although the values of k_x calculated by Logan's Method provides a useful initial estimation of the hydraulic conductivity within the layers, the continuous vertical calculation of the parameter based on geophysical logs can be upscaled to the nodes through an apparent

hydraulic conductivity estimation. From the log, the apparent horizontal hydraulic conductivity of fine-grained layers and coarse-grained layers can be assessed (refer to Section 2.4). Also, an acceptable approach is a zonation for the assignment of constant values of the parameter in specified areas of the flow domain.

Vertical anisotropy, represented by the ratio between horizontal and vertical hydraulic conductivity (k_x/k_v), prevails in many groundwater scenarios, attributed to stratigraphic features, fractures, and heterogeneity within a model layer, resulting in a preferential horizontal flow direction. Although vertical anisotropy can be measured through specialized tests (Kenoyer, 1988; Sterret et al., 2007) these tests are rarely performed in practice. Consequently, vertical anisotropy is typically estimated during the calibration process.

Regarding the effective porosity, even though it does not feature in the governing equation of groundwater flow, its significance becomes apparent in particle tracking applications, where it plays a crucial role in velocity calculations.

2.7.3 Boundary conditions

Boundary conditions are related to hydraulic conditions along the perimeter of the problem domain. They not only define the mathematical constraints in the solution of the flow equation but also serve as sources and sinks of water within the system (Kresic, 2006; Anderson et al., 2015). There are three primary mathematical approaches (**Table 2**) to representing them in the model:

Table 2. Principal mathematical method for depicting boundary conditions (Anderson et al., 2015).

Boundary type	Formal Name	Mathematical designation
Specified Head	Dirichlet	$h\,(x, y, z, t) = constant$
Specified flow	Neuman	$\frac{dh\,(x, y, z, t)}{dn} = constant$
Head-dependent flow	Cauchy	$\frac{dh}{dn} + ch = constant$

Note: 'h' represents head (measured in L), and 'n' denotes the directional coordinate normal to the boundary (measured in L), and c is a constant.

Specified head conditions, known as Dirichlet conditions, involve the imposition of a predetermined hydraulic head value at boundary locations within a hydrogeological model. Modflow, a widely-used groundwater flow modeling software, provides various packages, such as IBOUND and Time-Variant Specified Head, to facilitate the implementation of specified head conditions. Conversely, specified flux conditions, also termed Neumann conditions, entail the specification of the derivative of the hydraulic head at the boundary.

Modflow offers a suite of packages, including Flow and Head Boundary, Recharge, and Well, to incorporate specified flux conditions into the model setup (Wiston, 2018).

Additionally, head-dependent flux boundaries, known as Cauchy or mixed conditions, necessitate the application of Darcy's law to calculate flow across boundaries. This involves computing a gradient derived from the difference between a specified head outside the boundary and the head computed by the model at nodes situated on or near the boundary. Modflow provides a comprehensive array of options, including General-Head Boundary, Drain, Drain-Return, River, Evapotranspiration, Stream, Lake, Multi-Node Drawdown Limited Well, and Multi-Node Well packages, to accommodate head-dependent flux boundary conditions (Wiston, 2018).

Vertical Leakance, Resistance, and Conductance

The evaluation of vertical conductance assumes significance in regions where the interchange of water between surface water bodies and groundwater is influenced by sediments at the sediment-water interface, as denoted by **Equation 23**.

$$q_z = -k'_z \frac{h_{i,j,k} - h_s}{b'}, \quad \textbf{(23)}$$

where q_z denotes the vertical flux of water to or from a surface water body, $h_{i,j,k}$ represents the computed head beneath the surface water body, h_s signifies the surface water head specified by the modeler, k'_z stands for the vertical hydraulic conductivity at the interface between the groundwater system and the surface water body, and b' is the thickness of the interface.

In this context, vertical leakance is defined as the ratio of the vertical hydraulic conductivity of the sediments to their thickness (k'_z/b'). Vertical resistance, the reciprocal of leakance (b'/k'_z), and vertical conductance (C), is calculated by multiplying leakance by the horizontal area of the sediments within the cell, as expressed in **Equation 24**.

$$C = k'_z \frac{A}{L}, \quad \textbf{(24)}$$

where k'_z is the representative hydraulic conductivity, A denotes the representative area, and L represents the distance between the choosing location of the specific boundary head and the simulate cell. In practical implementation, the estimation of vertical leakance commonly occurs during the calibration of the model. Furthermore, achieving an accurate depiction of surface water features may necessitate fine spatial discretization, as emphasized by Anderson, et al. (2015). Calibration of these features involves alignment with field measurements of flux.

2.7.4 Calibration

The calibration process of the numerical model extends beyond merely comparing simulated values to observed data. It involves a systematic approach to iteratively refine model parameters and improve the model's predictive accuracy. Firstly, calibration objectives are established based on observed data, which typically include hydraulic heads measured at monitoring wells and fluxes observed at specified locations within the aquifer system. To initiate the calibration process, model parameters such as hydraulic conductivity, storativity, and boundary conditions are set within reasonable initial bounds. These bounds are often determined from prior knowledge, literature values, or preliminary model runs.

The calibration process then proceeds through a series of sequential forward runs of the model, during which parameters are adjusted incrementally within their specified bounds. The objective is to minimize the discrepancy between observed and simulated values, typically quantified using an objective function such as the sum of squared differences or the root mean square error. Statistical measures such as maximum, minimum, and mean values, along with confidence intervals, variances, or standard deviations, are often used to establish the bounds within which parameters are adjusted.

These measures provide a quantitative basis for assessing the variability and uncertainty associated with each parameter. Once a satisfactory level of agreement is reached between observed and simulated data, the calibrated model is validated using independent datasets to assess its robustness and reliability for predicting groundwater flow behavior under various conditions.

3 RESULTS AND DISCUSSION

3.1 Conceptual model of Southern Nyírség – Hajduság Groundwater Body

3.1.1 Hydrostratigraphic units and hydrofacies

The Southern-NHGWB stratigraphic model includes a three-dimensional geological description of an approximately 280-meter-deep section of Quaternary Sequences and partly of the Pannonian sedimentary deposits at the study site. A total of 24 cross-sections (Appendix B-1) were created for stratigraphic correlation, ensuring the interconnection between the 138 well-log data points. To illustrate, three cross-sections are depicted in **Figure 15**.

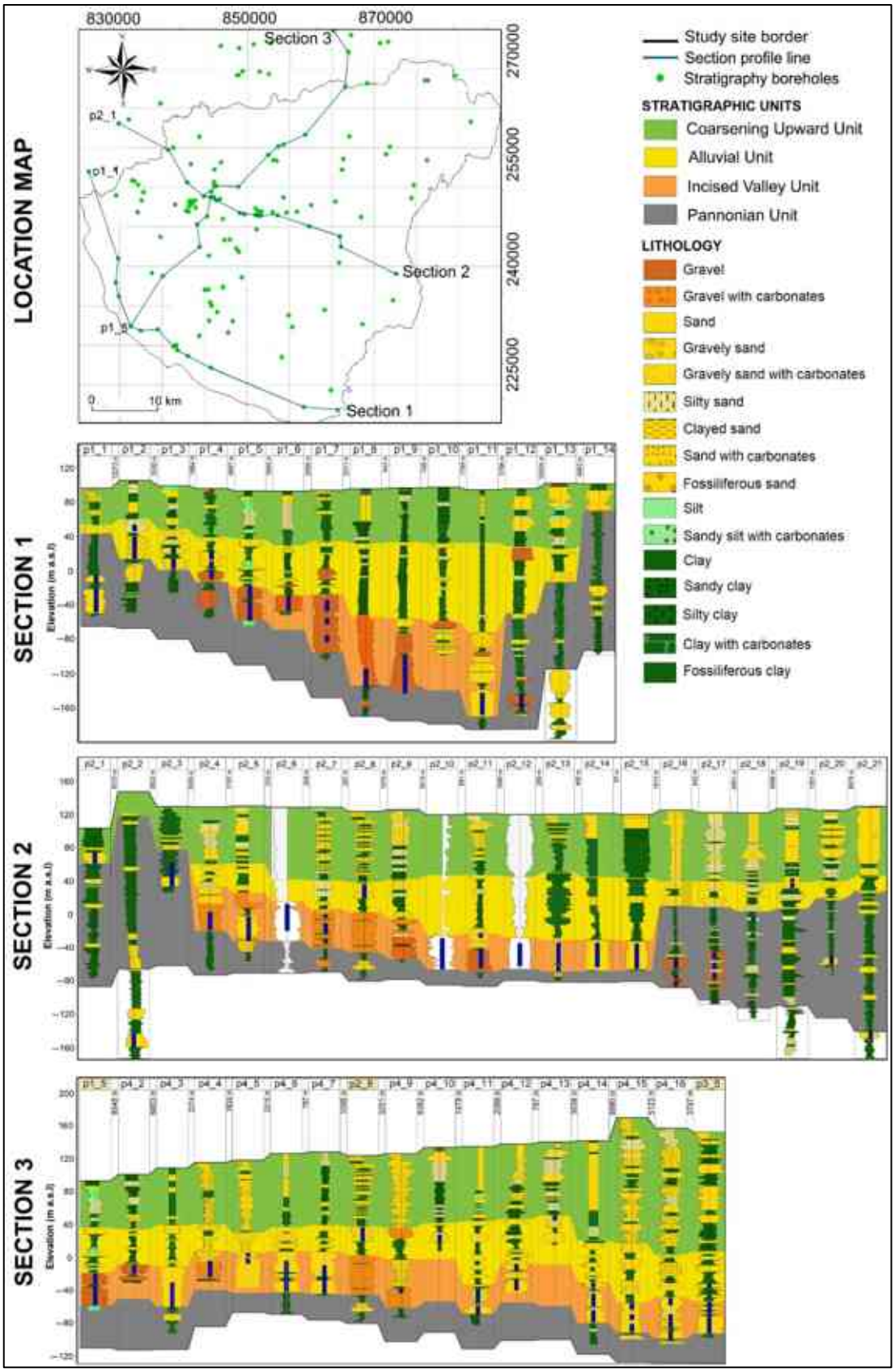

Figure 15. Location map displays stratigraphic data points and cross-section sets: Section 1 (Balmazújváros to Pocsaj), Section 2 (Józsa, Debrecen and Álmosd), and Section 3 (Hajdúszovát, Debrecen, Hajdúsámson and Nyíradony) with logs plotted equidistantly (Flores et al., 2023).

In this investigation were identified three stratigraphic bounding surfaces, four stratigraphic units, and 11 different facies based on the classification of sedimentary cycles, as shown in **Figure 16**.

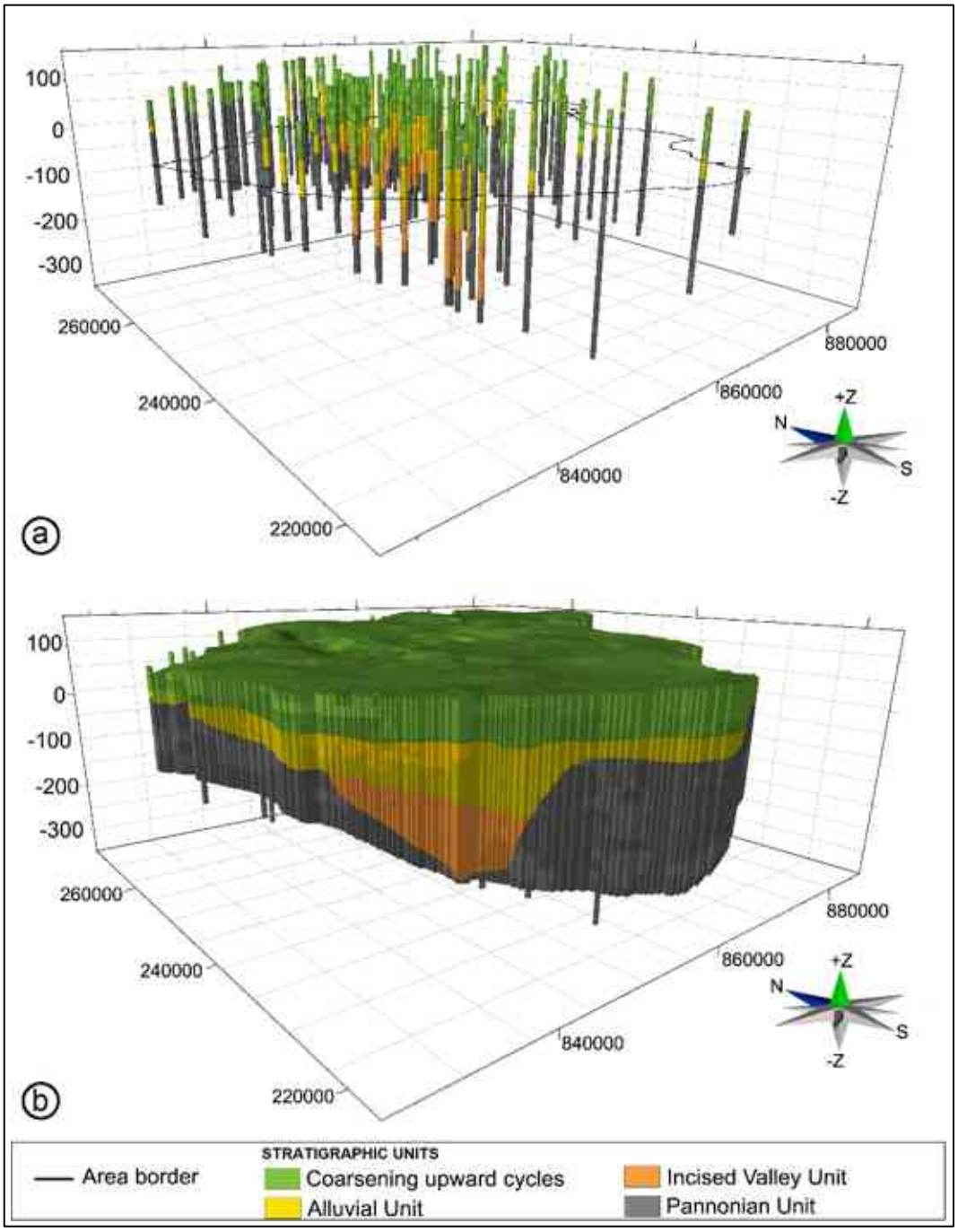

Figure 16. (**a**) Three-dimensional distribution of the lithological investigation points. (**b**) Three-dimensional visualization of the four interpreted stratigraphic units of the Southern-NHGWB (Flores et al., 2023).

The stratigraphic description was developed using available wire-line log records, employing high-resolution log correlation and geometrical convergence interpolation method, which was based on the following criteria: (1) changes in grain size, (2) erosional

basal contact, and (3) sedimentary structures and bedding thickness values (Cateneanu, 2022). The facies 3D model was generated through geostatistical modelling utilizing two stochastic methods (Appendixes D and E) according to the data availability for each stratigraphic unit. The key surfaces delineate the stratigraphic sequences in the well logs. These stratigraphic units are equivalent to system tracts in terms of their homogeneity in internal facies distribution, corresponding to a specific depositional trend (aggradation or degradation). Within these units, the facies exhibit lithological differences, representing individual depositional elements of the sequence.

The IVU-PU surface is a subaerial unconformity that separates the upstream-controlled sequences of the Pannonian (PU) from the Incised Valley (IVU) and Alluvial Unit (ALU), as illustrated in the example in **Figure 17**. Beneath it, one can observe sand or clay depositional elements that laterally connect with the aggradational elements of the Incised Valley Unit. The ALU-IVU surface is analogous to a flooding surface. It separates the high-amalgamation system tract of the Incised Valley Unit from the low-amalgamation system tract of the Alluvial Unit, as illustrated in **Figure 17**.

Below this surface, sand is present, while above it, clay is found. The CUU-ALU surface is analogous to the main flooding surface. It separates the low-amalgamation system tract of the Alluvial Unit from the hybrid upstream and downstream controlled sequences of the Coarsening Upward Unit (CUU). This surface can be identified throughout the study area, with silty material overlying it.

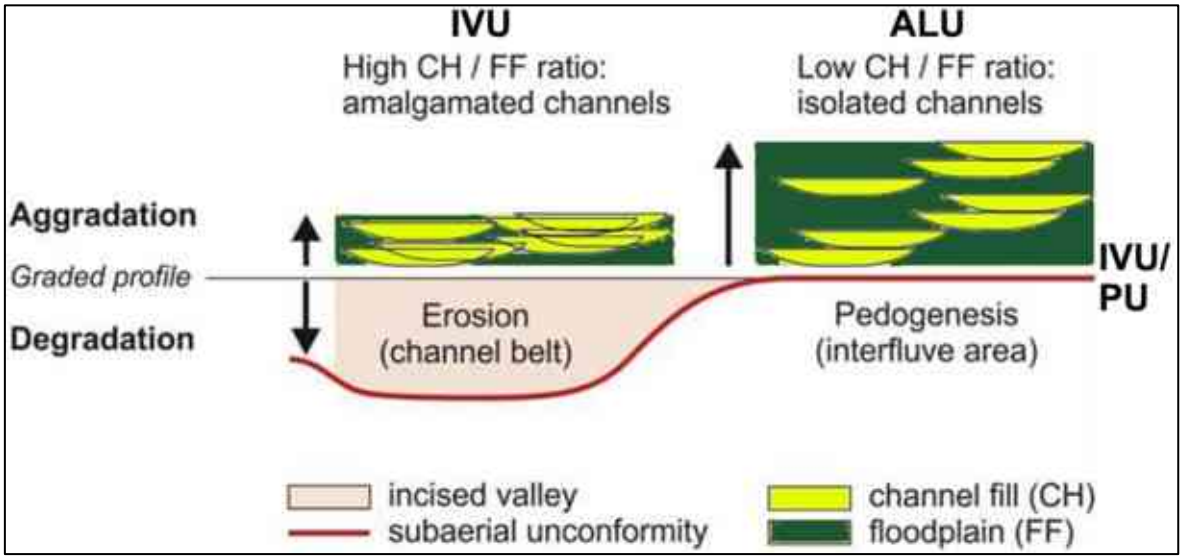

Figure 17. Depositional trends in fluvial settings. The stacking pattern depends on (1) the rate of aggradation; (2) the rate of lateral channel shifting, which is a function of the fluvial style; and (3) the frequency of avulsion (Cateneanu, 2022).

The Pannonian Unit (PU) constitutes the lowermost hydrostratigraphic unit and serves as the basal boundary of the study flow domain. Its modeled thickness varies from 10 m to 140 m, as depicted in **Figure 15** and **Figure 18b**. The top surface of the PU is situated on top of the Zagyva Unit; however, the total depth of the PU is not represented in the interpreted data. The coarse deposits transition from medium sand to silty sand, with a thickness ranging from 10.5 to 36.6 m. The fine deposits exhibit an aggradation character, consisting of mixed silty and clay materials with an average thickness exceeding 40 m. According to the well-logs, the hydrostratigraphic unit comprised 42% coarse-grained materials (sand and silty sand) and 58% fine-grained materials(silty), as shown in **Figure 18** and summarised in **Table 3**.

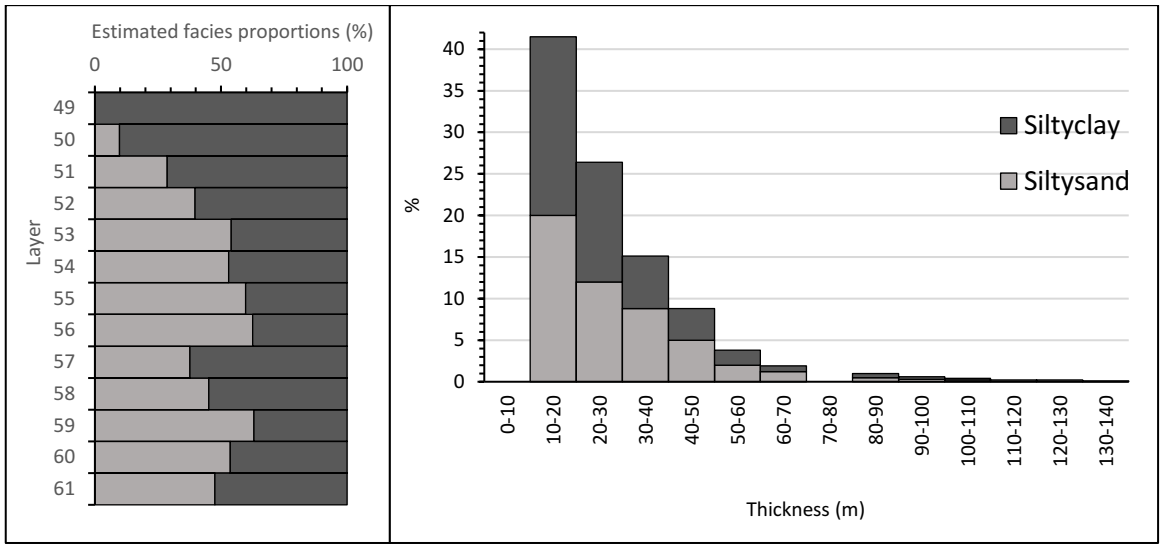

Figure 18. (**a**) Estimate facies proportions, and (**b**) thickness distribution of the Pannonian Unit.

Table 3. Maximum and minimum thickness of each facies in the Pannonian Stratigraphic Unit.

Facies	Min (m)	Mean (m)	Max (m)	Std. (m)	Proportion (%)
Pannonian Sand	10.5	36.6	114.9	22.94	42.33
Pannonian Silt	2	40.	134.9	28.34	57.67

The Incised Valley Unit (IVU) is the major aquifer in the region, exhibiting a thickness ranging from 10 m to 110 m, as illustrated in **Figure 15** and **Figure 19b**. According to the regional correlations (Püspöki *et al.*, 2013, 2016c), t has been dated to the Lower Pleistocene period (~2.5–1.9 million years ago). Isopach data analysis reveals a coarse sand body, approximately 10 to 13 kilometers wide, with an elongated shape oriented in an NNE–SSW direction.

This unit was deposited in a stratigraphic discontinuity overlying the Pannonian sediments. Stratigraphic interpretation results elucidate that the coarse sediments within this unit fill an incised valley that eroded the Pannonian Unit (PU). The IVU is characterized by

channel deposits of vertically stacked shapes, which are typical of channel complexes associated with anastomosing watercourses or translational meander development (Bridge, 2003; Miall, 2014). Well-logs indicate that the IVU is predominantly composed of coarse-grained sediments, with coarse sand and gravel making up 98% of its composition. Fine-grained sediments, such as clay, are nearly absent, as demonstrated in **Figure 19** and summarised in **Table 4**.

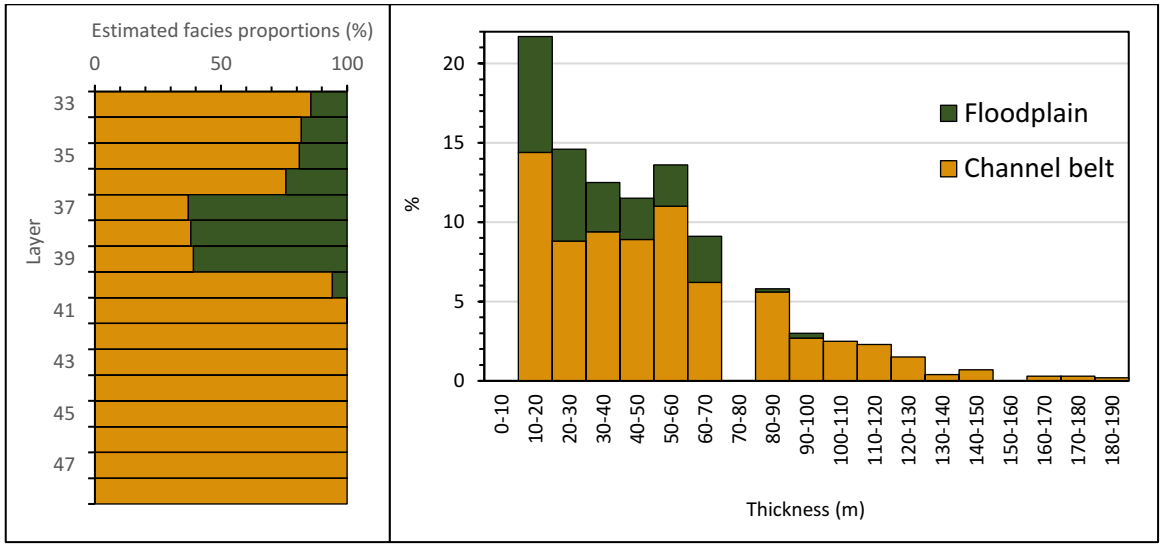

Figure 19. (**a**) Estimate facies proportions, and (**b**) thickness of the Incised Valley Unit.

Table 4. Maximum and minimum thickness of each facies in the Incised Valley Stratigraphic Unit.

Facies	Min (m)	Mean (m)	Max (m)	Std. (m)	Proportion (%)
Channel belt	8.3	40.2	94.4	15.67	98.4
Floodplain	7	7	7	0	1.6

The Alluvial Unit (AU) is a regional non-continuous extended semi-permeable aquifer with a thickness of 15 m to 140 m as shown in **Figure 15** and **Figure 20**. According to the regional correlations (Püspöki et al., 2013, 2016c), its age is Lower Pleistocene (~1.9–1.2 Ma). The boundary surface between the AU and the IVU was consistently picked in the logs at the first occurrence of several-meters-thick overbank deposits above the relatively flat top of the multiple-channel complex series as seen in **Figure 15**.

The AU is characterized by a general occurrence of overbank deposits that make up 47% of the unit volume. The single channel complexes, wherein the sand bodies exhibit fining upward porosity characteristic feature of meandering systems, account for up to 53% of the sediments as demonstrated in **Figure 20b** and **Table 5**.

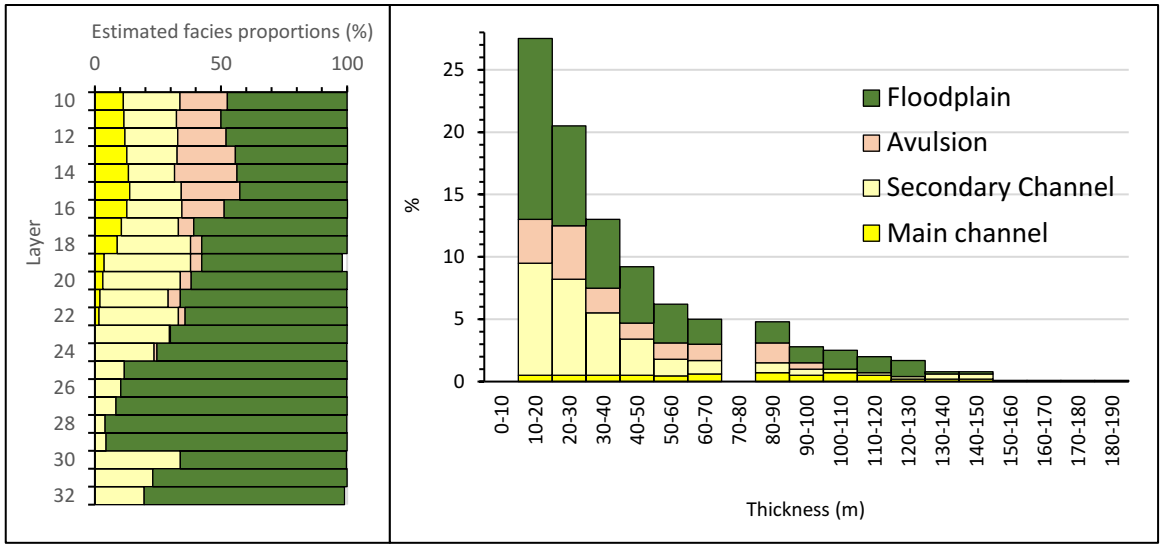

Figure 20. (**a**) Estimate facies proportions, and (**b**) thickness distribution of the Alluvial Unit.

Table 5. Maximum and minimum thickness of each facies in the Aluvial Unit.

Facies	Min (m)	Mean (m)	Max (m)	Std. (m)	Proportion (%)
Channel belt	0	19.3	46.3	13.95	16.67
Floodplain	0.2	12.6	98	13.7	47.04
Avulsion cycle	5	11.3	31.7	6.43	13.92
Secondary channel	0	9.9	34.4	4.99	21.80

The Coarsening Upward Unit (CUU) is an extensive hydrostratigraphic unit of thickness from 10 m up to 70 m and contains relatively highly permeable sand lenses as shown in **Figure 15**. According to the regional correlations (Püspöki et al., 2013, 2016c), its base corresponds to the Mid Pleistocene Transition (~1.2 Ma) and extends until today; however, perhaps with a few high-frequency unconformities. The findings of this research showed that 42.6% of the sediments are reported as coarse-grained (sand and fine sand) and 57.4% are described as fine-grained sediments (silt and clay) as demonstrated in **Figure 21** and **Table 6**. The CUU is the unconfined semi-permeable top aquifer layer of the system.

The above findings indicated that the Southern-NHGWB is a regional cross-formational porous aquifer system, extending from the Pannonian to the quaternary land surface sediments (Appendix F). The lithologic and stratigraphic considerations suggested that the PU, AU, and CUU differ from the IVU due to the general occurrence of fine-grained sediments. The vertically stacked character of the logs along the multiple channel complexes in the IVU implies low anisotropy and a high rate of facies continuity (Miall, 2006). Conversely, the overlying and underlying hydrostratigraphic units (**Figure 16**) are characterized by higher anisotropy and limited continuity of thinner coarse-sediment bodies, the fining upward stacked occurrence, which is caused by inclined heterolytic complexes consisting of couplets of clay intercalations and fine sand layers.

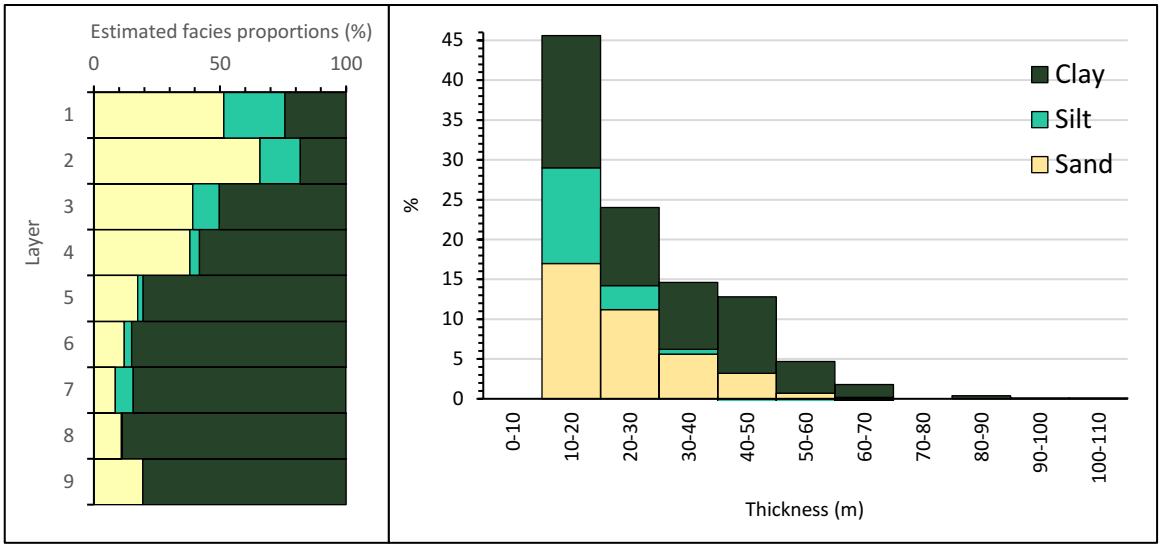

Figure 21. (**a**) Estimate facies proportions, and (**b**) their thickness distribution of the Coarsening Upward Sequences.

Table 6. Maximum and minimum thickness of each facies in the Coarsening Upward Sequences.

Facie	Min (m)	Mean (m)	Max (m)	Std. (m)	Proportion (%)
Sand	12.3	28.3	75	14.18	42.6
Silt	4.9	14.4	45	5.83	6.25
Clay	0.4	23.5	101.4	16.6	51.15

These results reveal a significant geological heterogeneity of particular interest when models are expanded from regional to local scales. It is worth noting that the stratigraphic discontinuity between the IVU and PU can be mistaken for other types of linear mathematical unconformities, such as faults (Szanyi, 2004). In line with Szany local model, the vertical compartmentalization of the Quaternary aquifer system was confirmed, occurring not only at the local scale but also at the regional scale, diverging from the representation of the Quaternary aquifer as a single hydrostratigraphic unit in the region, as was proposed by Marton (1982). Naturally, this study has limitations, including the horizontal uncertainty associated with the well-log correlation technique. However, it is important to emphasize that the evidence presented here relies on the correlation of the observed geometry with the patterns of hydrogeological variables analyzed below.

3.1.2 Horizontal hydraulic conductivity of sand bodies

The estimation of hydraulic conductivity and specific capacity was performed using data from 300 wells, classified based on the location of their screens in the sand bodies of the hydrostratigraphic units. Specifically, there were 70 wells screened in the CUU, 45 in the AU, 105 in the IVU, and 80 in the PU. The range of the estimated horizontal hydraulic conductivity (k_h) values for the coarse-grained lithologies in the study domain ranged from

0.1 to 43 m/d, as shown in **Figure 22**. Wells that screened the IVU had an average value of 11 m/d and exhibited a nearly normal distribution of the data. On the other hand, the PU, AU, and CUU exhibited average values of 4.6 m/d, 4.1 m/d, and 3.2 m/d, respectively. The data for all three semi-permeable aquifers had an unimodal right-skewed distribution.

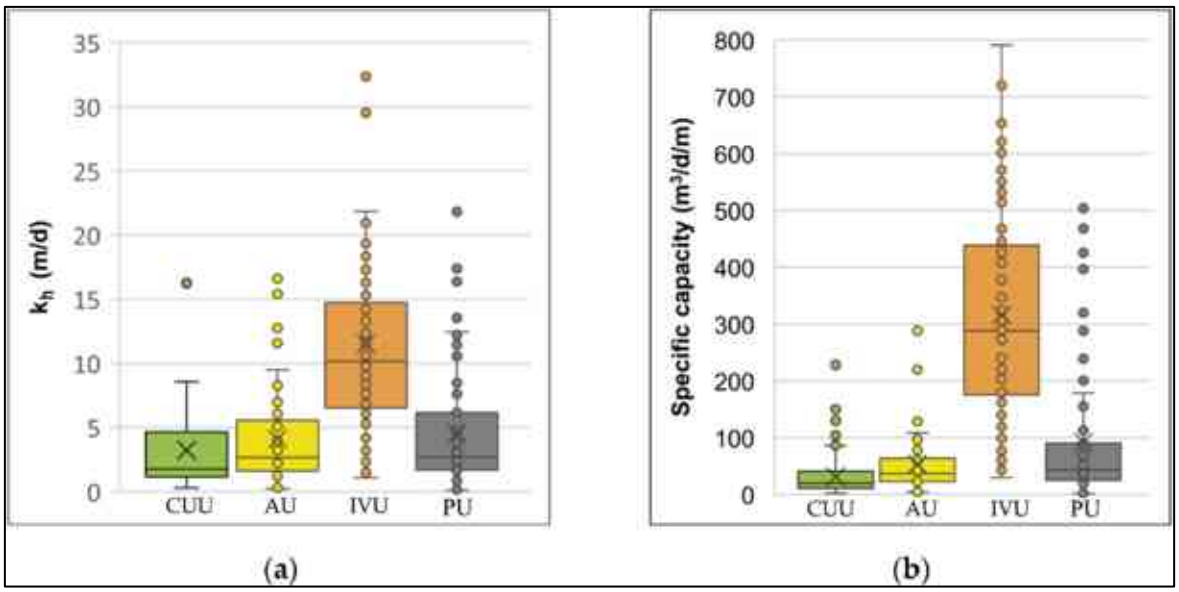

Figure 22. Range and distribution of (**a**) horizontal hydraulic conductivity (k_h) (**b**) and specific capacity (SC) for the screened sand bodies of the stratigraphic unit. The box plot presents the minimum, maximum, median, mean and quartile ranges for each hydrostratigraphic unit sand body (Flores et al., 2023).

The Logan's estimation of the horizontal hydraulic conductivity (k_h) reveals that the sand bodies of the IVU are higher flux conductive than the surrounding hydrostratigraphic units, and the normal distribution of the dataset aligned with the previous observation related to sediment homogeneity, porosity, and grain size in the IVU. Examining the spatial distribution pattern of the apparent hydraulic conductivity at the main aquifer depth corresponds with the geometry of the main aquifer (**Figure 23**).

Additionally, the proposed geometry aligns with the research conducted by Marton and Szany (2000) (**Figure 2**,**1993**) in Eastern Hungary regarding aquifer transmissivity at this depth. These findings provide strong evidence that the defined IVU functions as the main aquifer in the system, characterized by higher hydraulic parameters compared to the remaining semipermeable aquifers.

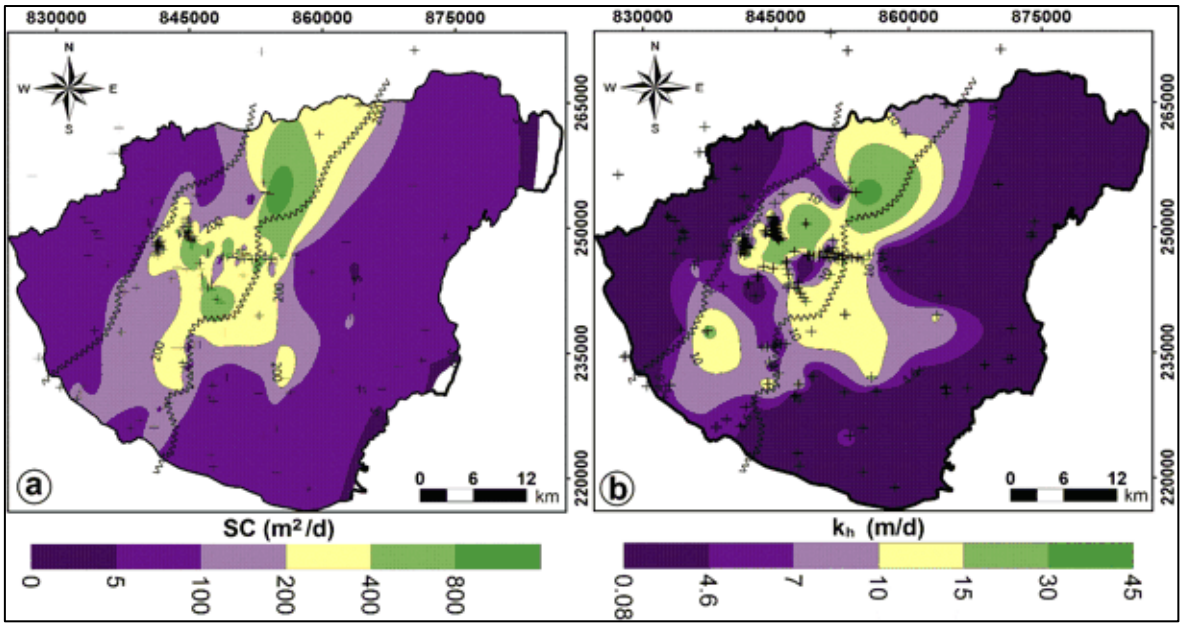

Figure 23. Range and distribution of (**a**) horizontal hydraulic conductivity (k_h) (**b**) and specific capacity (SC) for the screened sand bodies of the stratigraphic unit. The box plot presents the minimum, maximum, median, mean and quartile ranges for each hydrostratigraphic unit sand body (Flores et al., 2023).

3.1.3 Hydrodynamic conditions

The dynamic pressure (p_{dyn}) was calculated using hydraulic head data from 366 wells. The samples were categorized based on the location of their screens, with 115 wells screened in the CUU, 50 in the AU, 111 in the IVU, and 90 in the PU. The distribution and skewness of the data are presented in **Figure 24a**, while the pressure–depth profile is illustrated in **Figure 24b**. The hydrostatic pressure (p_{st}), represented by an average pressure gradient of $\gamma_{st} \approx 9.81$ kPa/m, it served as the reference, reflecting the water table and the upper hydraulic limit of the system.

The average dynamic pressure gradient (γ_{dyn}) was calculated from the linear trend of the dynamic pressure distribution (p_{dyn}) in each hydrostratigraphic unit (**Figure 24b**). The average dynamic pressure gradient (γ_{dyn}) exhibited values of 9.74 kPa/m for the CUU, 8.37 kPa/m for the AU, 6.06 kPa/m for the IVU, and 7.43 kPa/m for the PU. When comparing the results with the hydrostatic pressure gradient ($\gamma_{st} \approx 9.81$ kPa/m), it became evident that the aquifer system generally experienced under-hydrostatic pressure conditions ($\gamma_{st} < \gamma_{dyn}$). These findings followed the reported results of Marton (1982), and Tóth and Almási (2001) referring to the general hydraulic conditions of the Nyírség Region.

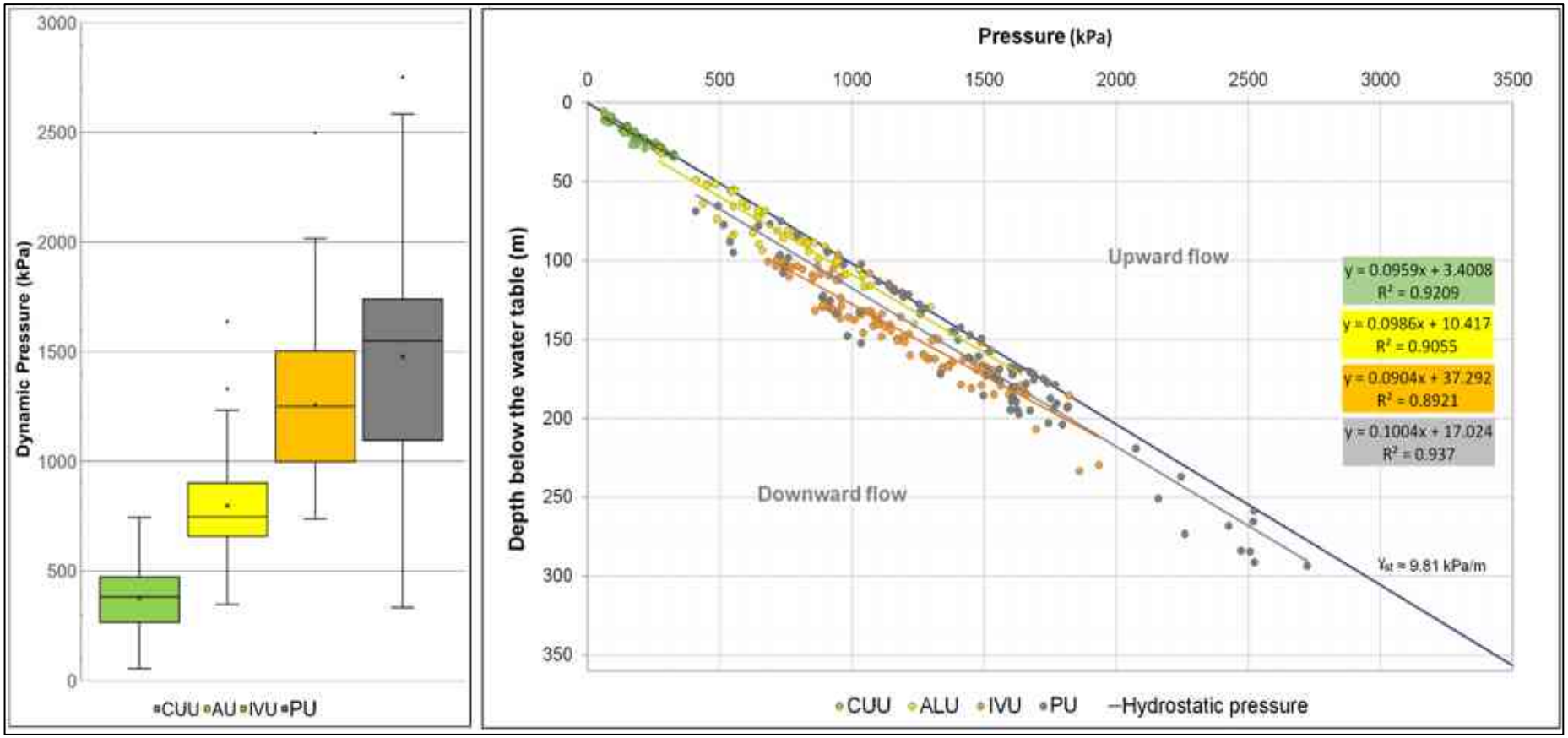

Figure 24. Range and distribution of dynamic pressure (p_{dyn}) for each stratigraphic unit in the study area. The box plot presents the minimum, maximum, median, mean and quartile ranges. (**b**) Pressure-depth profile. The plotting uses hydrostatic pressure as a reference. The hydrostatic pressure gradient (γ_{st}) is 9.81 kPa/m.

However, it was possible to identify that each hydrostratigraphic unit exhibited upward flow as well as horizontal flow directions in specific locations. Therefore, dynamic pressure increments (Δp) maps (**Figure 25b and 25d**) provide a comprehensive analysis of pressure variations between layers. These figures accurately illustrate the spatial locations of the downward flow regime ($-\Delta p$), representing recharge areas, and the upward flow regime ($+\Delta p$), representing discharge areas within the hydrostratigraphic units. The 0 kPa/m demarcates the boundary between the two flow regimes.

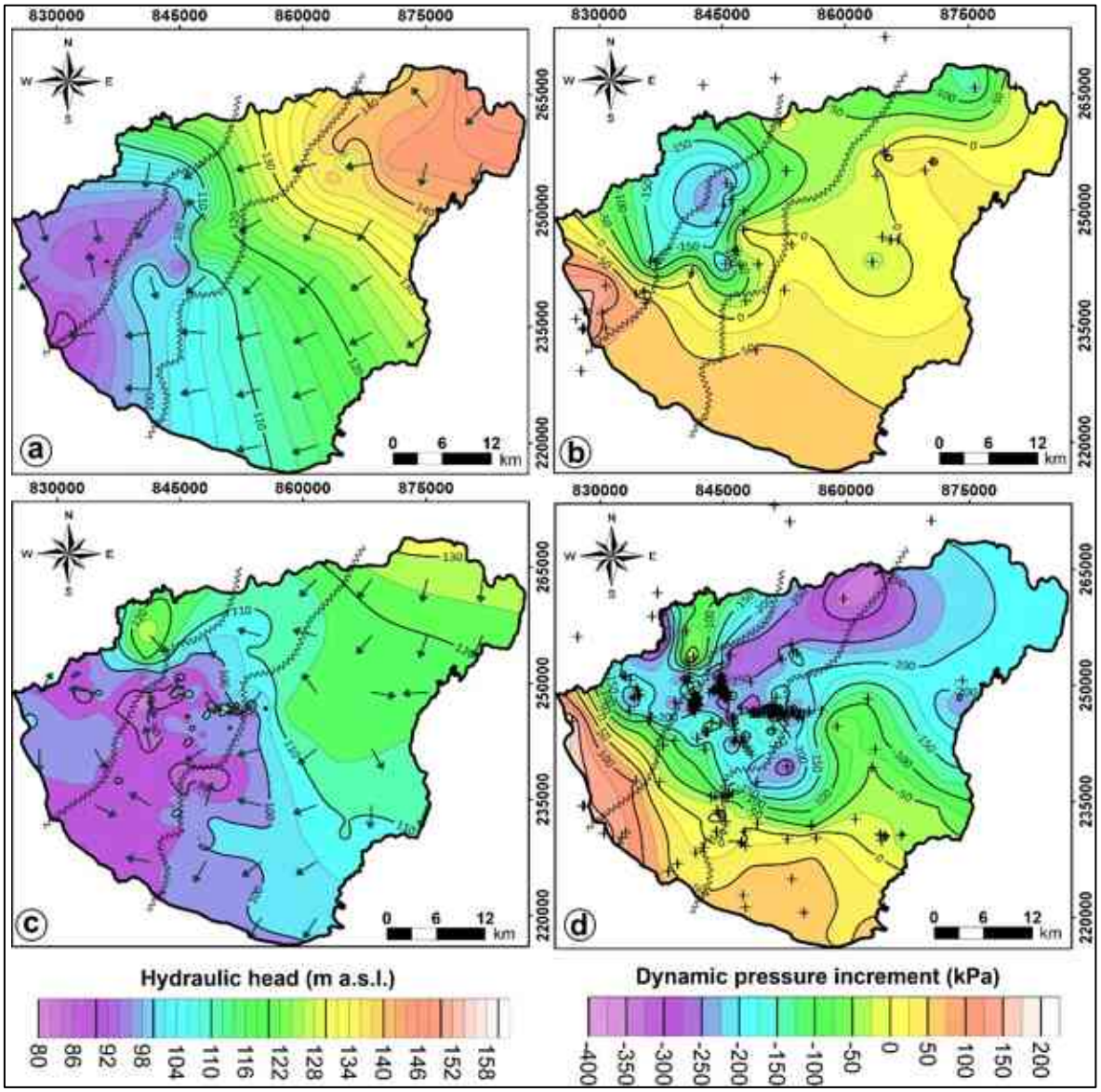

Figure 25. (**a**) Piezometric map of the AU. (**b**) Dynamic pressure increments map of the AU. (**c**) Piezometric map of the IVU-PU. (**d**) Dynamic pressure increments map of the IVU- PU. The arrows show the flow direction, and the points are the distribution of the total head measurement. The black undulated line represents the contact between IVU and PU (Flores et al., 2023).

The high production rates of the IVU, reported on the specific capacity data, have noticeable effects on the pressure condition of the system. It is evident by its lower average

dynamic pressure gradient ($\gamma_{dyn} = 6.06$ kPa/m). Additionally, the dynamic pressure maps indicated that these effects extend vertically up to the upper hydrostratigraphic unit (**Figure 25b**) and laterally into the PU (**Figure 25d**). There was found evidence of a hydraulic window in the central part of the study site, at the water extraction activities of the Debrecen Waterworks Site II.

The finding of hydraulic interactions between layers could have a significant effect on the chemical characteristics of the groundwater of the aquifer system with some differences and similarities. Three potential maps were generated to analyze the horizontal water flow pattern within the hydrostratigraphic units. The potential map of the CUU (**Figure 26**). illustrates the upper hydraulic boundary of the groundwater body in the study area. Higher hydraulic heads were observed between Nyírlugos and Nyírgelse in the north-eastern part of the region, while lower hydraulic heads were observed in the southwest around Hajdúszoboszló.

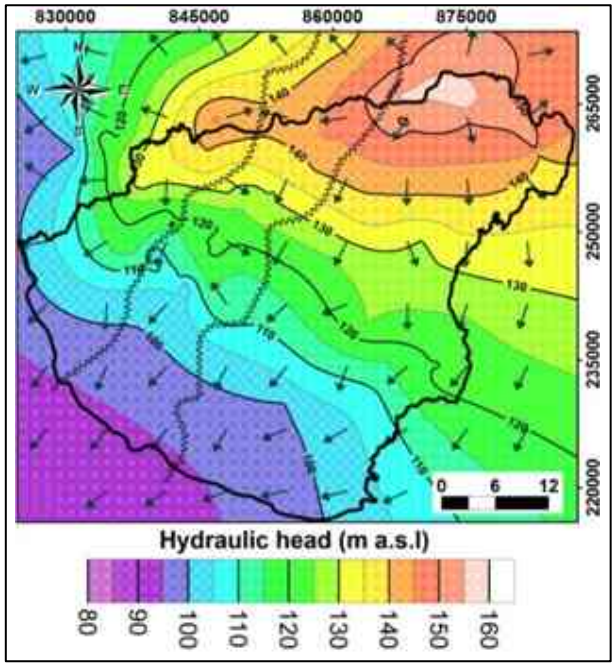

Figure 26. Hydraulic head map of the Coarsening Upward Unit.

The results reveal a regional flow direction from northeast to southwest. Overall, these findings followed the findings reported by the research of Marton (1982), and Tóth and Almasi (2001). In the potential map of the AU shown in **Figure 25a**, higher hydraulic heads were observed between Bocskaikert and Penészlek, passing through Nyíradony in the northeastern part of the region. Conversely, lower hydraulic heads were observed at two specific locations. The first location is in the west-central region, where the Debrecen Waterwork Sites operate, and the second location is in a depression between Hajdúszoboszló and Hajdúsovát.

Based on the stratigraphic interpretation presented in Appendix B, the PU and IVU exhibit similar depths at the P_{dyn} measurement points. Additionally, the pressure–depth plot in **Figure 24**, along with the dynamic pressure increment map (**Figure 25d**), provides evidence of the lateral hydraulic connection between the PU and IVU. Consequently, a unified piezometric map was generated for both hydrostratigraphic units. Higher hydraulic head values were observed in the northwest, near Józsa, while lower values were sampled in the west-central part, where the city of Debrecen and its waterworks sites are situated (**Figure 25b**). It is noteworthy that water production in Debrecen impacts the distribution of hydraulic heads. The observed pattern suggests a greater influence along the NE–SW axis compared to the NW–SE axis, indicating higher Darcy velocities within the IVU.

The hydraulic head maps plotted for the hydrostratigraphic units in the Southern NHGWB exhibit characteristics of a gravity-driven flow regime in a regionally unconfined system (Marton, 1982; Tóth and Almási, 2001). The flow regime shows a downward flow direction in the hilly area of the northeast and an upward flow direction in the lowlands near the East Main Canal. However, the high production rates from the IVU create a local hydraulic disturbance in the regional head distribution. This disturbance influences the hydraulic head distribution of the AU, resulting in a radial depression cone geometry (**Figure 25a**).

On the other hand, the head distribution of the Incised Valley Unit and Pannonian Unit is disrupted by a pronounced ellipsoidal depression cone geometry (**Figure 25b**). The regional horizontal flow direction presented in this research aligns with the one depicted by Marton; however, the vertical interpretation of the flow is presented as conforming to the newly proposed hydrostratigraphic framework of the conceptual model.

3.1.4 Geochemical model

Water samples were collected from 118 wells screening the Pannonian and Incised Valley Units. The location of the screens ranges from 67 m a.s.l. to 250 m b.s.l. (**Figure 27**). The sampling points are spatially distributed to cover the entire study area. The measured physical and chemical parameters include hydrogen potential (pH), temperature (T), electric conductivity (EC), total dissolved solids (TDS), and Na^+, Ca^{2+}, Mg^{2+}, K^+, Cl^-, SO_4^{2-}, HCO_3^- CO_3, and NO_3 ions. The concentration is expressed in mg/l. The minimum, maximum, average, and standard deviation values are reported in **Table 7**. It was noted from the average value that the cations were arranged in this order $Ca^{2+} > Na^+ > Mg^{2+} > K^+$ and the anions followed this order $HCO_3^- > SO_4^{2-} > Cl^- > NO_3$.

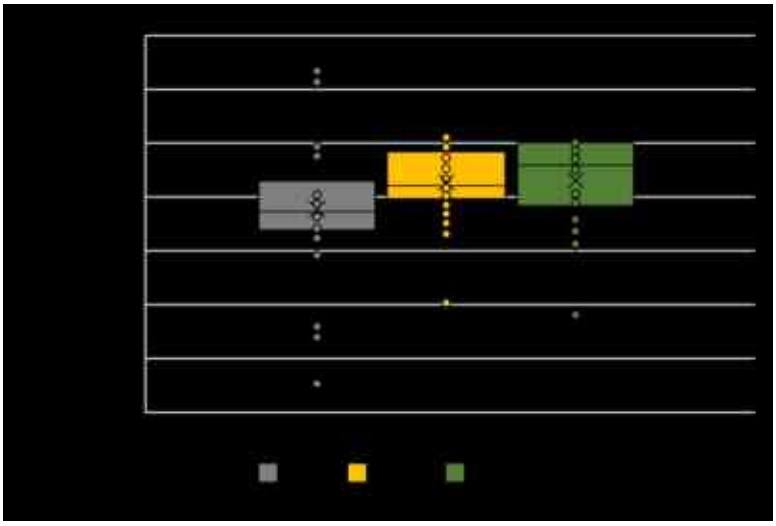

Figure 27. Box plot of the location of the screens of the sampled wells. The wells are separated into three groups: screening the Pannonian Unit (PU), screening the Incised Valley Unit (IVU), and screening both units at the time (MIX).

The physicochemical parameters were used to detect the geochemical evolution, water type, and geochemical modelling of the groundwater along the flow path, to determine the difference in the chemistry of water inside and outside the IVU. The reported results only refer to the change in water chemistry and water type through the flow path due to water-rock interaction, with limitation on the definition of water origin as was previously done by Marton (1982), illustrated in **Figure 1**.

Table 7. Summary statistics of the geochemical database.

	pH	T (°C)	Ec (uS/cm)	Na^+	K^+	Mg^{2+}	Ca^{2+}	Cl^-	SO_4^{2-}	HCO_3^-	CO_3^-	NO_3^-	TDS
Max	8.8	24.6	767.0	193.0	6.5	29.8	106.3	31.4	55.0	570.0	0.0	90.4	1304.0
Min	7.2	10.7	430.0	16.0	0.5	0.1	2.9	2.0	0.0	320.0	0.0	0.0	290.0
Mean	7.7	18.2	576.9	45.5	2.2	20.1	75.0	7.7	10.7	439.8	0.0	1.2	614.5
Media	7.6	18.0	566.5	33.4	2.2	21.4	81.1	7.0	8.6	440.0	0.0	0.0	604.0
St. Dev.	0.3	2.3	56.5	33.8	1.0	6.1	24.4	4.0	9.0	41.9	0.0	8.5	99.2

The collected water samples were classified into three hydrogeochemical facies, as shown in **Figure 28a**. Na-HCO_3 facies (Type 1) represent the samples outside of the Incised Valley, while the Ca-Mg-HCO_3 facies (Type 2) include the water samples of the IVU. This apparent spatial differentiation of facies Type 1 and 2 indicated the effects of valley-fill hydraulic performance, identified based on the hydrogeochemical facies of the enclosed pore water. The Na-HCO_3 facies were associated with advanced silicate weathering or ion exchange in the pore system of the Pannonian formations, while the Ca-Mg-HCO_3 character can be attributed to carbonate weathering or reverse ion exchange. A mixed Na-Ca-HCO_3 facies (Type 3) was observed in three samples; however, only one of them is located close

to the bounding surface of the incised valley, approximately 2.5 km northwest of Hajdúbagos. These facies indicated the mixing of two facies and suggested variable vertical flow intensity.

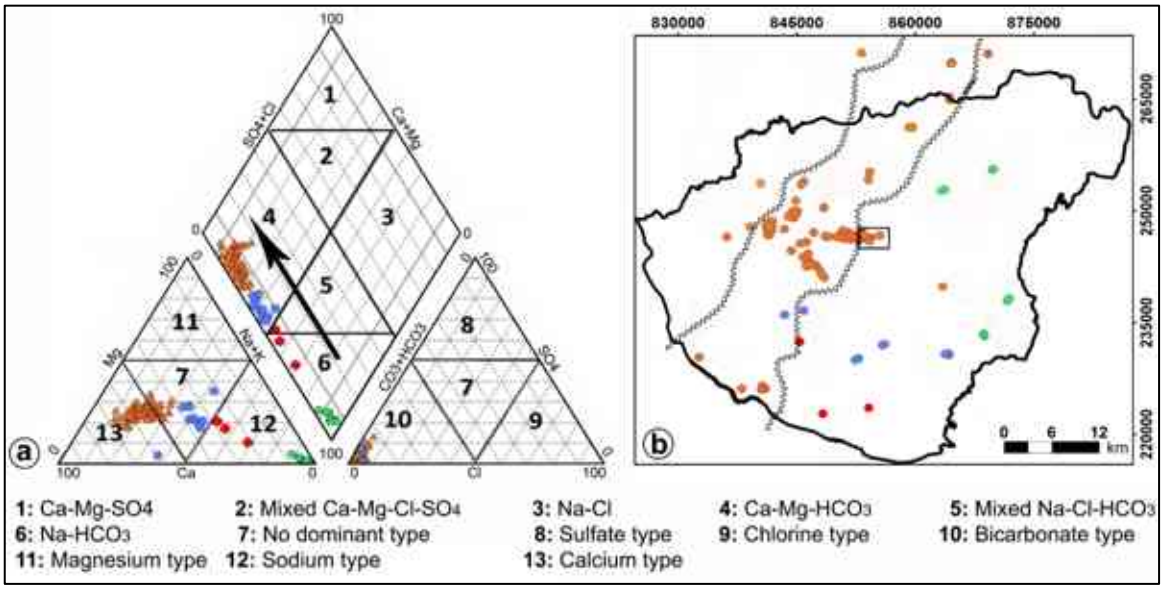

Figure 28. (**a**) Piper diagram and water type of the groundwater changing with flow direction. (**b**) Spatial distribution of the geochemical sampling points colored according to the water type to which it belongs (Flores *et al.*, 2023).

Exceptions included four samples showing Ca-Mg-HCO_3 facies in the center of the study area near the lateral bounding surface of the incised valley, but out of it (the rectangle in **Figure 28b**). This could be explained as a result of the over-exploitation of water by Debrecen Waterworks activities that shift the water mixing zone into the main aquifer since the hydraulic conductivity of the IVU is higher than the surrounding units, and demonstrated before by the hydraulic conditions of the system (**Figure 25**). Another exception was located in the southern part of the study area between Hajdúbagos and Létavértes. It was represented by six samples, the groundwater shows Ca-Mg-HCO_3 facies due to the local effect of the higher carbonate content of sediments in this region, as reported in the lithological logs.

The geochemical model was performed using PHREEQC. The saturation index (SI) of calcite, aragonite, dolomite, halite, gypsum and anhydrite minerals in the groundwater is calculated, and the analysis aims to detect the change in the saturation index inside and outside the incised valley along the flow paths. The minimum and maximum value of the SI for the minerals, shown in **Figure 29**, indicated that all the water samples were undersaturated concerning halite, gypsum, and anhydrite, showing the ability of water to dissolve more from these minerals all over the model domain, which is conversely for aragonite, calcite and dolomite.

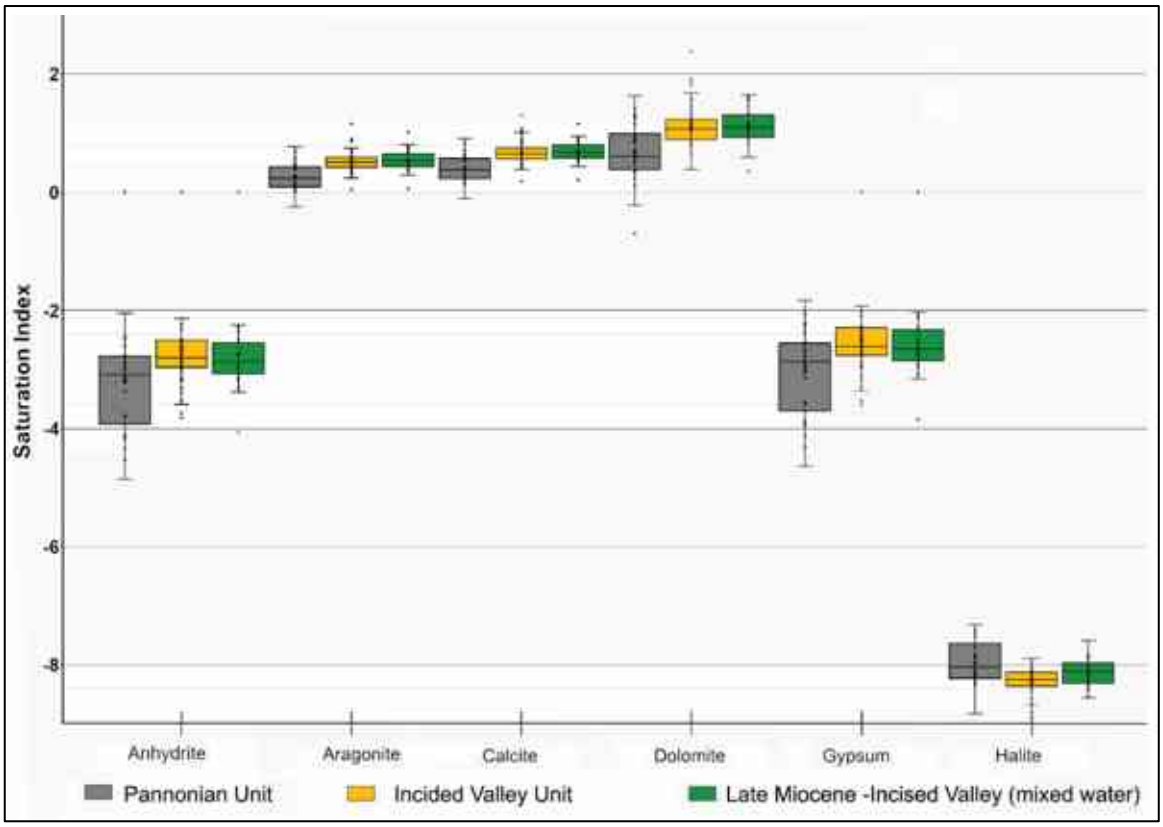

Figure 29. Range and distribution of mineral Saturation Index in the water samples from the Pannonian Unit, Incised Valley Unit, and Pannonian-Incised Valley Unit. The box plot presents the minimum, maximum, median and quartile ranges for each considered mineral.

The spatial distribution of saturation index (SI) values of calcite and dolomite (**Figure 30**) also revealed a reliable differentiation inside and outside the main aquifer. The water samples within the IVU were oversaturated regarding calcite and dolomite, with values that range from 0.5 to 1.2 and from 0.7 to 2.1, respectively. This suggested the ability of water to precipitate these minerals within the available pore space, decreasing the HCO_3 ion due to the precipitation of carbonate minerals, and increasing the $Ca^{2+} + Mg^{2+}$. Outside the valley, in the Pannonian Unit, the SI values concerning calcite and dolomite are lower, ranging from −0.2 to 0.5 and from −0.7 to 0.7, respectively. The negative value of the SI in the majority of the water samples from the PU indicated the ability of water to dissolve more calcite and dolomite approaching the valley; it begins to reach saturation with these minerals. The undersaturation in the PU may be the result of the non-carbonate origin of the waters or the advanced cation exchange. The outlying saturation index (SI) values outside the IVU between Hajdúbagos and Létavértes, showing high oversaturation, can be attributed to the higher carbonate content of the matrix.

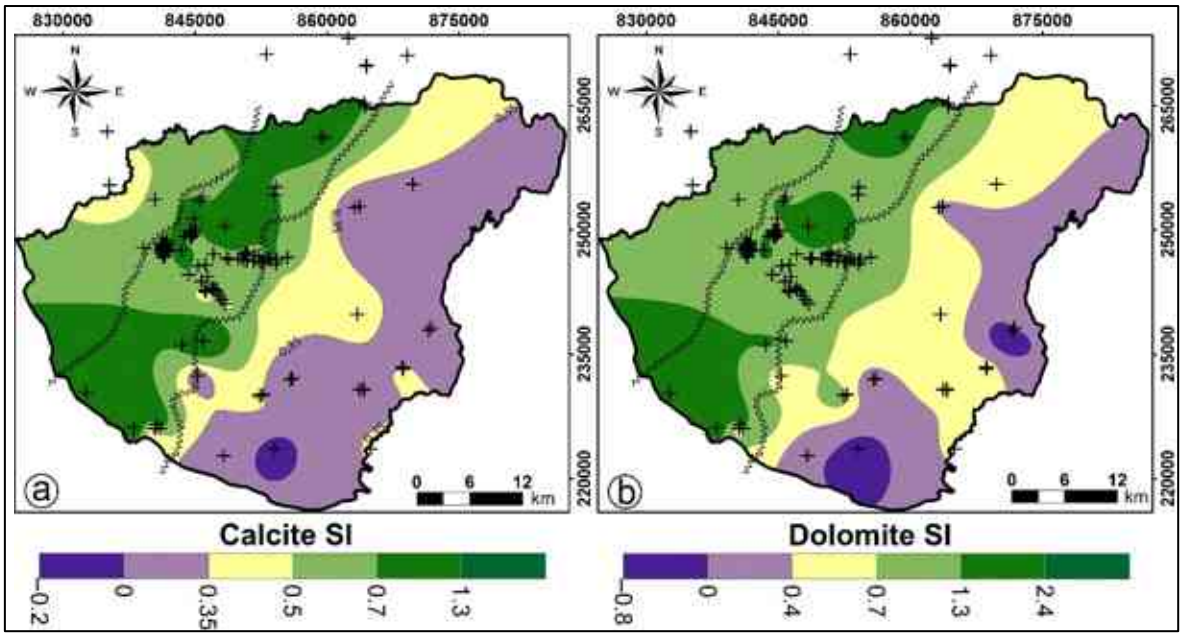

Figure 30. (**a**) Spatial correlation of Calcite Saturation Index. (**b**) Spatial correlation of Dolomite Saturation Index (Flores *et al.*, 2023).

However, since the carbonate content of the valley-fill sediments does not differ from or is even lower than that of the pre-Quaternary formations, the most probable sources of dissolved carbonate in the groundwater are the bio-carbonate minerals (such as gastropod shells, rhizoids and rhizoliths) present in the Quaternary layers between central Nyírség (Püspöki et al., 2013), which is the recharge area of the system. The direct recharge of the semi-confined aquifer has the potential to increase the saturation index (SI) from under-saturation to neutrality or even oversaturation when considering the joint interpretation of the flow pattern shown in **Figure 25**.

Spearman's correlation index was used to analyze the geochemical associations of the ions in the water samples. The results corroborated the previously presented findings concerning the geochemical reactions occurring within the hydrostratigraphic units due to water-rock interactions. **Table 8** presents the correlation index calculated from all the analyzed samples as a single group. The results revealed a strong-to-intermediate positive correlation of 0.74 between Ca^{2+} and Mg^{2+}, 0.6 between Ca^{2+} and HCO_3^-, 0.6 between HCO_3^- and EC, and 0.5 between Cl^- and EC. These strong-to-intermediate correlations indicate the significant contribution of these elements to mineralization processes and groundwater salinity (**Figure 31a**).

The samples are analyzed in three separate groups, classified based on the screen location of the well from where the sample was collected. For water samples taken from wells screening the Pannonian Unit (PU), the Spearman's correlation index reveals a strong-

to-intermediate positive correlation of 0.82 between Ca^{2+} and Mg^{2+}, 0.72 between Ca^{2+} and K^{+}, 0.72 between Mg^{2+} and K^{+}, and 0.66 between K^{+} and HCO_3^{-}. The strong correlation index is 0.6 between HCO_3^{-} and EC (**Figure 31b**). The strong correlation between Ca^{2+} and Mg^{2+}, and lower correlation with EC, suggest that the source of these ions are clay minerals such as montmorillonite ($(Na,Ca)_{0.3}(Al,Mg)_2Si_4O_{10}(OH)_2 \cdot nH_2O$), which hold the three ions in its chemical composition. The strong correlation of K^{+} with Ca^{2+}, Mg^{2+} and HCO_3^{-} supports this observation.

Table 8. Correlation matrix of the ions of the water samples used for geochemical analysis.

Parameters	Ec (uS/cm)	Na^+	K^+	Mg^{2+}	Ca^{2+}	Cl^-	SO_4^{2-}	HCO_3^-
Ec (uS/cm)	1	-0.01	0.05	0.21	0.36	0.5	0.27	0.6
Na^+		1	-0.38	-0.82	-0.88	-0.04	-0.17	-0.3
K^+			1	0.31	0.37	-0.01	0.02	0.13
Mg^{2+}				1	0.74	0.07	0.22	0.44
Ca^{2+}					1	0.3	0.27	0.6
Cl^-						1	0.25	0.34
SO_4^{2-}							1	0.16
HCO_3^-								1

Table 9. Correlation matrix of the major ions of the Pannonian Unit water samples.

Parameters	Ec (uS/cm)	Na^+	K^+	Mg^{2+}	Ca^{2+}	Cl^-	SO_4^{2-}	HCO_3^-
Ec (uS/cm)	1	-0.11	0.27	0.27	0.42	0.33	0.01	0.60
Na^+		1	-0.76	-0.86	-0.87	0.19	-0.49	-0.37
K^+			1	0.72	0.72	-0.14	0.40	0.66
Mg^{2+}				1	0.82	-0.13	0.37	0.49
Ca^{2+}					1	-0.02	0.47	0.47
Cl^-						1	0.34	0.09
SO_4^{2-}							1	0.13
HCO_3^-								1

Table 10. Correlation matrix of the major ions of the Incised Valley Unit water samples.

Parameters	Ec (uS/cm)	Na^+	K^+	Mg^{2+}	Ca^{2+}	Cl^-	SO_4^{2-}	HCO_3^-
Ec (uS/cm)	1	-0.22	-0.03	0.35	0.74	0.37	0.22	0.72
Na^+		1	0.36	0.11	-0.62	-0.17	-0.02	-0.35
K^+			1	-0.07	-0.23	0.11	0.09	-0.15
Mg^{2+}				1	0.25	0.23	0.09	0.39
Ca^{2+}					1	0.33	0.15	0.80
Cl^-						1	0.14	0.53
SO_4^{2-}							1	0.17
HCO_3^-								1

Table 11. Correlation matrix of the major ions of the Pannonian Unit- Incised Valley Unit (Mixed) water samples.

Parameters	Ec (uS/cm)	Na^+	K^+	Mg^{2+}	Ca^{2+}	Cl^-	SO_4^{2-}	HCO_3^-
Ec (uS/cm)	1	-0.05	0.08	0.34	0.65	0.65	0.14	0.64
Na^+		1	0.05	-0.27	-0.43	-0.14	-0.36	-0.35
K^+			1	0.28	0.13	0.27	0.04	0.16
Mg^{2+}				1	0.19	0.28	0.13	0.46
Ca^{2+}					1	0.72	0.20	0.81
Cl^-						1	0.06	0.72
SO_4^{2-}							1	0.20
HCO_3^-								1

Note(s): Concentration of the ions is measured in mg/l.

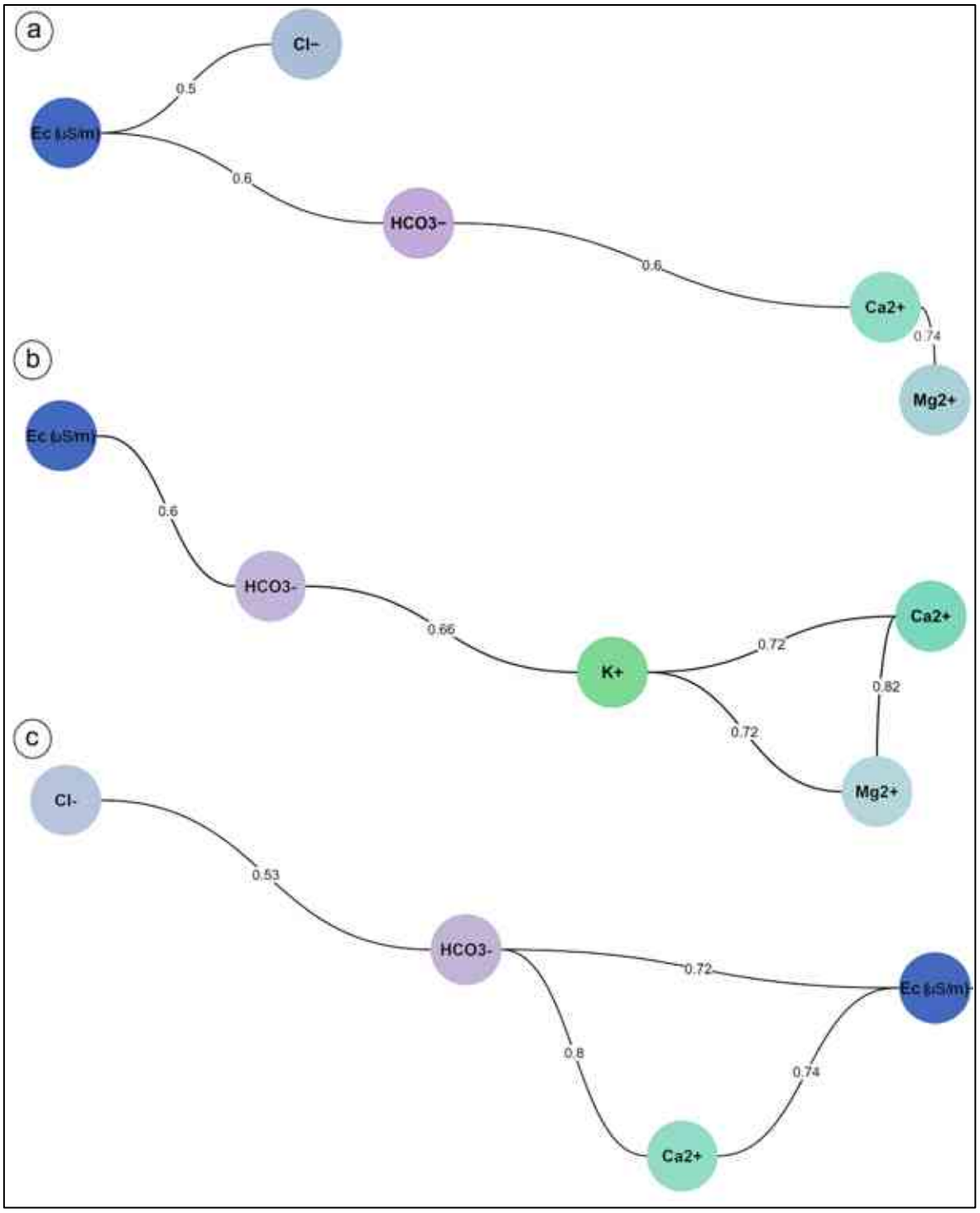

Figure 31. Geochemical association of the ions with a correlation index higher than 0.5, calculated considering (**a**) all samples, (**b**) samples from the Pannonian Unit, and (**c**) samples from the Incised Valley Unit. It is constructed in EzCorrGraph App (Campos and Licht, 2021).

For water samples taken from wells screening the Incised Valley Unit (IVU), the Spearman's correlation index (**Table 10**) reveals a strong-to-intermediate positive correlation of 0.74 between Ca^{2+} and EC, 0.80 between Ca^{2+} and HCO_3^-, 0.72 between HCO_3^- and EC, and 0.53 between Cl^- and HCO_3^- (**Figure 31c**). The strong correlation index

between Ca^{2+}, EC, and HCO_3^- suggests the dominance of carbonate dissolution in the Incised Valley Unit, while the lower correlation index between Mg^{2+} and EC, revealed that within this unit, the calcite has a greater effect on the salinity increase than dolomite.

Finally, for the water samples of mixed origin, where the well shares a screening section between Pannonian and Incised Valley Units, the Spearman's correlation (**Table 11**) reveals a strong-to-intermediate positive correlation of 0.81 between HCO_3^- and Ca^{2+}, 0.72 between HCO_3^- and Cl^-, 0.65 between Ca^{2+} and EC, and 0.64 between HCO_3^- and EC. In the samples of mixed origin, the strong correlation between HCO_3^-, Ca^{2+}, EC, and Cl^- indicates the signature of each unit in the water sample (**Figure 32**).

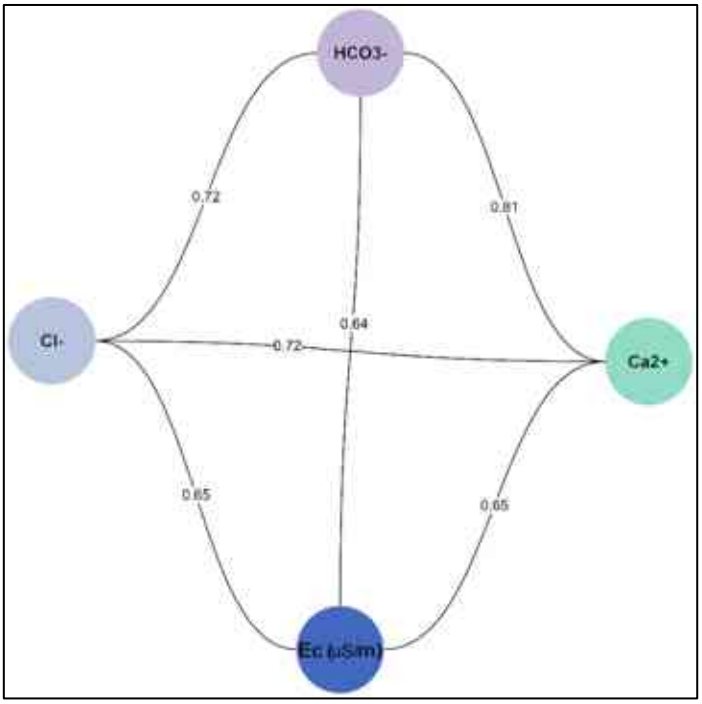

Figure 32. Geochemical association of the ions in the mixed water samples with correlation index higher than 0.5. The graph is constructed in EzCorrGraph App (Campos and Licht, 2021).

3.2 Regional numerical modelling

The numerical model for the Southern Nyírség-Hajdúság Groundwater Body was constructed using the control volume finite-difference approach of MODFLOW-USG code (Panday et al., 2013) in conjunction with the Groundwater Modelling System Interface (GMS GUI). This process followed the workflow steps numbered in **Figure 8** (Numerical Model, and Calibration), utilizing the information collected and analyzed during the conceptualization step (refer to Section 3.1). The results of the simulation are provided in an electronic version in Appendix G.

3.2.1 Spatial discretization

The spatial discretization of the model domain was achieved using a Quadtree Unstructured Grid (Quadtree), while temporal discretization occurred within a single stress period, operating under steady-state conditions. The active modeled area (**Figure 4**) is derived from the surface water basin definition combined with the reported borders of the groundwater bodies of the National General Directorate of Management, and also considering the regional groundwater flow net established by Marton (1982) (**Figure 1**). The numerical model was constructed using meters as length units and days as time units.

The grid of the model domain consists of 59,965 3D active cells, covering an area of 1,282 km² with an approximate thickness of 285 meters (Appendix G). The selection of the optimal cell size was based on considerations such as model-processing time, representation of property variability, and ensuring that there were more than three cells along the narrow aquifer side. The major axis of the grid is oriented at 52 degrees, aligning with the major dimension axis of the study area. The width-to-depth ratio is approximately 1:221 for the NE-SW axis and 1:202 for the NW-SE axis.

The chosen base dimension for the grid is 2000 meters, which was adjusted to a minimum of 250 meters at the domain's boundaries. Cell dimensions were further refined in the vicinity of well locations (WEL), ranging from a minimum of 50 meters to a maximum of 250 meters. Additionally, cells were adjusted in the location of the streams (DRN) to a size of 350 meters. Only convertible layers were utilized in the numerical model, considering the semi-confined nature of the aquifer, as previously stated in the hydraulic conditions of the system during the conceptual model development (see Section 3.1.3). The top view of the used Quadtree grid is illustrated in **Figure 33**.

Taking into account statements about vertical discretization from various authors (e.i. Haitjema et al. (2001); and Anderson et al. (2015)) emphasizing horizontal differentiation of heterogeneity was considered more effective in the studied case. Thus, the grid of the model domain is separated into four layers implemented in the model following the geological geometry revealed in the conceptual model (**Figure 15** and **Figure 16**).

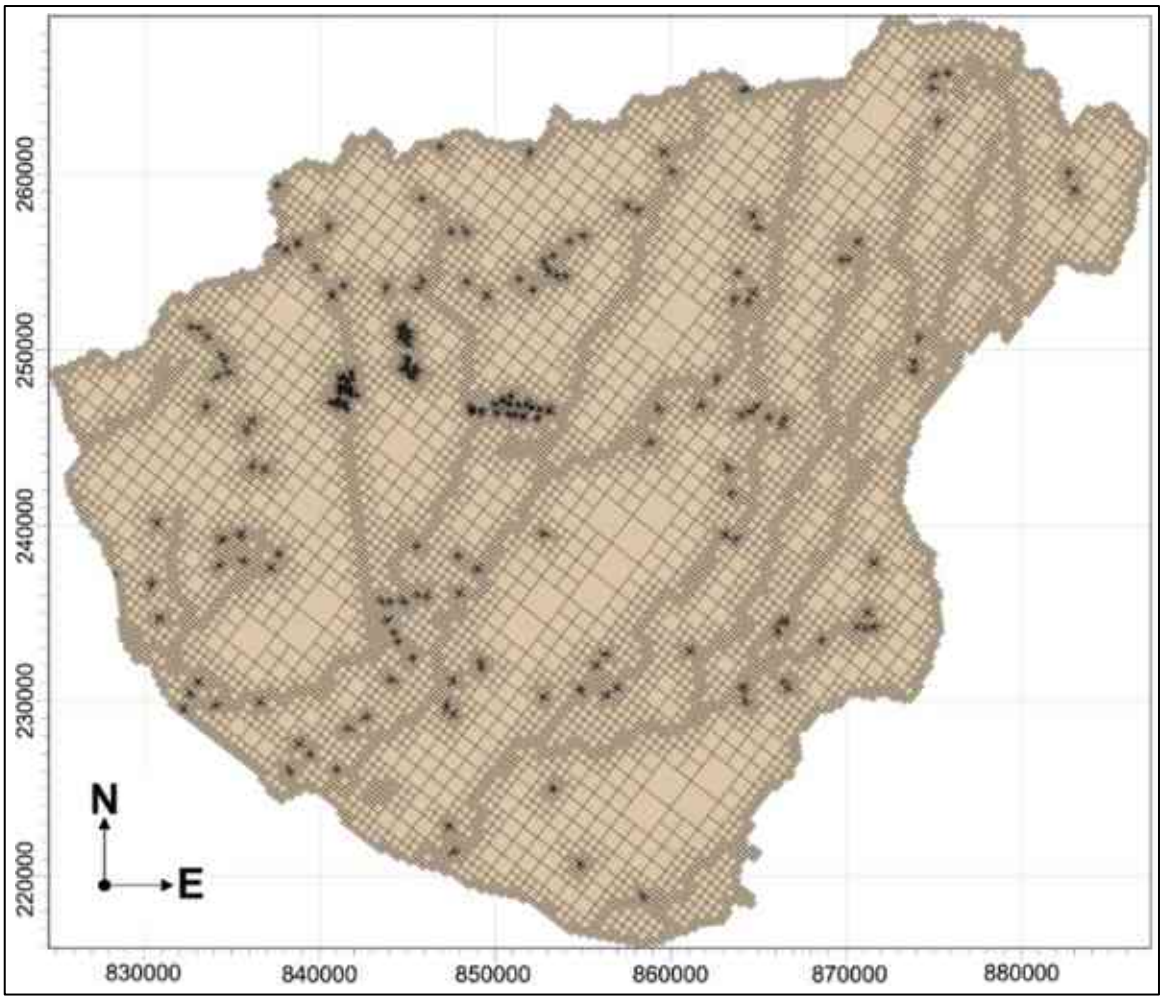

Figure 33. 2D view of the used Quadtree Unstructured grid of the model domain. The base size of the cell is 2000 m, with redefinition at lateral boundaries, sinks, and sources.

The first layer represents the Coarsening Upward Unit and its three lithologic facies: sand, silt, and clay. The second layer represents the Alluvial Unit and includes its four facies: major channel belt, floodplain, secondary channels, and avulsion cycle. The third layer represents the Incised Valley Unit and encompasses its two facies: channel belt and floodplain. Finally, the fourth layer represents the Pannonian Unit, comprising its two facies: sand and silty clay (see Section 3.1.1). The geometry of the top surfaces for each one of the layers is illustrated in **Figure 34**.

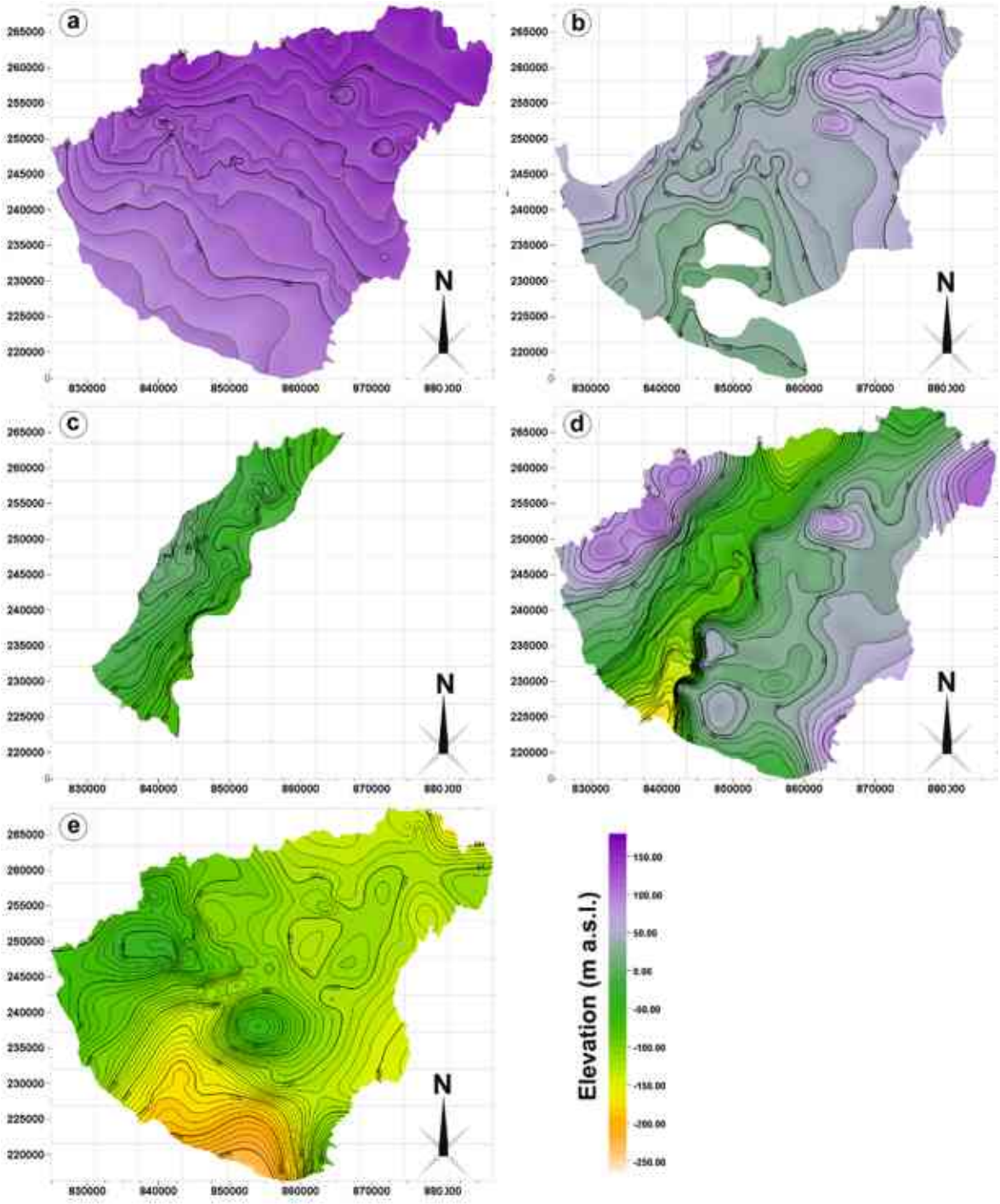

Figure 34. Contour lines of (**a**) the topographic surface or top of the model domain, (**b**) the top surface of the Alluvial Unit, (**c**) the top surface of the Incised Valley Unit, (**d**) the top surface of the Pannonian Unit, and (**e**) bottom surface of the model domain. Refers to Appendix F.

3.2.2 Initial conditions

Given the simulation's steady-state nature, only horizontal and vertical hydraulic conductivity were essential parameters to establish during *material properties configuration*. The apparent horizontal hydraulic conductivity of each stratigraphic unit was then calculated using findings from Mohammed et al. (2024) regarding horizontal hydraulic conductivity,

alongside the percentage contribution of each facies for every hydrostratigraphic unit derived from the 3D facies model (refer to Section 3.1.1 and Appendix G-1). Initial values utilized for horizontal hydraulic conductivity in the numerical model are outlined in **Table 12**.

Table 12. Maximum and minimum values of initial parameters of the facies in the study site.

Stratigraphic unit	Facies	K_h (m/d)	Facies contribution	Apparent K_h	Vertical anisotropy (k_h/k_v)
Coarsening Upward	Sand	2.2	0.426	0.96	1
	Clay	0.01	0.5115		
	Silt	0.23	0.0625		
Alluvial	Channel belt	2.2	0.1667	0.50	5
	Avulsion cycle	1.11	0.1392		
	Secondary Channel	1.09	0.218		
	Floodplain	0.05	0.4704		
Incised valley	Channel belt	3.5	0.984	3.45	10
	Floodplain	0.08	0.016		
Pannonian	Sand	2.2	0.4233	0.94	5
	Silt	0.02	0.5767		

While the computed hydraulic conductivity values of the sand bodies in the PU, ALU, and CUU (**Figure 22**) aligned with those reported by Mohammed et al. (2024), discrepancies were observed for the IVU. In this case, values derived from the multi-well clustering approach were favored due to their vertical definition and the availability of a more comprehensive dataset. For the vertical anisotropy ratio (k_h/k_v) initial values were selected as follows: 1 for the CUU, 8 for the ALU, 10 for the IVU, and 8 for the PU. These values will be subject to adjustment during the calibration process, alongside horizontal conductivity. For configuring the *initial head* in the model domain, the computed water table surface from the boreholes screening the unconfined aquifer layer (**Figure 26**), also called the Coarsening Upward Unit, was utilized in **Figure 35**.

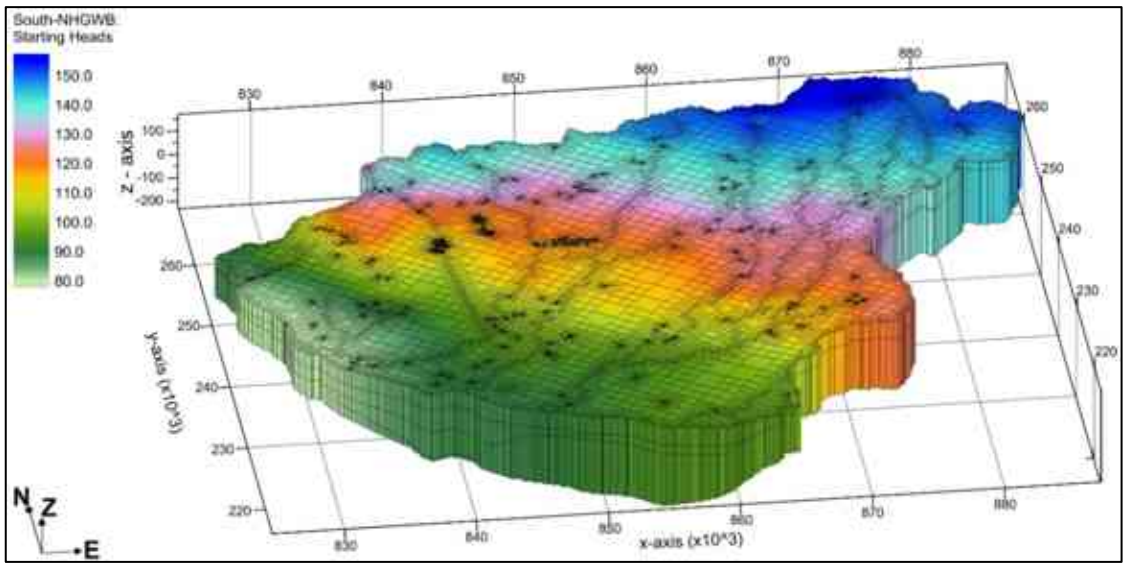

Figure 35. Initial head distribution in the model domain.

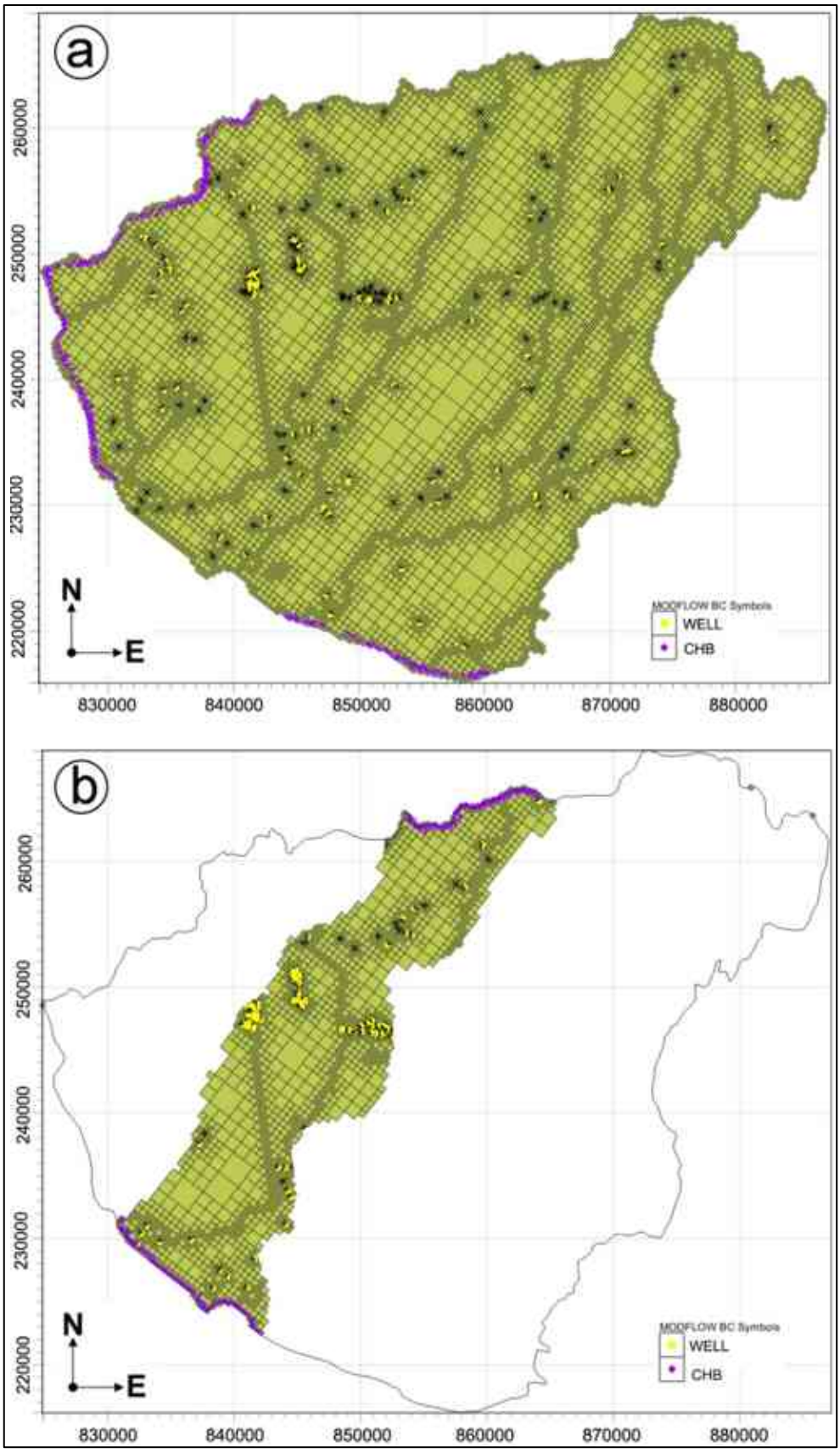

Figure 36. Location of the Constant Head Boundary condition set up for (**a**) the Pannonian Unit and (**b**) the Incised Valley Unit. Also, it is possible to visualize the location of the screens within each layer.

3.2.3 Boundaries conditions

The inflow and outflow components with the model domain were introduced aiming for the accomplishment of the boundary conditions configuration (**Figure 8, Numerical model**). It encompasses the lateral boundaries, sinks, and sources. Firstly, the *lateral flow boundaries* were established under Dirichlet conditions (**Table 2**), utilizing the Time-Variant Specified Head Package (CHB) of MODFLOW-USG. These conditions varied in terms of location, as depicted in **Figure 36**. The selection of location, as well as the values on the nodes on the arcs that represent the boundary condition (Appendix G), were specified according to the piezometric surface shown in **Figure 25c,** and considering the flow direction illustrated on it.

The recharge of the aquifer was introduced in the model using the Recharge package (RCH) of MODFLOW-USG, configured to be inserted into the highest active cell of the domain. It is spatially defined by the 30-year average of the effective infiltration values calculated based on the CARPATCLIM-HU measured climate parameters for the 1975-2004 climate period (NATéR, 2023). These values represent the annual recharge rate introduced by precipitation in the system after accounting for evapotranspiration occurrence, ranging from 0.00011 m/d to 0.00002 m/d, as depicted in **Figure 37**.

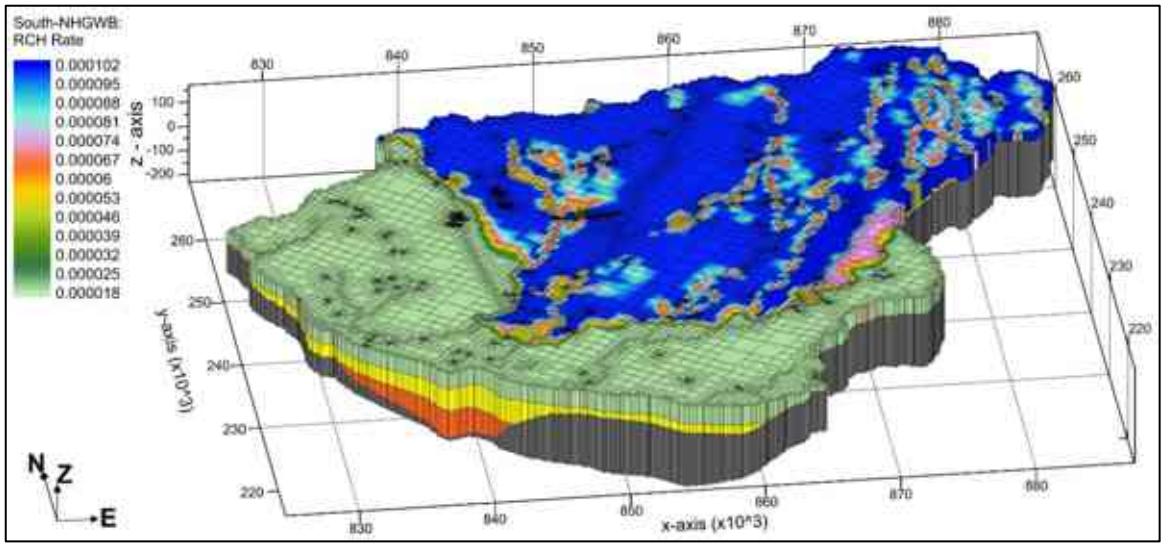

Figure 37. Implemented recharge package (RCH) and its spatial distribution on the model domain.

Subsequently, the production rates (Q) reported in the well books for the period 1969-1971 were incorporated to be simulated as withdrawals using the Well package (WEL). They were positioned within the model domain by activating "use screen location" in the conditions of the coverage layer. Following this, the streams existing within the model domain were simulated using the Drain package (DRN). The geometry of the streams is derived from the shape used and displayed in **Figure 4c**. The conductance is assumed to be

0.4 (m2/d)/m, and the bottom elevation at the nodes of the coverage was copied from the land surface elevation model.

3.2.4 Calibration

The Head Observation (OBS) package was used to compare simulated water-table altitudes to observed water-table altitudes collected from the field observations, recorded in the drilling wellbooks and previously employed to depict the piezometric surfaces for the layers (**Figure 25a**, **25c**, and **26**). Specifically, 40 observation targets were assigned to the Coarsening Upward Unit layer, 23 to the Alluvial Unit layer, 27 to the Incised Valley Unit, and finally 33 to the Pannonian Unit, as depicted in **Figure 38**.

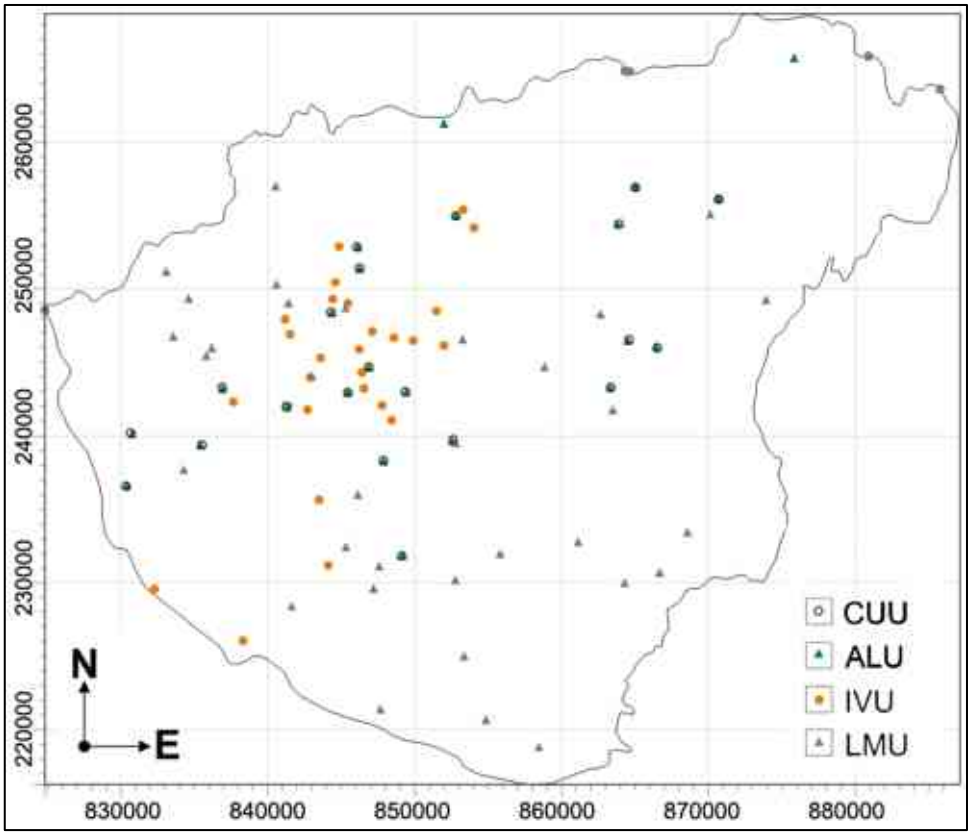

Figure 38. Hydraulic head calibration targets in the model domain.

The *first simulation* was done under the above-given setup conditions of the model domain for the Modflow-USG code performance, the stability of the model looks strong enough to maintain the budget percentage discrepancies in the solution under 1.0 % for the steady-state stress period. The reported water budget for the first simulation of the model domain was calculated as follows: a total of 127931 $m^{3/}d$ originated from effective infiltration of precipitation, 34050.6 m^3 entered from the specified head boundary sides, 20596.6 $m^{3/}d$ exited the system through the specified head boundaries, while 104178.1 $m^{3/}d$ were discharged through production wells, and 37212.3 $m^{3/}d$ are outflow from the rivers and

streams (Appendix G). The correlation between the calculated hydraulic head in the simulation and observed values in the area is strongly positive (r = 0.86), as illustrated in **Figure 39a**.

The residual heads vary between 31.3 and -26.1 m, as shown in **Figure 39b**. The total residual in the head for the first simulation is 897.17 m. The spatial distribution of the targets is illustrated in **Figure 40**, where targets with a variation between 0 and ±10 m are represented with green color boxplots, targets with a variation between ±10 and ±20 m are represented in yellow color boxplots, and targets with a variation higher than ±20 m are represented in red color boxplots.

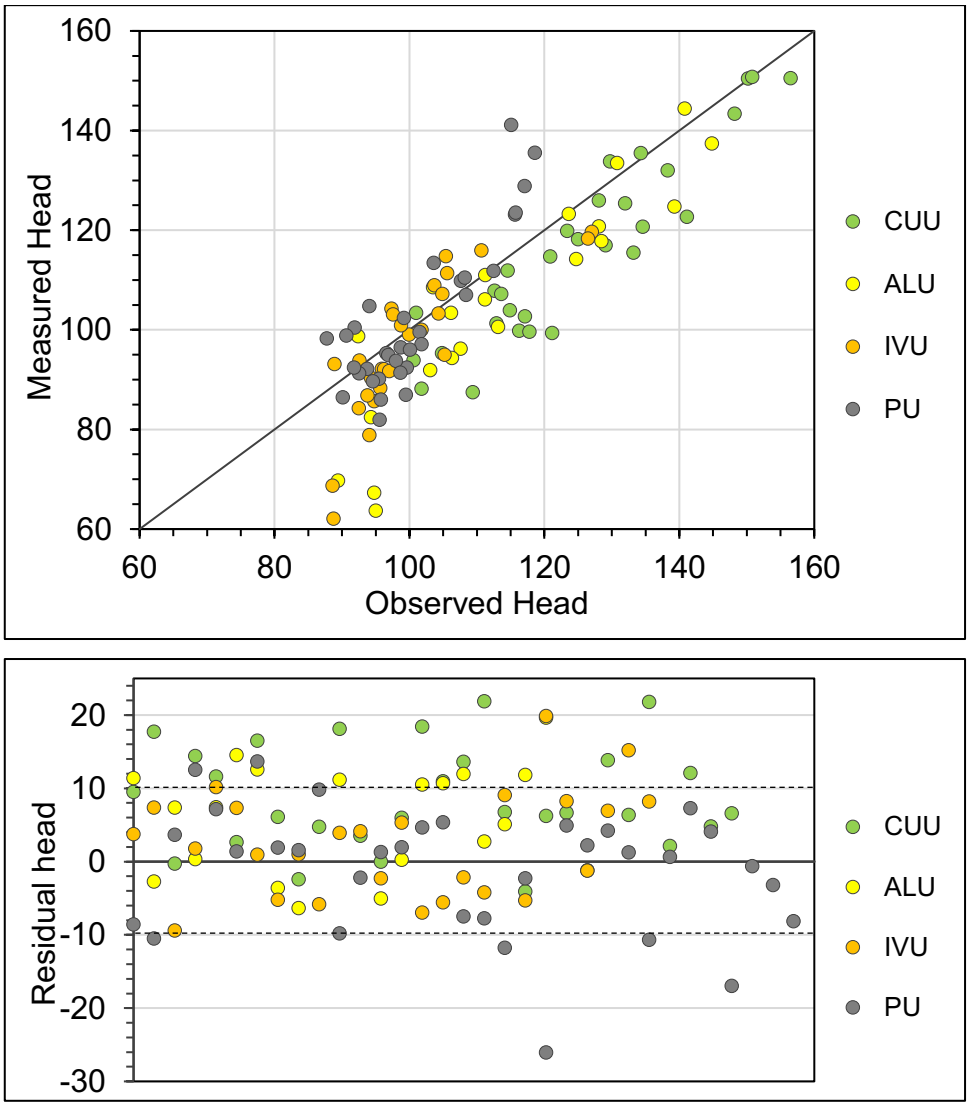

Figure 39. (**a**) Correlation between the values of the observed head and the measured head in the first simulation. (**b**) Report of the residual of the calculated head and the observed head values in meters.

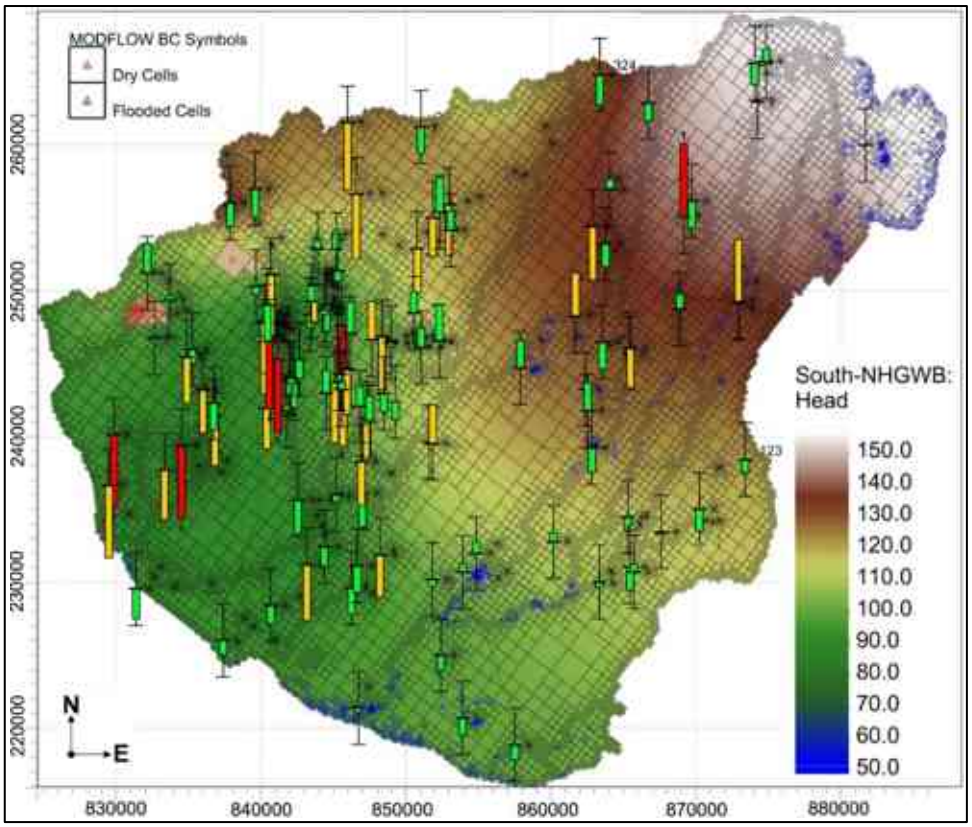

Figure 40. Boxplot of the calibration targets. They show the deviation of the calculated head from the observed head value.

Following this, the calibration process was methodically and manually executed. This involved the implementation of zonation for hydraulic conductivity in the Alluvial System Unit, utilizing the trend lines established for the Object-Based simulation (see Appendix F). The adjustment of the conductance value of the streams (DRN) was incorporated into the simulation. The values vary from 0.3 $(m^2/d)/m$ to 0.5 $(m^2/d)/m$ as shown in figure **Figure 41**. Furthermore, a progressive refinement of the input values for horizontal hydraulic conductivity and vertical anisotropy was undertaken to optimize the alignment between model-simulated piezometric surfaces and observed heads. The ultimate configuration of the hydraulic properties for the layers and zones is comprehensively detailed in **Table 13**.

The reported water budget for the calibrated model was calculated as follows: a total of 128058.2 $m^{3/}d$ originated from effective infiltration of precipitation, 36582.98 m^3 entered from the specified head boundary sides, 24769.3 $m^{3/}d$ exited the system through the specified head boundaries, while 103402.2 $m^{3/}d$ were discharged through production wells, and 36480.67 $m^{3/}d$ are outflow from the rivers and streams (Appendix G).

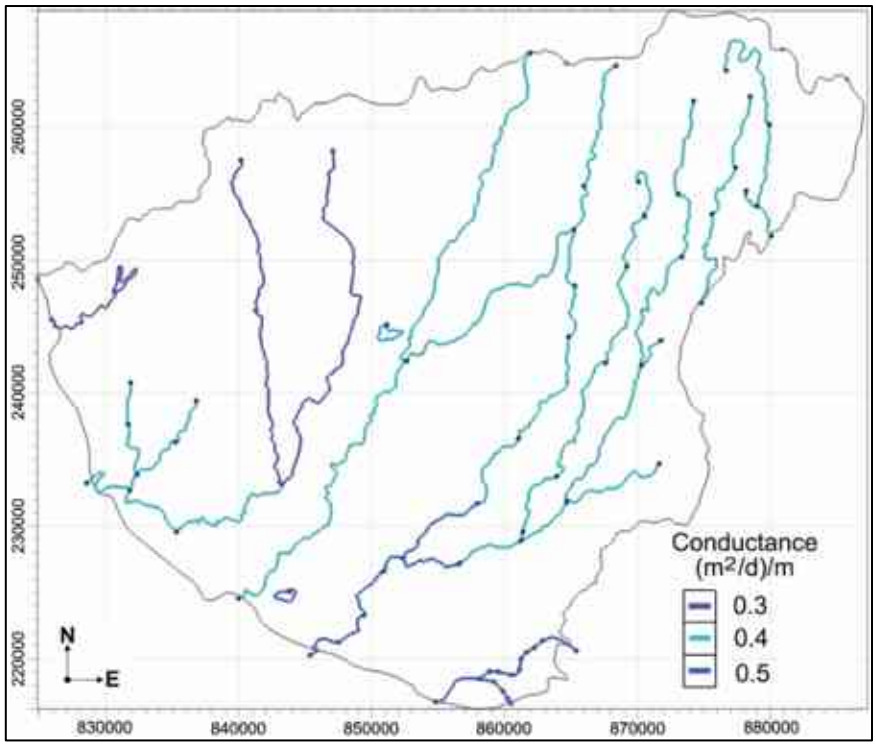

Figure 41. The drainage system is introduced in the model domain as a DRN package. The assigned conductance for the arcs varies between 0.3 to 0.5 (m^2/d)/m.

Table 13. Configuration of the hydraulic properties of the layers after calibration.

Hydrostratigraphic Unit	Zones	k_h (m/d)	Vertical anisotropy (k_h/k_v)
Coarsening Upward	Sand	0.95	1
	Clay		
	Silt		
Alluvial	Channel belt	2.2	15
	Avulsion cycle	1.1	15
	Secondary Channel		
	Floodplain	0.0002	1
Incised valley	Channel belt	3.5	15
	Floodplain		
Pannonian	Sand	1.8	3
	Silt		

The correlation between the calculated hydraulic head in the simulation and observed values in the area is strongly positive (r = 0.896), as illustrated in **Figure 42a**. The residuals vary between 20 m and -15 m, as shown in **Figure 42b**. The total residual in the head for the first simulation is 676.12 m. The spatial distribution of the targets is illustrated in Figure 41, where targets with a variation between 0 and ±10 m are represented with green color boxplots, targets with a variation between ±10 and ±20 m are represented in yellow color boxplots, and targets with a variation higher than ±20 m are represented in red color boxplots (**Figure 43**).

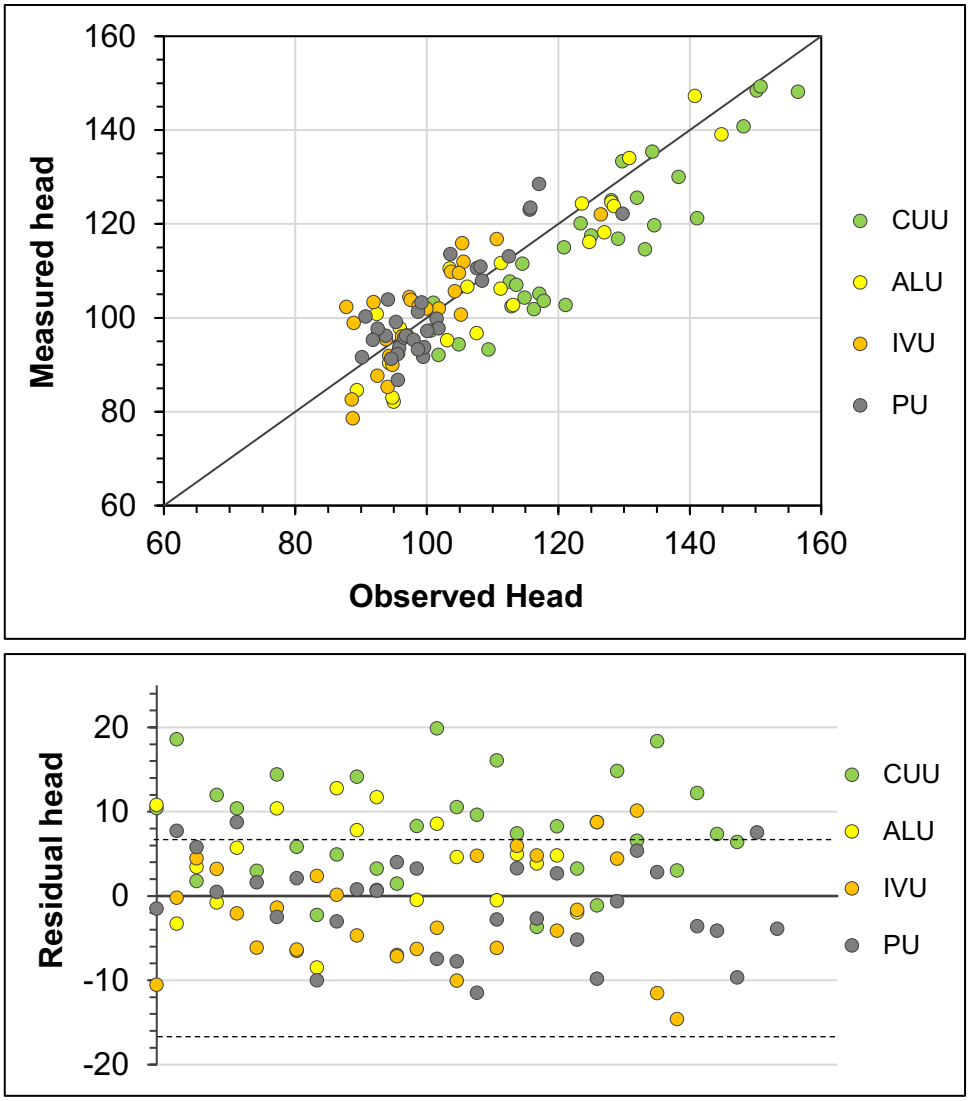

Figure 42. (a) Correlation between the values of the observed head and the measured head in the calibrated simulation. (b) Report of the residual of the calculated head and the observed head values in meters.

The hydrogeological model calibration process was conducted meticulously to ensure accuracy and reliability. The implementation of zonation for hydraulic conductivity in the Alluvial System Unit, informed by Object-Based simulation trend lines, allowed for a detailed representation of aquifer heterogeneity. Adjustments to stream conductance values further refined the model's depiction of surface water-groundwater interactions.

Through progressive refinement of input parameters such as horizontal hydraulic conductivity and vertical anisotropy, the model was optimized to closely match observed piezometric surfaces and hydraulic heads. The comprehensive detailing of hydraulic properties for different layers and zones in **Table 13** provides valuable insights for future modeling efforts. Then, the strong positive correlation (r = 0.896) between calculated and observed hydraulic heads indicates the model's effectiveness in capturing the system's

behavior, also supported by the residual head analysis further validated the model's performance, with minor deviations observed between simulated and observed heads considering the regional dimension of the model domain. The spatial distribution of target variations provided additional context, highlighting areas of agreement and potential areas for further investigation or refinement.

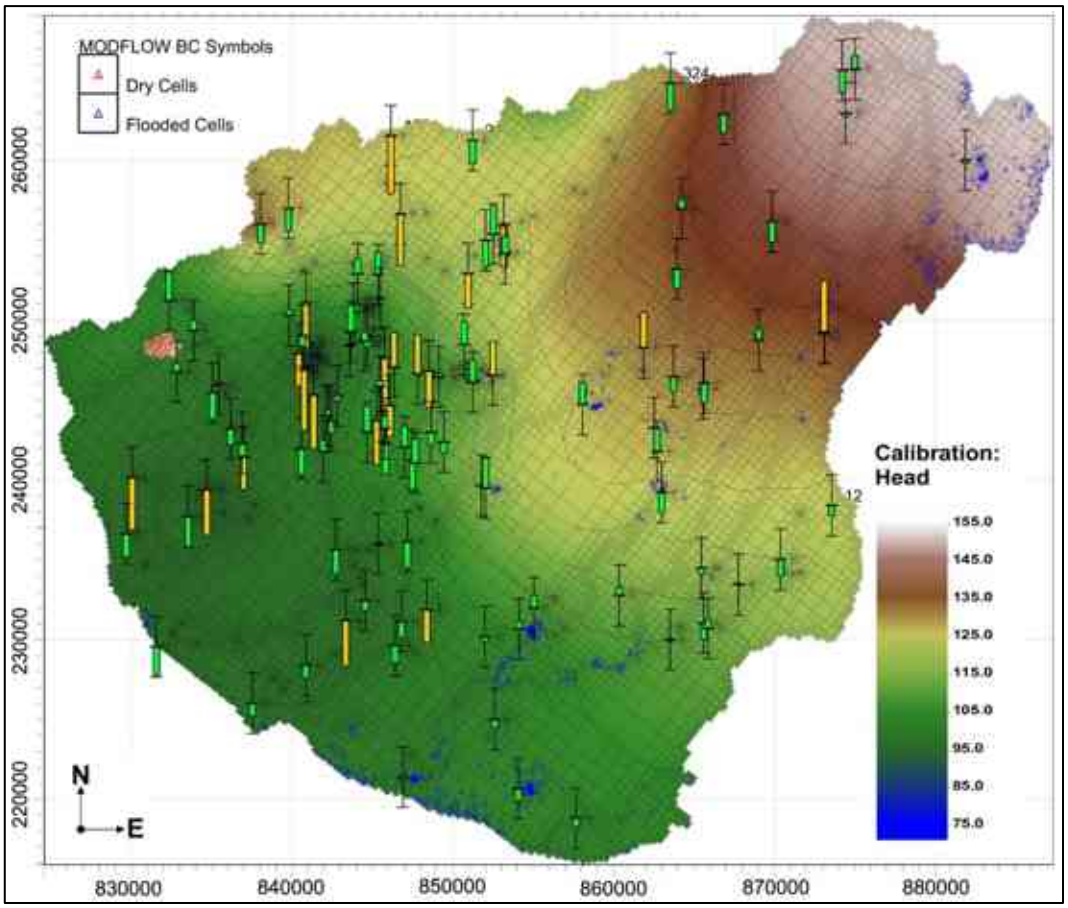

Figure 43. Boxplot of the calibration targets. They show the deviation of the calculated head from the observed head value.

4 NEW SCIENTIFIC RESULTS

4.1 Thesis of the research

Following the established workflow for the application of the above-exposed methods on the constructed database of the Southern Nyírség-Hajdúság Groundwater Body, I was able to achieve the next new scientific results:

Thesis 1. 3D stratigraphic units definition

I have constructed the 3D geological interpretation of the Southern Nyírség-Hajdúság Groundwater Body applying high-resolution log correlation, identifying 3 bounding surfaces within 285 meters depth of the sedimentary record. The developed 3D

geological model defines the spatial continuity of the stratigraphic units within the study area. Also, I was enabled to identify an incised valley deposited in stratigraphic discordance on Pannonian sediments, subsequently buried by an alluvial sequence and a fluvial-lacustrine sequence, verifying the hypothesis of Püspöki (2016a, b).

Thesis 2. Correlation between geological framework and hydrodynamic patterns

In the absence of 2D geophysical data in the region, I supplemented log correlation at the studied depth with hydrogeological and hydrogeochemical data as independent sources to validate stratigraphic contacts and delineate the hydrostratigraphic units of the aquifer system. Horizontal uncertainty between logs was assessed by examining patterns observed on piezometric surfaces, pressure conditions, and geochemical characteristics, which serve as expressions of the geometric distribution of the geological framework. Through the estimation of horizontal hydraulic conductivity of the sand bodies using the Logan Method, I was able to identify coarser grain sizes for the Incised Valley Unit compared to the surrounding units. The spatial distribution of the estimated hydraulic conductivity aligns with the proposed geometry of the paleo-valley, with a noticeable change in values occurring at the boundary of the defined stratigraphic unit.

From the analysis of the hydrodynamic conditions, I was able to discern the hydraulic connectivity of the layers through hydraulic windows occurring in areas with high water extraction rates. This resulted in the development of a semi-confined hydraulic behavior within the aquifer system. Additionally, I was able to corroborate the gravity-driven flow regime mentioned previously by other researchers. I also observed two main disturbances in the regional flow direction: (1) A perturbation was observed in the form of an elongated disturbance along the same strike direction as the paleo valley, attributed to the higher hydraulic conductivity pathway within the Incised Valley Unit. (2) Another perturbation resulted from the presence of hydraulic windows, with the IVU-AU vertically and IVU-LMU horizontally, leading to a depression in the dynamic pressure increment and hydraulic head at the center of the study area, specifically at the Debrecen Waterworks Sites.

Furthermore, I recognized the dominance of a downward flow direction and under-hydrostatic pressure conditions ($\gamma_{st} < \gamma_{dyn}$) in the system. The Incised Valley Units exhibited the highest depression, with a hydrostatic gradient (γ_{dyn}) of 6.06 kPa/m, compared to the surrounding units where the pressure gradient (γ_{dyn}) exhibited values of 9.74 kPa/m for the CUU, 8.37 kPa/m for the AU, and 7.43 kPa/m for the LMU.

Finally, from the geochemical analysis, I established that the primary aquifer is distinguished by a Ca-Mg-HCO_3 water type, whereas the lateral surrounding aquifer exhibits Na-HCO_3 water type. Furthermore, the saturation index values indicated a transition from under-saturated to supersaturated states for calcite and dolomite minerals along the spatial extent of the Incised Valley Unit (IVU). These findings align with the observation that the heterogeneity introduced by the primary aquifer significantly influences the flow pattern, resulting in higher flow velocities within the IVU.

Thesis 3. 3D facies modelling

I developed a facies model for the stratigraphic units to characterize the complexity and geological heterogeneity within them. Utilizing the density of available well-log information, I applied object-based simulation to stochastically model the 3D spatial distribution of depositional elements for the Alluvial Unit and Incised Valley Unit facies. Simultaneously, I employed sequential indicator simulation to describe the spatial distribution of lithofacies within the Coarsening Upward Unit and Pannonian Unit.

Using the 3D facies model, I assessed the volume of each facies and subsequently calculated the apparent hydraulic conductivity for the four aquifer layers. Hydraulic conductivity values were determined as a continuous log using the Csókás method for 19 selected boreholes, as reported in the research conducted by Mohammed et al. (2024)

Thesis 4. 3D regional numerical modelling

I have performed a numerical simulation of the created conceptual model of Southern Nyírség-Hajdúság Groundwater Body to prove the hydraulic behavior of the geological framework. I have addressed an acceptable calibration of the model implementing layer zoning for the distribution of horizontal hydraulic conductivity. The zonation is done according to the facies model insights. This decision was driven by the constraint that the model could not achieve a higher level of vertical discretization for the layers, primarily due to limitations within the modelling code, particularly concerning cell saturation and the wide-to-depth ratio of the model.

I could report a water budget for the calibrated model domain at a regional water scale was calculated as follows: a total of 128058.2 m^3/d originated from effective infiltration of precipitation, 36582.98 m^3 entered from the specified head boundary sides, 24769.3 m^3/d exited the system through the specified head boundaries, while 103402.2 m^3/d were discharged through production wells, and 36480.67 m^3/d are outflow from the rivers and streams. The comparison between the calculated hydraulic head in the simulation and observed values of it. The residual heads vary between 20 m and -17 m.

4.2 Practical applicability

In this study, the newly acquired scientific results offer profound insights into the regional-scale hydrogeological interpretation of the Southern Nyírség-Hajdúság Groundwater Body. By delivering a comprehensive three-dimensional geological description of one of Hungary's most critical aquifer systems, this research effectively addresses a notable gap in our understanding.

The significance of this aquifer system has been underscored by continuous research efforts aimed at various water utilization purposes, thereby amplifying the relevance and substance of the findings presented here. The meticulously tested and calibrated aquifer system geometry, based on data spanning from 1969 to 1971, holds immense potential for updating hydraulic conditions and formulating new scale exploration models ranging from local to regional scales. These findings are poised to drive progress in sustainable groundwater management practices within the region, particularly amidst escalating water demands from local communities, agricultural activities, and industrial sectors. The reported results constitute invaluable contributions to informed decision-making and the formulation of efficient strategies aimed at ensuring the long-term accessibility and optimal utilization of groundwater resources in the area.

Furthermore, the methodology employed in this research has introduced a practical approach that capitalizes on the strong correlation between geological geometry and hydrogeological patterns. This methodology facilitates the construction of a reliable conceptualization of porous media aquifer systems, especially in scenarios where 2D geological information collection is hindered by geological conditions such as depth, compaction, heterogeneity, and horizontal extension. Moreover, this approach has demonstrated its efficacy in conducting hydrogeological modeling, thereby ensuring a comprehensive understanding of the three-dimensional nature of aquifer characteristics.

Overall, the findings and methodology presented in this research offer tangible practical applicability, guiding future endeavors in groundwater management and resource utilization while advancing our understanding of complex hydrogeological systems.

5 SUMMARY

The 3D geological characteristics of the groundwater system in the Southern Nyírség–Hajdúság Groundwater Body, located in East Hungary, have been examined through an integrated analysis of geological, hydrogeological, and geochemical data. This study developed a comprehensive conceptualization that effectively describes the

hydrogeological framework and hydrological system of the porous media aquifer system under investigation. This conceptualization served as a crucial prerequisite before initiating the application of numerical modelling.

The gathered results revealed a previously unexplored stratigraphic unconformity within the complex Quaternary sedimentary sequences of the Great Hungarian Plain. Through the successful application of high-resolution log correlation, the study identified four hydrostratigraphic units within the studied depth interval. Among these units, the primary aquifer was found within an incised paleo valley, measuring approximately 10 to 13 kilometers in width and oriented along an NE–SW axis. This aquifer primarily comprises coarse-grain sediments. It was deposited unconformably on the eroded surface of the Pannonian Units, subsequently becoming buried beneath an alluvial stratigraphic sequence and a series of sediments exhibiting a coarsening-upward trend, with an undefined sedimentary environment.

Despite the limited availability of 2D geophysical data, the geometry of the stratigraphic units was effectively demonstrated through their positive correlation with the spatial distribution of hydraulic conductivity, as well as the horizontal and vertical flow patterns and the geochemical evolution of the water. The estimated horizontal hydraulic conductivity of the sand bodies consistently aligned with the grain size information reported in the wellbooks for each identified hydrostratigraphic unit. This alignment indicated a coarser grain size for the Incised Valley Unit compared to the surrounding units. The spatial distribution of hydraulic conductivity conformed to the geometry of the paleo valley, with a noticeable change in hydraulic conductivity values occurring at the boundary of the Incised Valley Unit's presented geometry.

The hydrological characteristics of the aquifer were revealed through the analysis of fluid potential patterns. These patterns demonstrated the hydraulic connectivity of the layers via hydraulic windows, particularly in areas with high water extraction rates, resulting in the development of a semi-confined hydraulic behavior within the aquifer system. Additionally, they corroborated the gravity-driven flow regime mentioned previously by other researchers, as evidenced by the similarities between the water table and topography. In this context, recharge predominantly occurs in the highland areas, while discharge primarily takes place in the lowland regions. Lastly, the flow potential patterns indicated that the flow within the region is primarily governed by under-pressure conditions, leading to a downward flow direction. This condition is substantiated by the observation that the average pressure gradient within the hydrostratigraphic units is lower than the hydrostatic pressure gradient.

An intriguing observation worth noting is that the regional flow direction, originally described as flowing from the northwest to the southeast, exhibited two significant perturbations. The first perturbation was observed in the form of an elongated disturbance along the same strike direction as the paleovalley, caused by the higher hydraulic conductivity pathway within the Incised Valley Unit. The second perturbation resulted from the presence of hydraulic windows, with the IVU-AU vertically and IVU-PU horizontally, leading to a depression in the dynamic pressure increment and hydraulic head at the center of the study area, specifically at the Debrecen Waterworks Sites.

The geochemical analysis conducted led to the conclusion that the primary aquifer is distinguished by a Ca-Mg-HCO_3 water type, whereas the lateral surrounding aquifer exhibits a Na-HCO_3 water type. Furthermore, the saturation index values indicated a transition from under-saturated to supersaturated states for calcite and dolomite minerals along the spatial extent of the Incised Valley Unit (IVU). These findings align with the observation that the heterogeneity introduced by the primary aquifer significantly influences the flow pattern, resulting in higher flow velocities within the IVU.

After confirming the stratigraphic units, a geostatistical facies model was employed to assess the internal grain size variability within these units. The Pannonian unit was categorized into sand (42.33%) and silt (57.67%) lithological facies. The Incised Valley Unit primarily consisted of channel belt facies (98.4%) with smaller floodplain facies (1.6%). In contrast, the Alluvial Unit exhibited four distinct facies: a primary channel belt (16.67%), three secondary channels (21.80%), an avulsion cycle (13.92%), and floodplain deposits (47.04%). Finally, the Coarsening-Upward Sequences were represented by three lithologic facies, comprising sand (42.6%), silt (6.25%), and clay (51.15%).

The conceptual model of the four hydrostratigraphic units within the semi-confined Southern Nyírség–Hajdúság Groundwater Body was employed for discretization. This was carried out using an unstructured grid comprising 71,948 3D active cells distributed across four layers. This choice of four layers was made based on the consideration that, in regional modelling, the addition of multiple layers to the numerical model does not yield significant improvements. This is due to the relatively small thickness of the aquifer system in comparison to its lateral extent, which primarily results in a horizontal flow direction.

The apparent horizontal hydraulic conductivity was calculated based on the facies proportions within each unit, using the hydraulic conductivity results obtained by Mohammed et al. (2024)calculations applied to selected geophysical logs in the study area. Throughout the calibration process of the numerical model, the spatial distribution of these

facies played a significant role in fine-tuning the hydraulic conductivity, primarily in response to variations in the concentration of sand or clay within the area.

The initial hydraulic head conditions in the model were set based on the hydraulic head values reported in the wellbooks of wells that screened the first layer. Boundary conditions were defined using production wells (Well Package), effective infiltration (Recharge Package), and specific head (Time-Variant Head). The simulation was conducted using the MODFLOW-USG code within the GMS GUI.

This research finalized with the presentation of a comprehensive 3D regional hydrogeological model of the porous media aquifer system within the Southern Nyírség–Hajdúság Groundwater Body. This model was constructed based on the newly developed 3D stratigraphic and facies model, which accurately characterizes the complex Quaternary Sedimentary Sequences within the established model domain. This meticulously tested and calibrated aquifer system geometry, based on data spanning from 1969 to 1971, holds immense potential for updating hydraulic conditions and formulating new scale exploration models ranging from local to regional scales, driving progress in sustainable groundwater management practices within the region, particularly amidst escalating water demands from local communities, agricultural activities, and industrial sectors.

ACKNOWLEDGEMENTS

In the course of my thesis work, I have been fortunate to receive invaluable support and guidance from numerous individuals who have played pivotal roles in the successful completion of this research.

First, I would like to express my deepest appreciation and gratitude to my two dedicated supervisors, Prof. Dr. Péter Szűcs and Dr. Zoltán Püspöki, for their immense generosity in sharing their time, expertise, and unwavering commitment to my academic and professional growth. Their guidance has been instrumental in shaping the trajectory of this research.

I would also like to express my sincere gratitude to the scientific consultants who shared their profound knowledge and offered invaluable insights, helping me overcome various challenges encountered during the investigation process. Your willingness to lend your expertise has been truly invaluable.

Additionally, I extend my thanks to the teachers, colleagues, and administrative personnel at the institute who have provided assistance, support, and encouragement throughout this journey.

I am deeply appreciative of the collaborative spirit and collective contributions of all these individuals, without whom this research would not have been possible. Thank you for being an integral part of this academic pursuit.

Finally, I would like extend a special thanks to Rock Flow Dynamics, which, through the company Petroaptos Oil Engineering Company of Ecuador, has granted the use of a license to the tNavigator software to meet the objectives of the study.

REFERENCES

Alabert, F.G. (1987) Stochastic imaging of spatial distributions using hard and soft information. MSc Thesis. Stanford University. Stanford.

Anderson, M.P., Woessner, W.W. and Hunt, R.J. (2015) *Applied Groundwater Modelling. Simulation of Flow and Advective Transport*. 2th Edition. London: Academic Press. DOI: 10.1016/c2009-0-21563-7.

Appelo, C.A.J. and Postma, D. (2005) *Geochemistry, groundwater and pollution*. 2th Edition. London: CRC Press. DOI: 10.1016/0016-7037(94)90585-1.

Aquaveo LLC (n.d.) *Groundwater Modelling System*. Viewed 3 October 2023, <https://www.xmswiki.com/wiki/Main_Page>.

Bayer, P. et al. (2011) Three-dimensional high resolution fluvio-glacial aquifer analog - Part 2: Geostatistical modelling. *Journal of Hydrology* 405(1–2): 10–23. DOI: 10.1016/j.jhydrol.2011.03.037.

Bianchi, M. and Pedretti, D. (2017) Geological entropy and solute transport in heterogeneous porous media. *Water Resources Research* 53(6): 4691–4708. DOI: 10.1002/2016WR020195.

Bloch, S. (1991) Empirical Prediction of Porosity and Permeability in Sandstones. AAPG Bulletin 75 (7): 1145-1160. DOI: 10.1306/0C9B28E9-1710-11D7-8645000102C1865D

Borsy, Z. (1982) 'Hordalékkúpok fejlődése az Alföldön', Scientific Publications in the BGYTF, p. 37.

Borsy, Z. (1990) 'Evolution of the alluvial fans of the Alföld'. In: A. Rachocki and M. Church (eds) *Alluvial Fans: A Field Approach*. New York: John Wiley & Sons Inc., pp. 229–246.

Brassington, F.C. and Younger, P.L. (2010) A proposed framework for hydrogeological conceptual modelling. *Water and Environment Journal* 24(4): 261–273. DOI:10.1111/j.1747-6593.2009.00173.x.

Bridge, J.S. (2003) *Rivers and Floodplains: Forms, Processes, and Sedimentary Record*. Bodmin: Wiley - Blackwell. ISBN: 978-0-632-06489-2.

Buday-Bódi, E., Buday, T. and McIntosh, R.W. (2019) Geology and Utilization of Porous Thermal Water Reservoirs, NE Hungary. Presented at *European Geothermal Congress,* Den Haag, Netherlands, 11-14 June.

Buday, T. et al. (2015) Sustainability aspects of thermal water production in the region of Hajdúszoboszló-Debrecen, Hungary. *Environmental Earth Sciences* 74(12): 7511–7521. DOI:10.1007/s12665-014-3983-1.

Buday, T. and Püspöki, Z. (2011) B05 Facies Variations Detected by Well Log Correlation in a Geothermal Reservoir (Újfalu Formation) around Debrecen, Hungary, presented at *6th Congress of Balkan Geophysical Society*, Budapest, 03-06 October.

Campos, F.F. de and Licht, O.A.B. (2021) Correlation diagrams: Graphical visualization of geochemical associations using the EzCorrGraph app. *Journal of Geochemical Exploration* 220: 106657. DOI:10.1016/j.gexplo.2020.106657.

Cateneanu, O. (2022) *Principles of sequence stratigraphy*. Second Edition. Radarweg: Elservier. ISBN: 9780444533531.

Cooley, R.L. (2004) A theory for modelling ground-water flow in heterogeneous media. U.S.G.S, Reston, Virginia. DOI: 10.3133/pp1679.

Csillag, G. et al. (2023) 'Kvarter'. In: E. Babinszki et al. (eds) *Magyarország litosztratigráfiai egységeinek leírása II. Kainozoos képződmények*. Budapest: Szabályozott Tevékenységek Felügyeleti Hatósága, pp. 144–147. ISBN: 9789636713294

Csókás, J. (1995) Determination of yield and water quality of aquifers based on geophysical well logs. *Magyar Geofizika* 35(4): 176–203.

Darcy, H. (1856) *Les fontaines publiques de la ville de Dijon*. Edited by V. Dalmont. Paris: Libraire des Corp Impériaux des ponts et chussées et des Mines.

Debreceni Vizmű Zrt. (2017a) *The history of Debrecen Water Works*. Viewed 16 May 2023, <https://www-debreceni--vizmu-hu.translate.goog/cegunkrol/cegtortenet?_x_tr_sl=hu&_x_tr_tl=en&_x_tr_hl=es-419&_x_tr_pto=wapp>.

Debreceni Vizmű Zrt. (2017b) Documentumtár-Water management legislation. Viewed 30 March 2022, <https://www.debreceni-vizmu.hu/dokumentumtar>.

Deutsch, C. V. and Journel, A.G. (1998) *GSLIB: geostatistical software library and user's guide*. 2th Edition. Edited by A.G. Journel. Oxford University Press.

Deutsch, C. V. and Tran, T.T. (2002) FLUVSIM: A program for object-based stochastic modelling of fluvial depositional systems. *Computers & Geosciences* 28(4): 525–535. DOI:10.1016/S0098-3004(01)00075-9.

Deutsch, C. V and Wang, L. (1996) Hierarchical Object-Based Stochastic Modelling of Fluvial Reservoirs. *Mathematicul Geology* 28(7): 857-800. DOI: 10.1007/BF02066005.

Dutton, S.P., Flanders, W.A. and Barton, M.D. (2003) Reservoir characterization of a Permian deep-water sandstone, East Ford field, Delaware Basin, Texas. *AAPG Bulletin* 87(4): 609–627. DOI:10.1306/10100201085.

Emery, D. and Myers, K. (1996) *Sequence Stratigraphy*. 1st Edition. Uxbridge: Blackwell Science. ISBN-10: 0632037067.

Enemark, T. et al. (2019) Hydrogeological conceptual model building and testing: A review. *Journal of Hydrology* 569: 310–329. DOI:10.1016/j.jhydrol.2018.12.007.

Erdélyi, M. (1976) Outlines of the hydrodynamics and hydrochemistry of the Pannonian Basin. *Acta Geologica Academiae Scientiarum Hungaricae* 20(3-4): 287-309.

ESRI Magyarország Kft. (2015) *Víztestek a vízgyűjtőkön*. Viewed 19 April 2022, <http://geoportal.vizugy.hu/vizgyujtogazd01/>.

Fetter, C.W. (2014) *Applied Hydrogeology*. 4th Edition. U.K.: Pearson. ISBN-10: 1292022906

Flores, Y. G. (2019) Complex analysis of hydrogeological behaviour of Hajduszoboszlo aquifer to demonstrate the advantage of fluvial facies interpretation. MSc Thesis. University of Miskolc. Miskolc.

Flores, Y.G. et al. (2023) Integration of Geological, Geochemical Modelling and Hydrodynamic Condition for Understanding the Geometry and Flow Pattern of the Aquifer System, Southern Nyírség–Hajdúság, Hungary. *Water* 15(16): 2888. DOI: 10.3390/w15162888.

Fogg, G.E. and Kreitler, C.W. (1981) Ground-Water Hydrology around salt domes in the East Texas Basin: A practical approach to the contaminant transport problem1. *Environmental & Engineering Geoscience* 18(4): 387–411. DOI: 10.2113/gseegeosci.xviii.4.387

Freeze, R.A. and Cherry, J.A. (1979) *Groundwater*. Edited by C. Brenn and K. McNeily. Upper Saddle River: Pretice Hall.

Gábris, G. and Nádor, A. (2007) Long-term fluvial archives in Hungary: response of the Danube and Tisza rivers to tectonic movements and climatic changes during the Quaternary: a review and new synthesis. *Quaternary Science Reviews* 26(22–24): 2758–2782. DOI: 10.1016/j.quascirev.2007.06.030.

Gribovszki, K. and Szeidovitz, G. (2006) Investigation of earthquakes' geo-surroundings in the Pannonian Basin by using GIS tools. *Acta Geodaetica et Geophysica Hungarica* 41(3–4): 441–460. DOI: 10.1556/AGeod.41.2006.3-4.15.

Haas, J. et al. (2014) *Geology of the pre-Cenozoic basement of Hungary. Explanatory notes for 'Pre-Cenozoic geological map of Hungary (1:500000)*. Edited by O. Piros. Geological and Geophysical Institute of Hungary.

Haitjema, H. Kelson V. and de Lange W. (2001) Selecting MODFLOW cell sizes for accurate flow fields. Groundwater 39(6): 931-938.

Haitjema, H. (2006) The Role of Hand Calculations in Ground Water Flow Modeling. *Groundwater* 44(6): 786–791. DOI: 10.1111/j.1745-6584.2006.00189.x.

Hubbert, M.K. (1940) The Theory of Ground-Water Motion. *The Journal of Geology* 48(8,1): 785–944. DOI: 10.1086/624930.

Jelmer J. Nijp, Klaas Metselaar, Juul Limpens, Harm P.A. Gooren, Sjoerd E.A.T.M. van der Zee. (2017). A modification of the constant-head permeameter to measure saturated hydraulic conductivity of highly permeable media. *MethodsX* 4: 134-142. DOI: 10.1016/j.mex.2017.02.002.

Kenoyer, G.J. (1988) Tracer test analysis of anisotropy in hydraulic conductivity of granular aquifers. *Groundwater Monitoring & Remediation* 8(3): 67–70. DOI: 10.1111/j.1745-6592.1988.tb01086.x.

Kinokow, L.F. and Bredehoeft, J. (2020) *Groundwater Resource Development: Effects and Sustainability*. Edited by J.A. Cherry and E.P. Poeter. Guelph: Groundwater Project.

Kirsch, R. (2009) *Groundwater Geophysics. A tool for hydrogeology*. 2th Edition. Berlin: Springer-Verlag. DOI: 10.1007/978-3-540-88405-7.

Kresic, N. (2006) *Hydrogeology and Groundwater Modeling*. 2th Edition. Boca Raton: CRC Press. DOI:10.1201/9781420004991.

Kozeny, J. (1927) Ueber kapillare Leitung des Wassers im Boden. *Sitzungsber Akad. Wiss., Wien* 136(2a): 271-306.

Logan, J. (1964) Estimating Transmissibility from routine production tests of water wells. *Groundwater* 2(1): 35–37. DOI: 10.1111/j.1745-6584.1964.tb01744.x.

Lóki, J., Hertelendi, E. and Borsy, Z. (1994) New dating of blown sand movement in the Nyírség. *Acta Geographica ac geologica et meteorologica Debrecina* 32: 67–79.

Mádl-Szőnyi, J. and Tóth, J. (2009) A hydrogeological type section for the Duna-Tisza Interfluve, Hungary. *Hydrogeology Journal* 17(4): 961–980. DOI: 10.1007/s10040-008-0421-z.

Mádl-Szőnyi, J. and Simon, S. (2016) Involvement of preliminary regional fluid pressure evaluation into the reconnaissance geothermal exploration-Example of an

overpressured and gravity-driven basin. *Geothermics* 60: 156–174. DOI: 10.1016/j.geothermics.2015.11.001.

Maekawa, T., Matsumoto, Y. and Namiki, K. (2007) Interpolation by geometric algorithm. *Computer-Aided Design* 39(4): 313–323. DOI: 10.1016/J.CAD.2006.12.008.

Ben Mahrez, H. et al. (2023) Hydrostratigraphic decomposition of fluvio-deltaic sediments inferred from seismic geomorphology and geophysical well logs in the Pannonian Basin, Hungary. *Global and Planetary Change* 230: 104285. DOI: 10.1016/j.gloplacha.2023.104285.

Maliva, R.G. (2016) *Aquifer Characterization Techniques Schlumberger Methods in Water Resources Evaluation Series No. 4*, Springer International Publishing. DOI: 10.1007/978-3-319-32137-0.

Marton, L. (1982) Izotóphidrológiai modellek és számítási eljárások a felszín alatti vizek mozgásának tanulmányozásához. *Hidrológiai Közlöny* 62(12): 525–572.

Marton, L., Erdélyszky, Z. and Vinzenz, R. (1980) A környezeti izotópok vizsgálata Debrecen és a Nyírség rétegvizeiben. *Hidrológiai Közlöny* 2: 85–94.

Marton, L. and Szanyi, J. (1997) Kelet-magyarországi pleisztocén üledékek geostatisztikai vizsgálata. 1. A transzmisszivitás térképezése. *Hidológiai Közlöny* 77(5): 233–248.

Marton, L. and Szanyi, J. (2000) A talajvíztükör helyzete és a rétegvíz termelés kapcsolata Debrecen térségében'. *Hidrológiai Közlöny* 80(1): 3–13.

McCord, J.T., Gotway, C.A. and Conrad, S.H. (1997) Impact of geologic heterogeneity on recharge estimation using environmental tracers: Numerical modelling investigation. *Water Resources Research* 33(6): 1229–1240. DOI: 10.1029/96WR03755.

Miall, A.D. (2006) *The Geology of Fluvial Deposits. Sedimentary Facies, Basin Analysis, and Petroleum Geology*. Fourth Edition. Springer.

Miall, A.D. (2014) *Fluvial depositional systems*. Springer International. DOI: 10.1007/978-3-319-00666-6.

Mizuno, T.A. and Deutsch, C. V (2022) Sequential Indicator Simulation (SIS). Alberta. Viewed 20 September 2023. <https://geostatisticslessons.com/pdfs/sequentialindicatorsim.pdf>

Mohammed, MusaabA.A. et al. (2024) Multi-well clustering and inverse modelling-based approaches for exploring geometry, petrophysical, and hydrogeological parameters of the Quaternary aquifer system around Debrecen area, Hungary. *Groundwater for Sustainable Development* 24: 101086. DOI: 10.1016/j.gsd.2024.101086.

NATéR (2023) *National Adaptation Geo-information System*. Viewed 10 May 2023, <https://map.mbfsz.gov.hu/nater/>.

Oliver, M.A. and Webster, R. (2014) A tutorial guide to geostatistics: Computing and modelling variograms and kriging. *Catena* 113: 56–69. DOI: 10.1016/j.catena.2013.09.006.

Országos Vízügyi Főigazgatóság (2013) *Vízügyi Honlap*. Viewed 3 Nov. 2023, < https://www.vizugy.hu/?mapModule=OpTalajviz&mapData=TalajvizTajekoztatok#mapModule >.

Panday, S. et al. (2013) MODFLOW – USG Version 1: An Unstructured Grid Version of MODFLOW for Simulating Groundwater Flow and Tightly Coupled Processes Using a Control Volume Finite-Difference Formulation. USGS, Reston, Virginia. DOI: 10.3133/tm6A45

Parkhurst, D.L. and Appelo, C.A.J. (2013) Description of input and examples for PHREEQC version 3—A computer program for speciation, batch-reaction, one-dimensional transport, and inverse geochemical calculations. USGS, Denver, Colorado. DOI: 10.3133/tm6A43.

Piper, A.M. (1944) A graphic procedure in the geochemical interpretation of water-analyses. *Eos, Transactions American Geophysical Union* 25: 914–928. DOI: 10.1029/TR025i006p00914.

Püspöki, Z. et al. (2013) Tectonically controlled Quaternary intracontinental fluvial sequence development in the Nyírség-Pannonian Basin, Hungary. *Sedimentary Geology* 283: 34–56. DOI: 10.1016/j.sedgeo.2012.11.003.

Püspöki Z. (ed) (2016a) *A Debrecen I – II vízmű telepek és környezetének szekvenciasztratigráfiai feldolgozása* (Report on sequence stratigraphic investigation in the sourroundings of I – II well fields of Debrecen). Budapest, SARA data store.

Püspöki Z. (ed) (2016b) *A debreceni TEVA telephely rétegsorának értelmezése az I – II vízmű telepek és környezetük szekvenciasztratigráfiai modelljében* (Interpretation of the TEVA site in the sequence stratigraphic model performed for the sourroundings of I – II well fields of Debrecen). Budapest, SARA data store.

Püspöki, Z. et al. (2016c) Magnetic susceptibility as a possible correlation tool in quaternary alluvial stratigraphy. *Boreas* 45(4): 861-875. DOI: 10.1111/bor.12196.

Püspöki Z. ed (2018) *Nagy felbontású fácies korrelációs vizsgálat Debrecen-Dél területen* (High resolution log correlations at Debrecen-South region). Budapest, SARA data store.

Pyrcz, M.J. and Deutsch, C. V. (2014) *Geostatistical Reservoir Modelling*. 2th Edition. Oxford University Press.

Rajmohan, N. and Elango, L. (2004) Identification and evolution of hydrogeochemical processes in the groundwater environment in an area of the Palar and Cheyyar River Basins, Southern India. *Environmental Geology* 46: 47–61. DOI: 10.1007/s00254-004-1012-5.

Reilly, T.E. (2001) System and Boundary Conceptualization in Ground-Water Flow Simulation. USGS, Denver, Colorado.

Risser, D. (2010) Factors Affecting Specific-Capacity Tests and their Application--A Study of Six Low-Yielding Wells in Fractured-Bedrock Aquifers in Pennsylvania. USGS, Reston, Virginia.

Rock Flow Dynamics (2020) Characterising your model using facies modelling. Viewed 03/06/2024 <https://www.youtube.com/watch?v=XLpe3KyXsO8&t=6s>.

Sasamoto, H., Yui, M. and Arthur, R.C. (2004) Hydrochemical characteristics and groundwater evolution modelling in sedimentary rocks of the Tono mine, Japan. *Physics and Chemistry of the Earth* 29(1): 43–54. DOI: 10.1016/j.pce.2003.11.003.

Simon, S. et al. (2023) Wetland Management in Recharge Regions of Regional Groundwater Flow Systems with Water Shortage, Nyírség Region, Hungary. *Water* 15(20): 3589. DOI: 10.3390/w15203589.

'Spearman Rank Correlation Coefficient' (2008) in The Concise Encyclopedia of Statistics. New York, NY: Springer New York, pp. 502–505. DOI:10.1007/978-0-387-32833-1_379.

Sterret, R. et al. (2007) *Groundwater and Wells*. 3rd Edition. Edited by R.J. Sterrett. New Brighton: Johnson Screens. ISBN-13: 97809787793

Szanyi, J. (2004) Felszín alatti víytermelés környezeti hatásai Dél-Nyírség péeldáján. PhD Thesis. Szegedi Tudományegyetem. Szeged.

Sztanó, O. and Magyar, I. (2023) 'Felső miocén - pliocén'. In: E. Babinszki et al. (eds) *Magyarország litosztratigráfiai egységeinek leírása II. Kainozoos képződmények.* Budapest: Szabályozott Tevékenységek Felügyeleti Hatósága, pp. 117–137. ISBN: 9789636713294

Szűcs, P. and Madarász, T. (2006) Complex hydrogeological modelling of multifunctional artificial recharge options of the Great-Forest Park in Debrecen, Hungary. *WIT Transactions on Ecology and the Environment*, 95: 177–188. DOI: 10.2495/WP060181.

Torrado, L. et al. (2020) Integrated seismic and well-log analysis for the exploration of stratigraphic traps in the Carbonera Formation, Llanos foreland basin of Colombia. *Journal of South American Earth Sciences* 104. DOI: 10.1016/j.jsames.2020.102607.

Tóth, J. (2009) *Gravitational Systems of Groundwater Flow. Theory, evaluation, utilization*. New York: Cambridge University Press. DOI: 10.1017/CBO9780511576546.

Tóth, J. (2015) Geothermal phenomena in the context of gravity-driven basinal ground flow. *Central European Geology* 58(1-2): 1-27. DOI: 10.1556/24.58.2015.1-2.1.

Tóth, J. and Almási, I. (2001) Interpretation of observed fluid potential patterns in a deep sedimentary basin under tectonic compression: Hungarian Great Plain, Pannonian Basin. *Geofluids* 1: 11–36. DOI: 10.1046/j.1468-8123.2001.11004.x.

VKKI, V. és K.K.I. (2010) *Vízgyűjtő-Gaszdálkodási Terv. Tisza Reszvízgyűjtő*. Viewed March 2024, http://www2.vizeink.hu/files/Reszvizgyujto_VGT_Tisza_13.pdf.

Wiston, R.B. (2018) *Online guide to MODFLOW NWT—Suggested input values for the NWT input file.* U.S.G.S, viewed 3 October 2023, <https://water.usgs.gov/ogw/modflow-nwt/MODFLOW-NWT-Guide/ground-water_flow_process.html>.

Wórum, G. et al. (2020) *Young geological deformations in Hungary*. Geomega, viewed 29 January 2024, < http://www.geomega.hu/letoltes/>.

APPENDIX A. TNavigator License Certificate

Mr. César Calvachi
General Manager of
PetroAptos Oil Engineering Company

CERTIFIES

That, PETROAPTOS PETROLEUM ENGINEERING COMPANY has granted **YETAZABEL GERARDA FLORES CARPIO** the use of an academic license for tNavigator, software developed by Rock Flow Dynamics.

tNavigator may be used in the development of scientific research entitled "HIGH-RESOLUTION FACIES INTERPRETATION OF QUATERNARY SEDIMENTARY SERIES FOR HYDROGEOLOGICAL MODELING OF THE NYÍRSÉG-HAJDÚSÁG GROUNDWATER BODY, NE HUNGARY".

It is worth mentioning that this license is granted exclusively for scientific activities related to the development, fulfillment and publication of the results of the specified topic.

In exchange, the beneficiary will include the following text in the credits of the publication of their results: "Special thanks to ROCK FLOW DYNAMICS, which, through the company PETROAPTOS OIL ENGINEERING COMPANY of Ecuador, has granted the use of a license to the tNavigator software, "very useful tool to meet the objectives of the study"

21 de febrero del 2024, Quito, Ecuador

Eng. César Calvachi, MBA.
General Manager
PetroAptos Oil Engineering Company C. Ltda.

Appendix A-1. Letter of permission for tNavigator license use.

APPENDIX B. High-resolution log correlation.

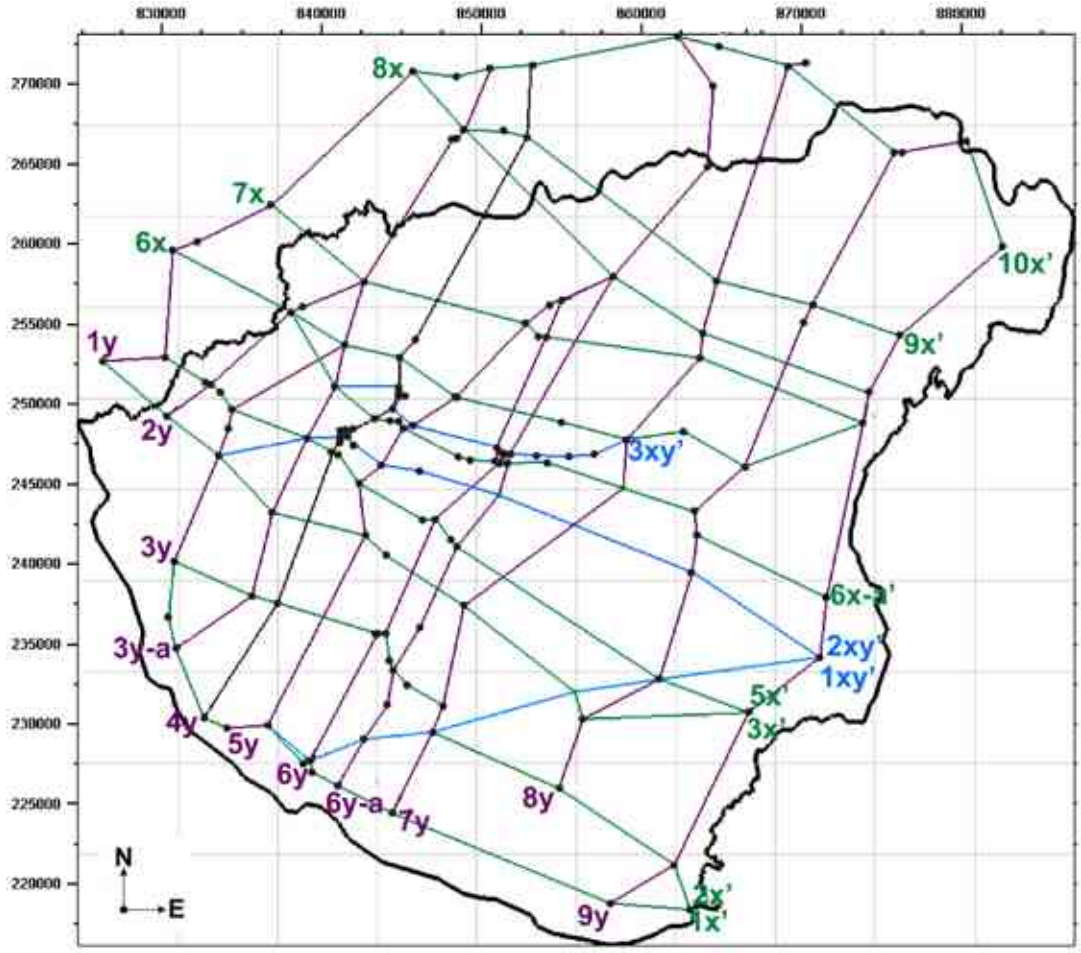

Appendix B-1. Location Map of the presented cross-sections in the study area. Sections running in the NW-SE direction are marked with 'X,' while those running in the SW-NE direction are marked with 'Y.' Additionally, three extra sections are denoted with the notation 'XY'.

Appendix B-2. Simbology for the cross-secctions. The stratigraphic units are displayed in the background of the sections, meanwhile, the lithology fills the space between the logs.

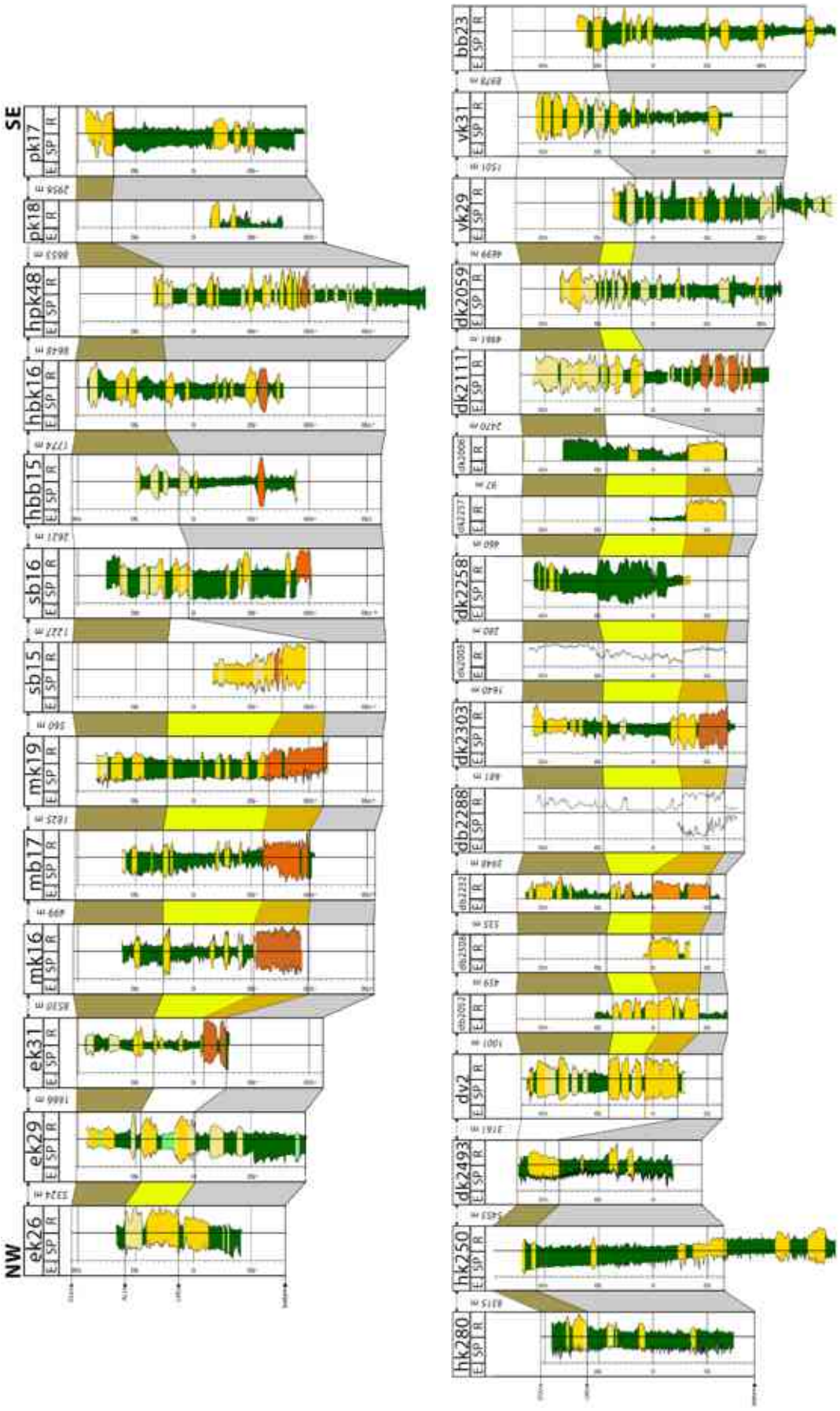

Appendix B-3. Cross-section 2x and cross-section 6x-a The well logs are equidistantly plotted, showing the GR and SP log at the left, and R log at the right, and the geological log filling between the curves.

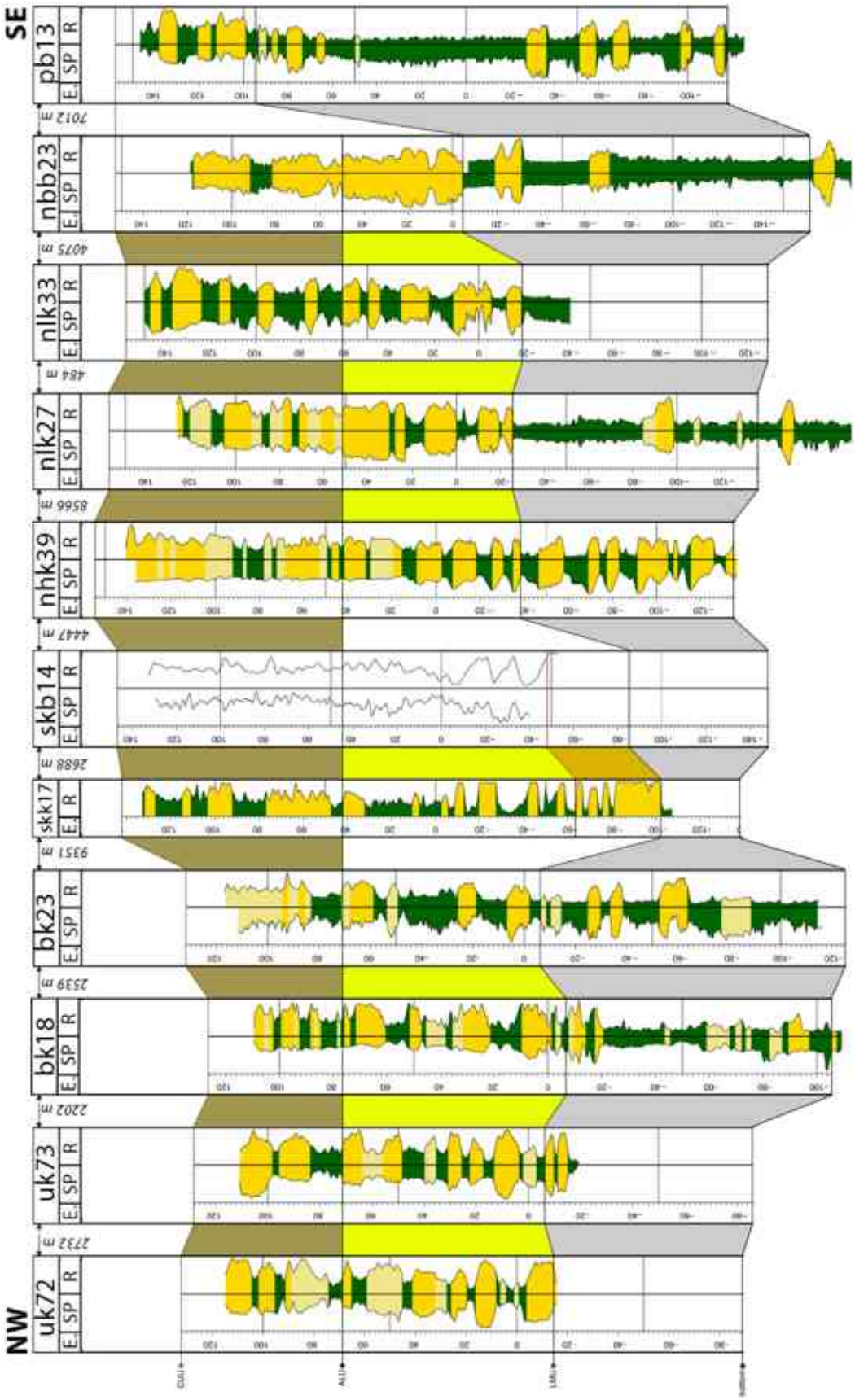

Appendix B-4. Cross-section 10x. The well logs are equidistantly plotted, showing the GR and SP log at the left, and R log at the right, and the geological log filling between the curves.

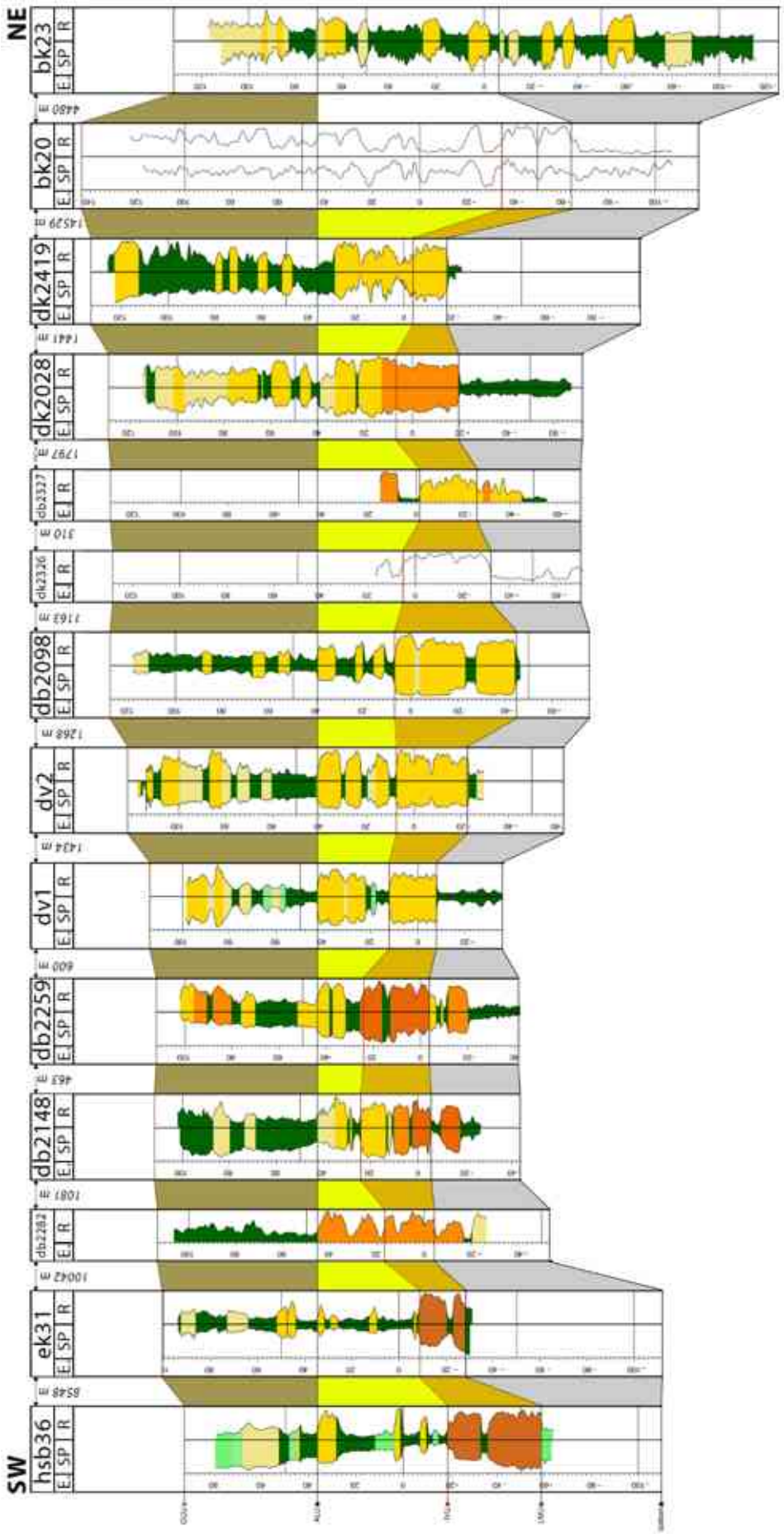

Appendix B-5. Cross-section 4y. The well logs are equidistantly plotted, showing the GR and SP log at the left, and R log at the right, and the geological log filling between the curves.

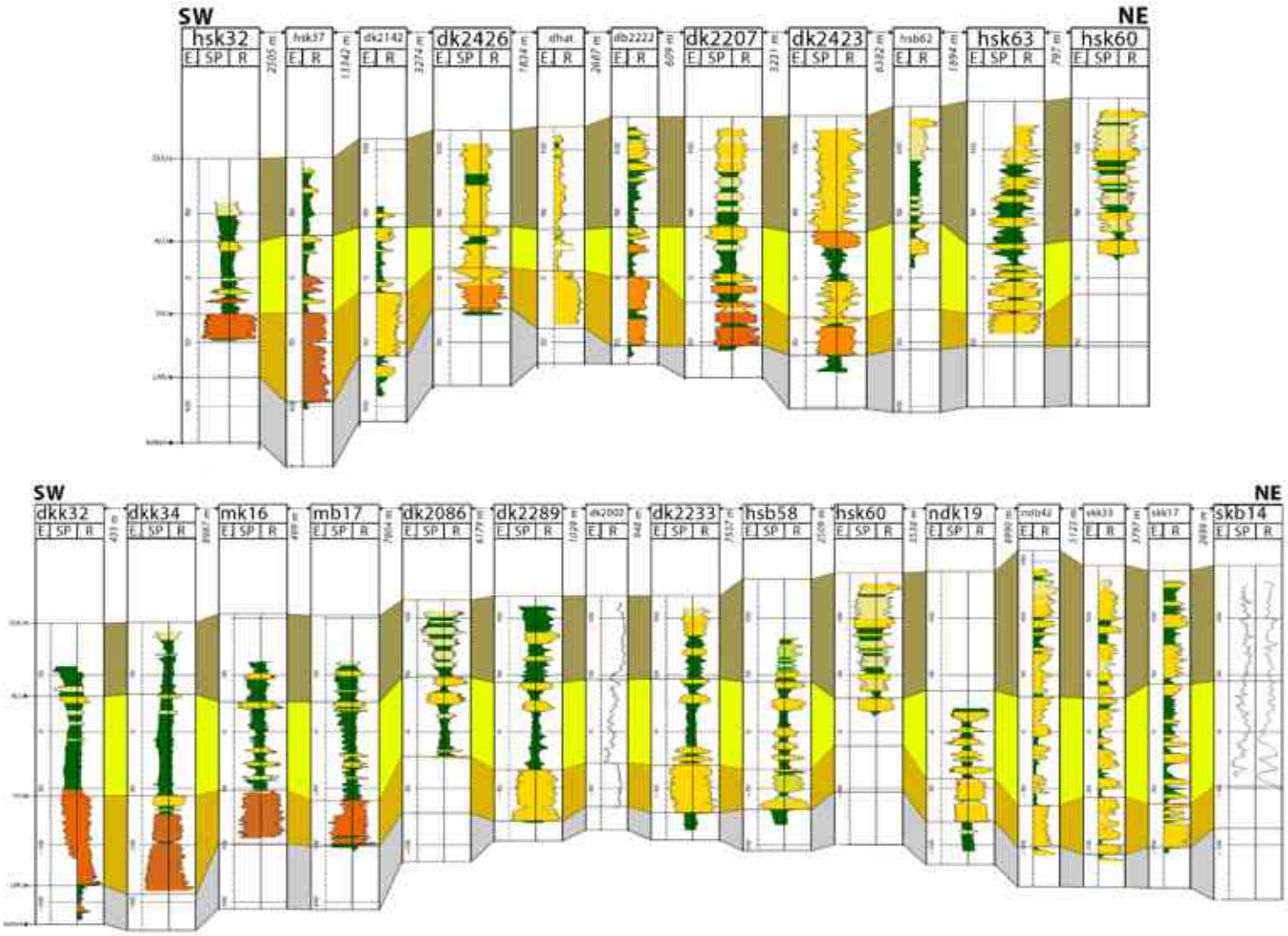

Appendix B-6. Cross-section 5y and cross.-section 6y. The well logs are equidistantly plotted, showing the GR and SP log at the left, and R log at the right, and the geological log filling between the curves.

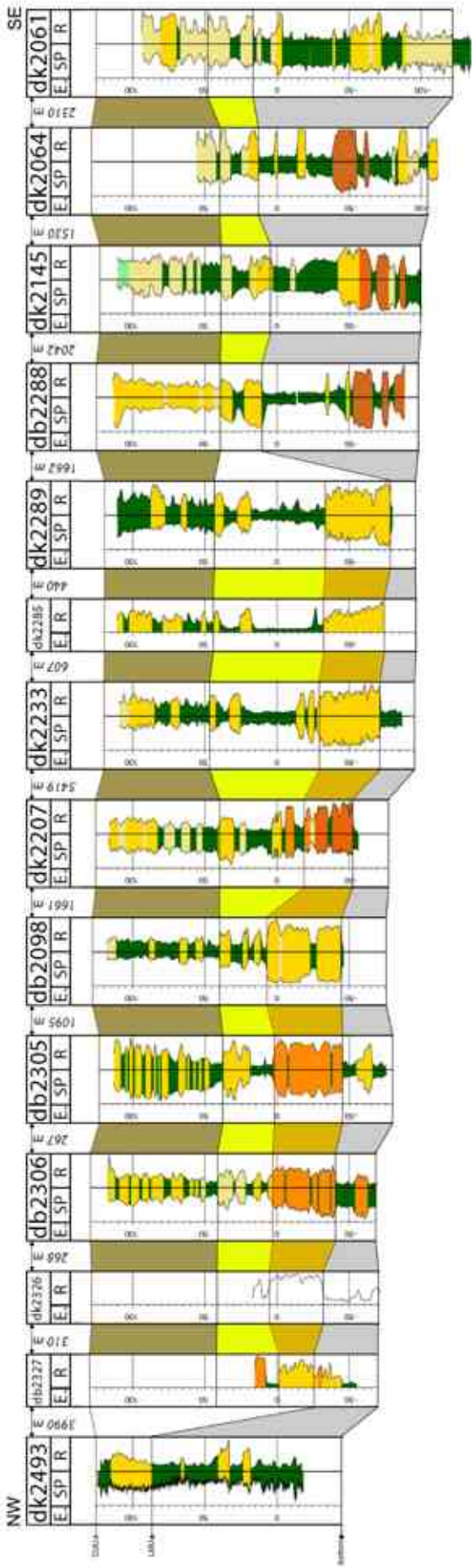

Appendix B-7. Cross-section 3xy. The well logs are equidistantly plotted, showing the GR and SP log at the left, and R log at the right, and the geological log filling between the curves.

APPENDIX C. Trend model of the defined facies generated for the upscaled logs

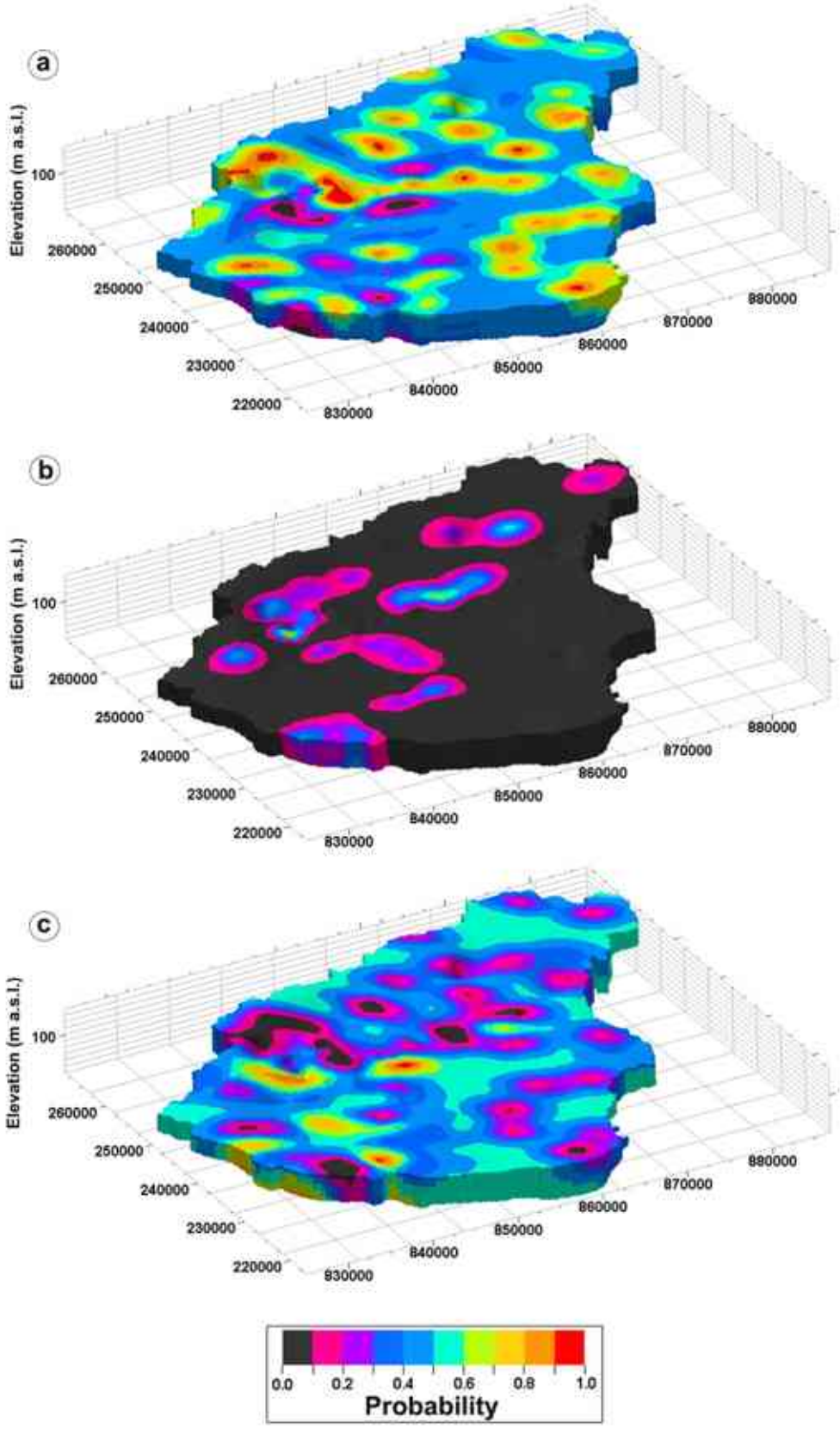

Appendix C-1. Probability of occurrence of (**a**) sand facies, (**b**) silt facies, and (**c**) clay facies in the Coarsening Upward Unit.

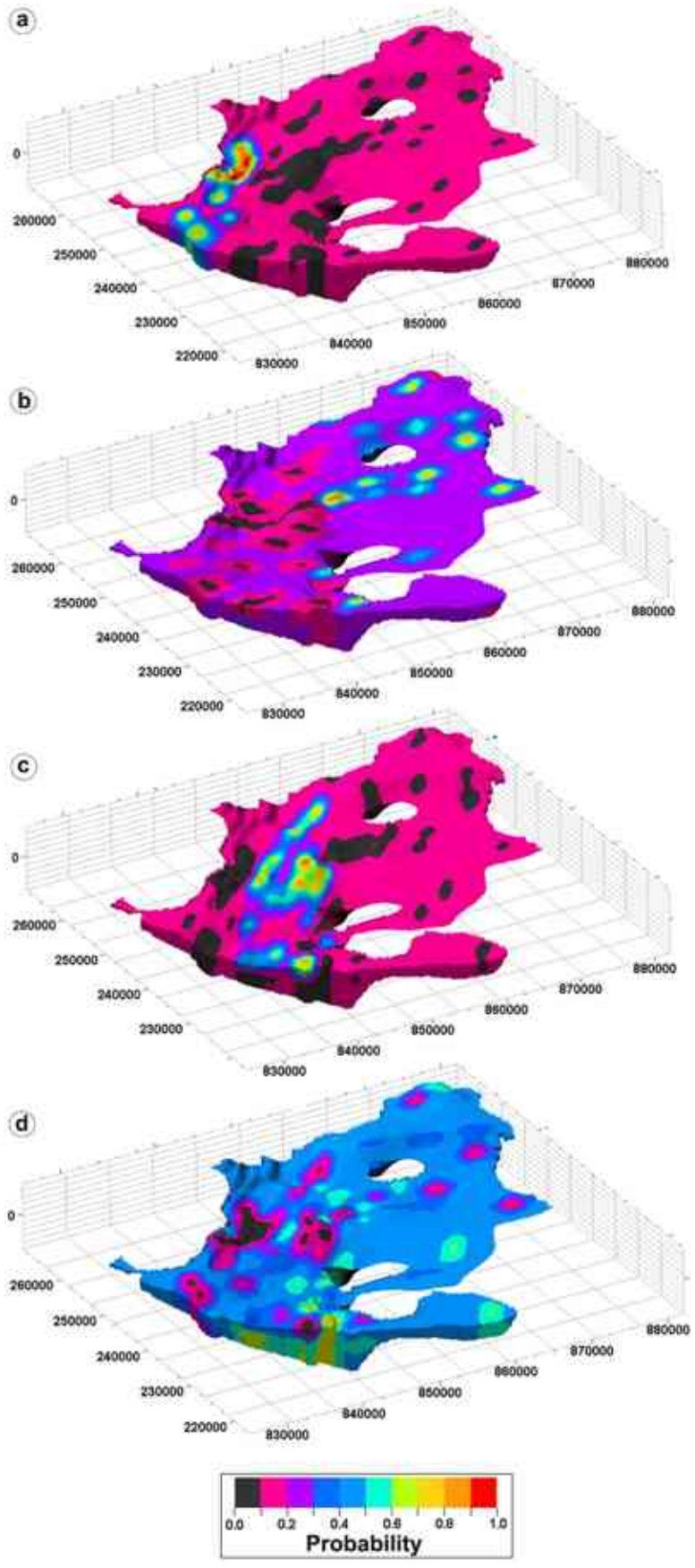

Appendix C-2. Probability of occurrence of (**a**) main channel facies, (**b**) secondary channel facies, (**c**) avulsion facies, and (**d**) floodplain facies in the Alluvial Unit.

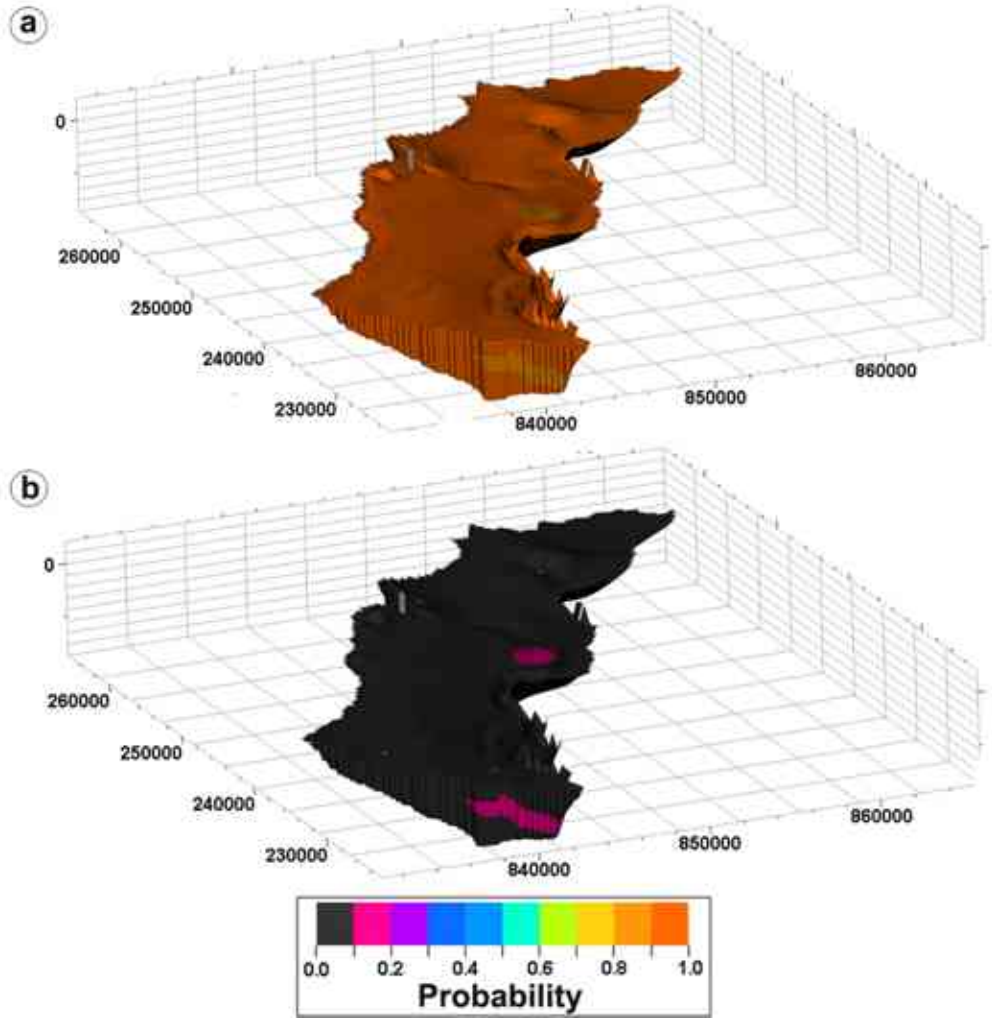

Appendix C-3. Probability of occurrence of (**a**) channel facies, and (**b**) floodplain facies in the Incised Valley Unit.

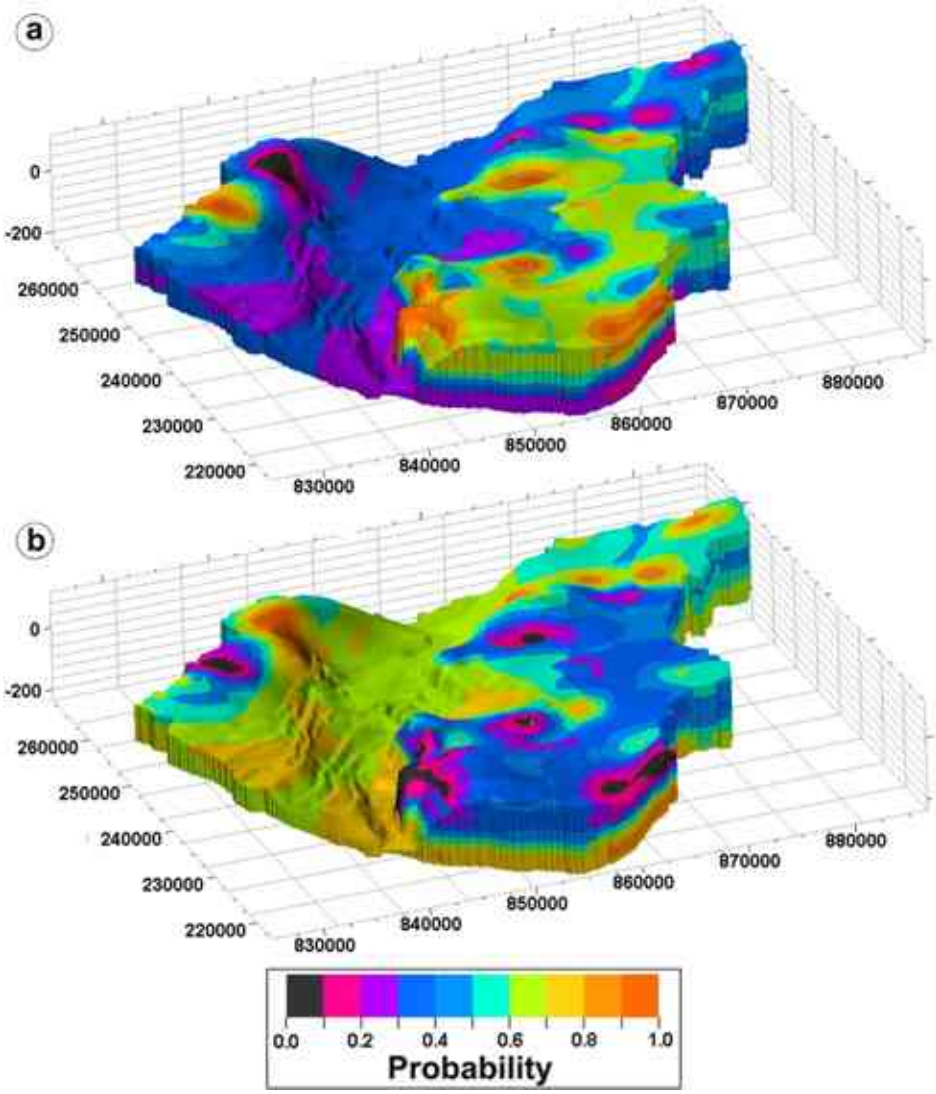

Appendix C-4. Probability of occurrence of (**a**) sand facies, and (**b**) clay facies Pannonian Unit.

APPENDIX D. Variograms for application of the Indicator Kriging Simulation of Pannonian Stratigraphic Unit and Coarsening Upward Sequences

Pannonian Stratigraphic Unit

Variogram model	
Type	Exponential
Sill	0.7705
Major range	5253.538
Minor range	5389.353
Vertical range	52.537
Nugget	0.0001
Sill	0.7706

Experimental variogram									
	Azimuth	Dip	Number lags	Lag distance	Search radius	Bandwidth	Tolerance angle	Lag tolerance	Thickness
Vertical	NA	90	7	17.7	123.9	17.7	45	50	NA
Major	35.3	0	24	1721	41304	1721	45	50	0.001
Minor	305.3	0	24	1721	41304	1721	45	50	0.001

Coarsening Upward Stratigraphic Unit

Variogram model - Clay	
Type	Spherical
Sill	0.8804
Major range	4666.667
Minor range	6147.353
Vertical range	33.609
Nugget	0.0001
Sill	0.8805

Experimental variogram - Clay									
	Azimuth	Dip	Number lags	Lag distance	Search radius	Bandwidth	Tolerance angle	Lag tolerance	Thickness
Vertical	Vertical	NA	90	7	8.6	60.2	8.6	45	50
Major	Major	300.6	0	23	1039.9	23917.7	1721	45	50
Minor	Minor	210.6	0	23	2120	48760	1721	45	50

Variogram model - Silt	
Type	Spherical
Sill	0.9352
Major range	3702.749
Minor range	4903.78
Vertical range	26.568
Nugget	0.0001
Sill	0.9353

Experimental variogram - Silt									
	Azimuth	Dip	Number lags	Lag distance	Search radius	Bandwidth	Tolerance angle	Lag tolerance	Thickness
Vertical	NA	90	5	13.1	65.5	13.1	45	50	NA
Major	349.4	0	24	1177.5	28260	1691	45	50	0.001
Minor	259.4	0	24	1691	40584	1691	45	50	0.001

Variogram model - Sand	
	Structure 1
Type	Spherical
Sill	0.9116
Major range	6626.607
Minor range	3275.44
Vertical range	37.224
Nugget	0.0001
Sill	0.9117

Experimental variogram - Sand									
	Azimuth	Dip	Number lags	Lag distance	Search radius	Bandwidth	Tolerance angle	Lag tolerance	Thickness
Vertical	NA	90	5	17.4	87	13.1	45	50	NA
Major	305.8	0	24	1362	32688	1691	45	50	0.001
Minor	215.8	0	24	915.7	21976.8	1691	45	50	0.001

APPENDIX E. Geometric parameters used in the Object-Based Simulation for the Incised Valley Unit (IVU) and Alluvial Unit (ALU)

	Facies	Orientation		Amplitude				Wavelength		
		Min	Med	Max	Min	Med	Max	Min	Med	Max
IVU	Channel	24	30	35	1000	1500	1800	1000	1500	1800
ALU	Main channel				1100	1700	2000	13000	20000	24000
	Avulsion channel	Derived from flow lines			1100	1700	2000	13000	20000	24000
	Secondary river 1				600	800	1000	25000	30000	43000
	Secondary river 2				600	800	1000	25000	30000	43000
	Secondary river 3				600	800	1000	25000	30000	43000
	Secondary river 4				600	800	1000	25000	30000	43000

	Facies	Orientation		Width			Thickness		
		Min	Med	Min	Med	Max	Min	Med	Max
IVU	Channel	24	30	3000	3300	3600	20	40	50
ALU	Main channel			1100	1460	2000	5	16	30
	Avulsion channel	Derived from flow lines		1030	1150	1260	5	12	16
	Secondary river 1			600	900	1000	4	10	15
	Secondary river 2			600	900	1000	4	10	15
	Secondary river 3			600	900	1000	4	10	15
	Secondary river 4			600	900	1000	4	10	15

APPENDIX F. Cross-sections of facies modelling.

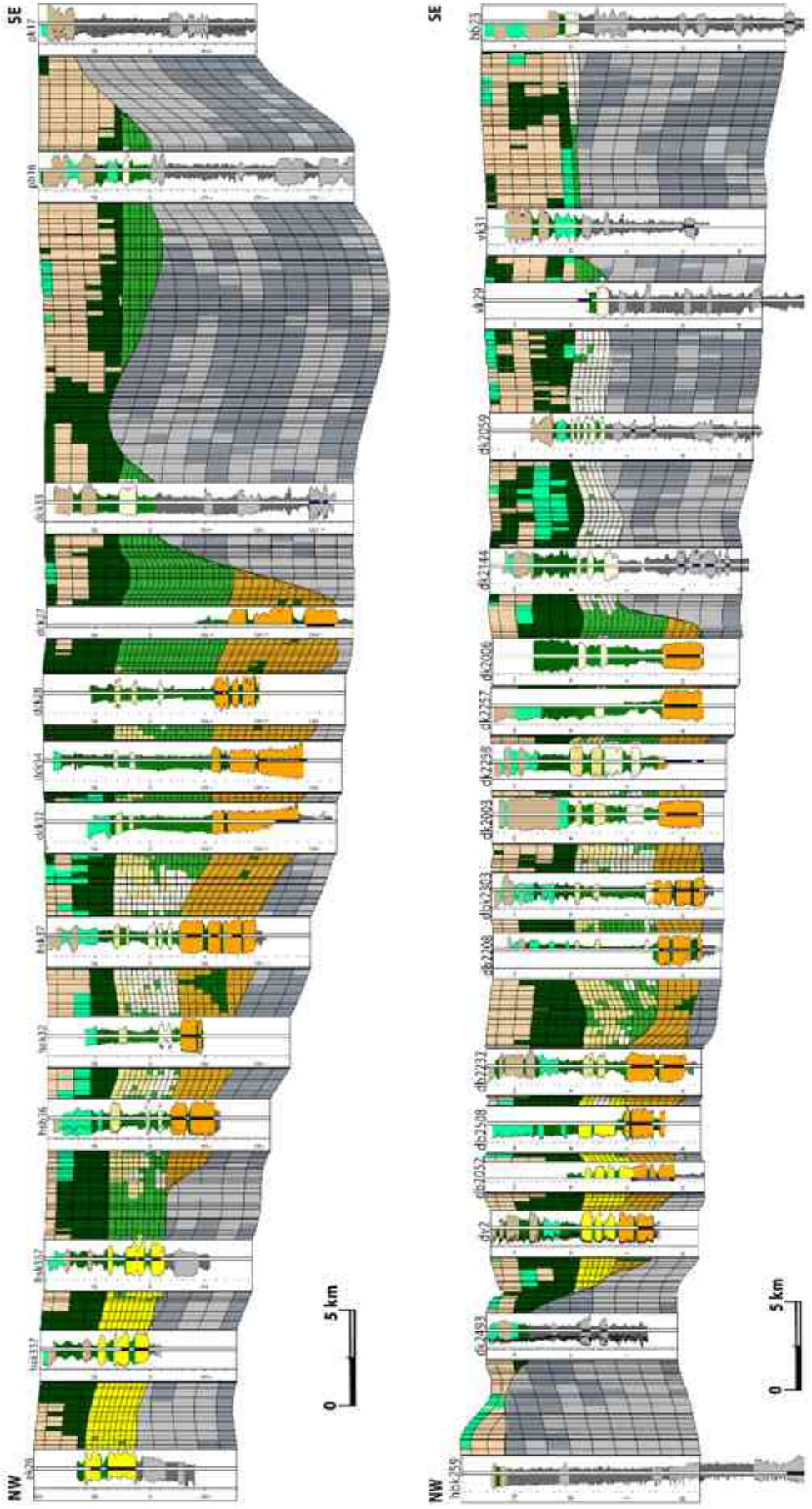

Appendix F-1. Cross-section 1x and cross-section 6xa. The well logs are equidistantly plotted, showing the GR and SP log at the left, and R log at the right, is filled with the Facies log. In the background is visible the simulation results.

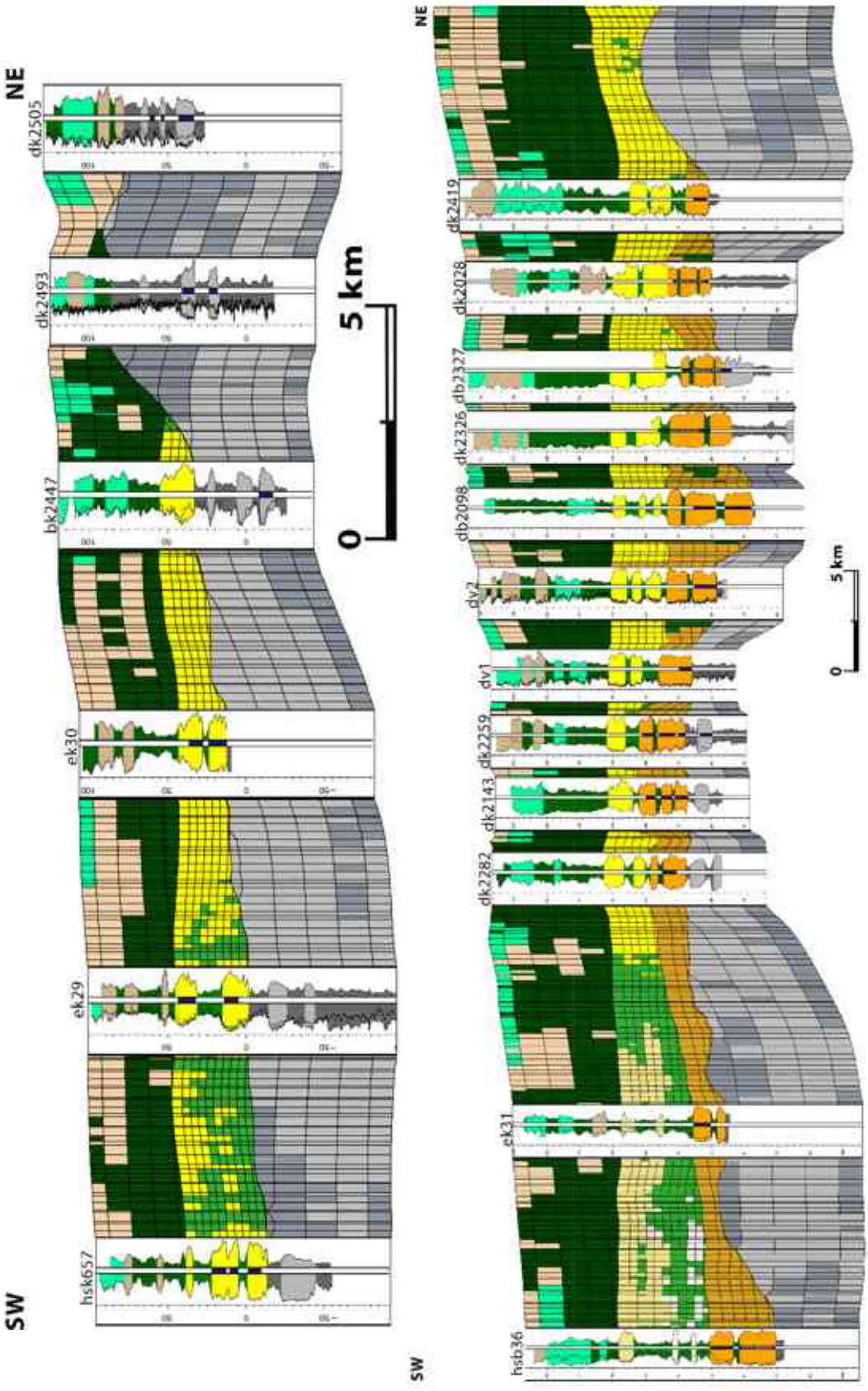

Appendix F-2. Cross-section 3y_a and cross-section 4y. The well logs are equidistantly plotted, showing the GR and SP log at the left, and R log at the right, is filled with the Facies log. In the background is visible the simulation results

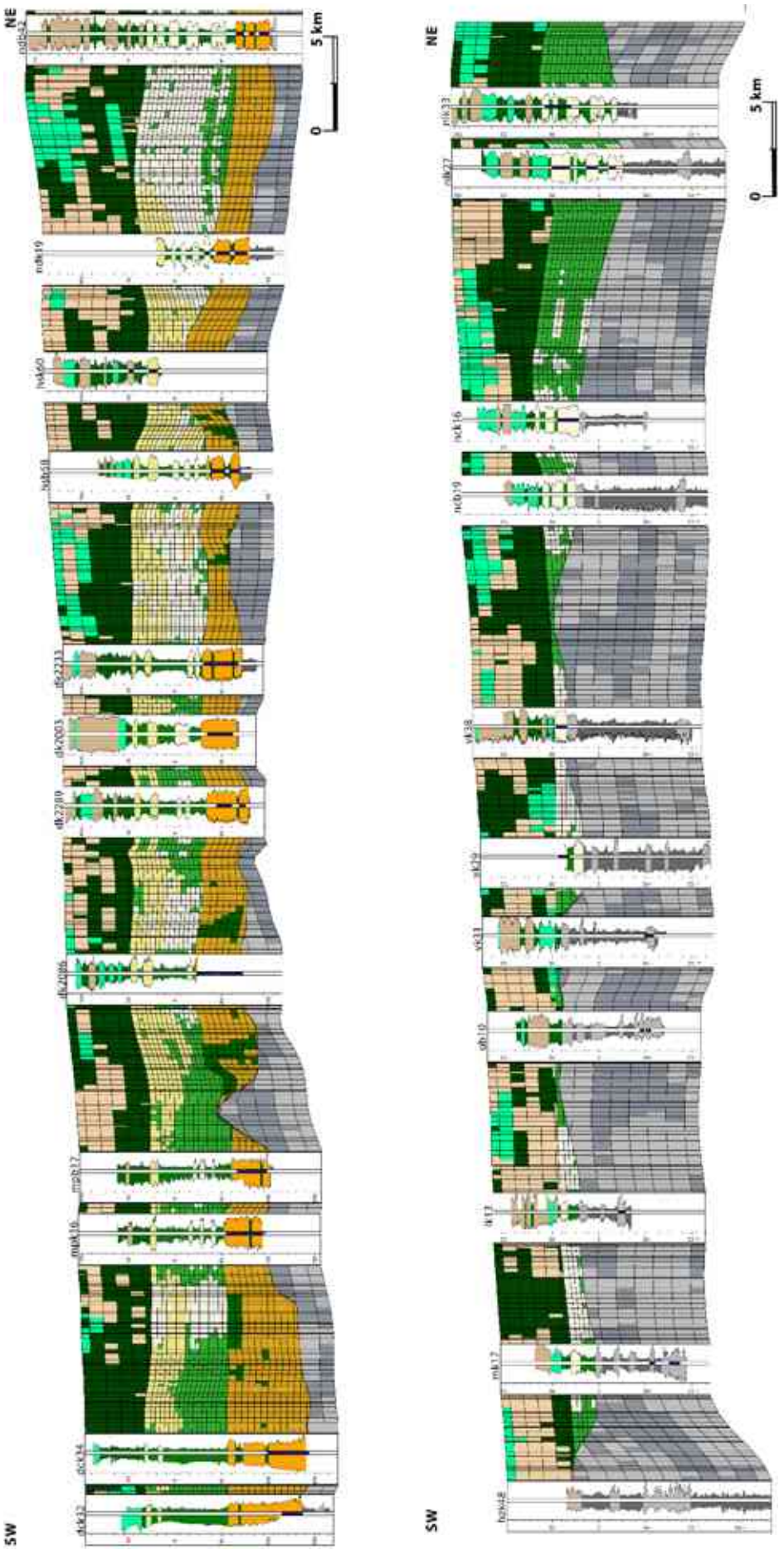

Appendix F-3. Cross-section 6y and cross-section 8y. The well logs are equidistantly plotted, showing the GR and SP log at the left, and R log at the right, is filled with the Facies log. In the background is visible the simulation results

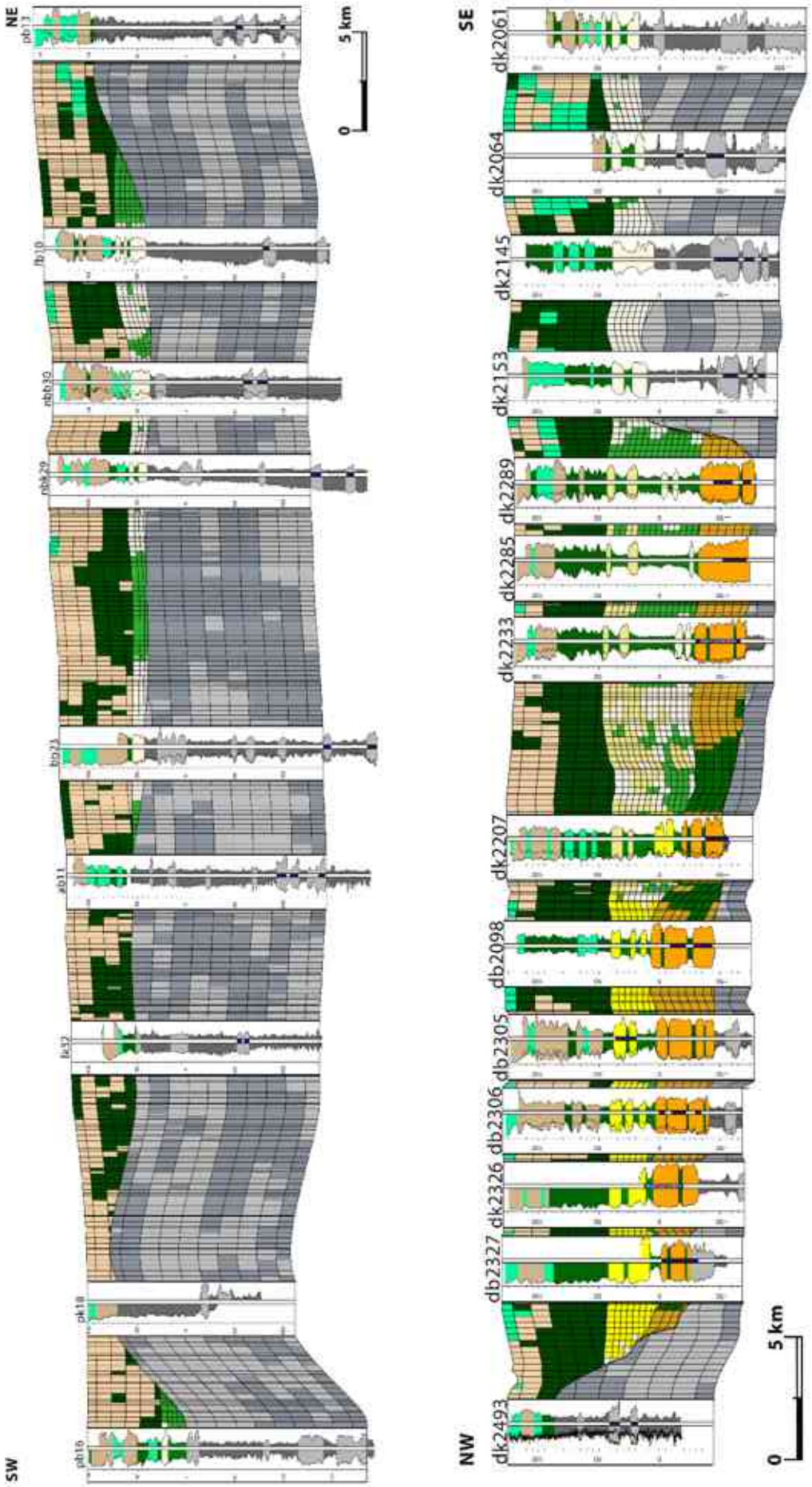

Appendix F-4. Cross-section 9y and cross-section 3xy. The well logs are equidistantly plotted, showing the GR and SP log at the left, and R log at the right, is filled with the Facies log. In the background is visible the simulation results.

APPENDIX G. Hydrogeological numerical model of Southern-NHGWB.

Appendix G is the electronic attachment that contains the numerical model of the Southern Nyírség-Hajdúság Groundwater Body. The simulation is performed using Modflow USG in the graphic interface of the Groundwater Modelling System (GMS).

Two versions will be found in the attachment, including the first simulation and the calibrated model.